SURFACE-INITIATED RING OPENING METATHESIS POLYMERIZATION FROM THE VAPOR PHASE TO PREPARE COMPOSITIONALLY VERSATILE THIN FILMS

By

Xuanli Deng

Dissertation
Submitted to the Faculty of the
Graduate School of Vanderbilt University
in partial fulfillment of the requirements
for the degree of

DOCTOR OF PHILOSOPHY
in

Chemical Engineering

December 15, 2018

Nashville, Tennessee

Approved:

G. Kane Jennings, Ph.D.

Paul E. Laibinis, Ph.D.

Clare M. McCabe, Ph.D.

Douglas E. Adams, Ph.D.

To the family and friends

who encouraged me along the way

ACKNOWLEDGEMENTS

I would like to express my deepest appreciation to my advisor, and my committee chair, Professor Kane Jennings, for all the support, encouragement and patience throughout my PhD life. The completion of this journey would not have been possible without his guidance and nurturing. I would also like to thank him for his advice, support, and friendship on my professional and personal development. I would like to extend my deepest gratitude to my committee members: Dr. Paul Laibinis, Dr. Clare McCabe, Dr. Douglas Adams for their time, insight, and valuable suggestions.

It is my fortune to be in the Jennings Lab and work with my outstanding labmates. In particular, I would like to thank Dr. Ian Njoroge for his valuable ideas, guidance, and support on my research work. I would like to thank all the current and previous Jennings and Laibinis group members: Maxwell T. Robinson, Siyuan Yang, Faustin Mwambutsa, Josh Passantino, and Liudmyla Prozorovska, Bradley Baker for their support and friendship. I would also like to thank all the passionate and hardworking undergraduates who I had pleasure to work with. They includes, Jason B. Delony, Kenneth J. Anderson, and Joshua L. Livingston.

It is my privilege to experience a five-year study here at the Chemical and Biomolecular Engineering department. I would like to thank all the faculties for their guidance and advice. I would also like to thank Felisha C. Baquera, Angie Pernell, Mark Holmes, Mary Gilleran, Rae Uson for all their support, patience, assistance, and guidance in solving administrative and repairing challenges.

I would like to thank the National Science Foundation and the U.S. Department of Energy for their financial support of the research through the grants CMMI-1300406 and DE-NE0008712. I would also like to thank the Vanderbilt Institute of Nanoscale Science and Engineering (VINSE) for their support of my research in the form of instrumentation access. In particular, I would like to express my appreciation to Dr. Dmitry S. Koktysh for his patience and support on my research projects.

Finally, I would like to thank my family, my friends and all other people who motivated, inspired, supported me along the journey. It's my pleasure to have experienced such a fantastic journey with all of you.

TABLE OF CONTENTS

LIST OF TABLES

LIST OF FIGURES

CHAPTER I

INTRODUCTION

Surface and interfacial properties of materials attract considerable attention from both industry and academia due to their impact on many applications in areas of science and technology. From industry operation to microchip fabrication,[1,2] from energy conversion to biomaterials synthesis,[3–5] from environmental remediation to aerospace vehicles,[6,7] the careful consideration of material surface properties is an inevitable requirement in almost every engineering design. Ample research has been performed in the past decades on the design and modification of surface properties.[8–12] Functional polymer films are one system that provide the ability to tailor the properties of surfaces[13,14] and furthermore, can impart corrosion resistance,[8] wear resistance,[9] lubrication,[10,11] biocompatibility,[5,12] and "smart" switchability of properties based on stimuli in the environtment.[15,16] Over the past decades, many polymer film preparation techniques have been developed, such as spin coating,[17] dip coating,[18] layer-by-layer assembly,[19] and Langmuir–Blodgett deposition.[20] Most of these techniques require the synthesis of a bulk polymer in liquid or solution phase and its deposition onto the surface via physical or chemical bonding.

Among the many techniques of polymer film preparation, surface-initiated polymerization (SIP) is special approach that provides improved performance in constructing a stable, controllable, and tunable polymer film.[21–24] Figure 1.1 shows the basic illustration of SIP. In SIP, the initiators are chemically coupled to the surface, often via the spontaneous chemisorption of a self-assembled monolayer (SAM), so that the polymerization happens directly from the surface. The chemical interactions between the polymer film and the surface contributes to the enhanced

robustness of the film as a coating. Polymer coatings can be formed onto surfaces of any geometric shape and nearly any size by using SIP,[22,23,25] and various well-developed polymerization methods can be utilized within SIP, which enables the controllability and tunability of film preparation on the surface.

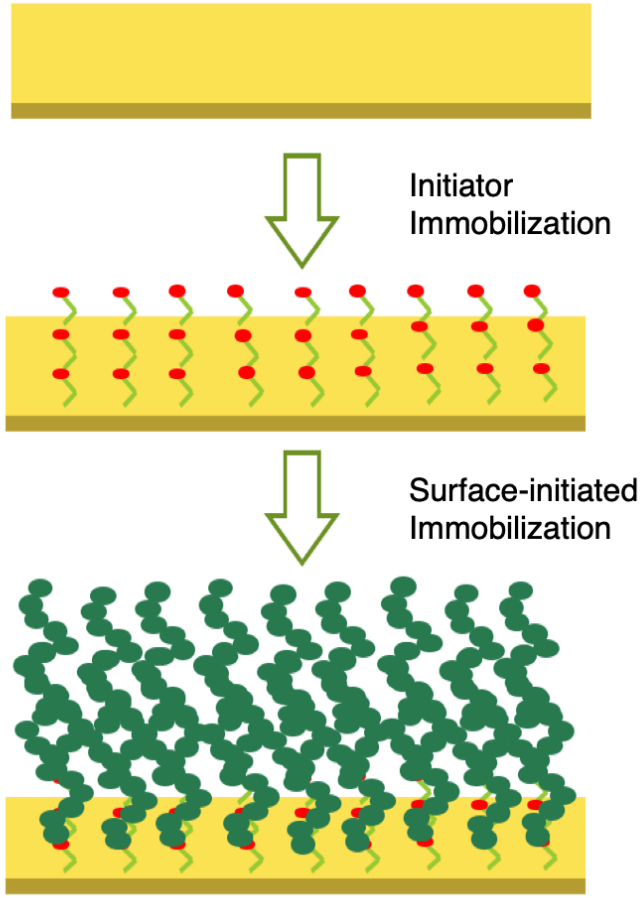

Figure 1.1. Illustration of surface-initiated polymerization

Many researchers have investigated the preparation of functional polymer films by SIP with different polymerization methods.[26–30] Among those methods, surface-initiated versions of atom-transfer radical polymerization (SiATRP) and ring-opening metathesis polymerization (SiROMP) are two that provide high control over the polymerization process, generally under mild

and non-stringent conditions. ATRP has already been well established and utilized in many research studies due to the control over film thickness and the tremendous variety of commercially available functional monomers that can undergo ATRP.[31,32] In contrast, ROMP has attracted less attention even though ROMP exhibits significantly fast initiation and polymerization, even at ambient conditions, and enables the preparation of high molecular weight polymers with preservation of olefin functionality.[33–35]

There are several limitations in the SiROMP of monomers with functional groups. As a ring-opening process, ROMP is thermodynamically driven by release of the energy of ring-strain, which establishes key requirements for the selection of ROMP monomers.[27,33,35] The most commonly used ROMP monomers are norbornene derivatives due to the high ring strain of the norbornene structure. However, not all norbornene-based monomers can be successfully polymerized from surfaces. The ease of the polymerization depends on the type of functional groups added to the norbornene structure due to either their reactivity with the catalyst or steric limitations. For example, norbornene carboxylic acid has not been directly polymerized into polymer films through SiROMP in the literature. Protection and deprotection processes are required to obtain polymers with carboxylic acid groups via SiROMP. [36,37] Therefore, for some important, chemically versatile functional groups, the polymer coating cannot be directly achieved via SiROMP. Furthermore, for some other groups of norbornene-based monomers, although they are suitable for SiROMP, they are not commercially available. Time-consuming and costly monomer syntheses are required before SiROMP can yield the polymer coating.[23,38] These requirements for ROMP monomers has limited the development of functional polymers by this polymerization method.

Finding accessible new methods that can impart multiple functionalities to polymer films grown by SiROMP is critical. This dissertation describes the work that I have performed in introducing multiple functionalities and properties into polymer thin films prepared by SiROMP. In this thesis, I demonstrate the feasibility of preparing chemically versatile thin film platforms by SiROMP as well as first steps toward the utilization of these platforms in applications.

In Chapter IV, I report the SiROMP of trans-5-norbornene-2,3-dicarbonyl chloride (NBDAC) as a versatile platform to achieve many functional polymer films via simple exposure of the pNBDAC film to reagents. This modification strategy owes to the fast and high-yield reaction of acyl chlorides with alcohols, amines, water, and other molecules. The polymerization of NBDAC is performed with monomer in the vapor phase and exhibits rapid kinetics, producing ~400 nm thick films within 5 min. Due to the high reactivity of the acyl chloride groups in the film, the pNBDAC films are easily modified to produce side chains of carboxylic acids, esters, and amides via the reaction of the acyl group with water, alcohols, and amines, respectively. Alcohols with different hydrocarbon chain length are used to modify the pNBDAC film, and the properties of the resulting comb films with hydrocarbon carbon chains are investigated. As we increase the carbon chain length (n), film thickness increases linearly and methylene crystallinity is improved. Large changes in water contact angle from 40° to 117° and a four-order-of-magnitude increase in the resistance to ion transfer are measured as the carbon chain length is increased from 0 (pendant carboxylate) to 16 (pendant hexadecyl ester).

In Chapter V, the functional polymer preparation method introduced in Chapter VI is applied to produce polynorbornene films that contain pendant hydroxamic acid groups. The hydroxamic acid-modified film is prepared by the reaction of acyl chloride groups in the pNBDAC films with hydroxylamine. The main characteristic of the hydroxamic acid groups is their ability

to chelate transition metal ions, which can be used in metal ion caption from aqueous solutions. The chelation ability of our hydroxamic acid-modified film was investigated to show that the polymer film can chelate most divalent ions such as Fe^{2+}, Cu^{2+}, Ni^{2+}, Co^{2+}, and Zn^{2+}, with a 70% chelation degree, even at solution concentrations as low as 30 μM. Lower extents of chelation are achieved when the hydroxamic acid-modified polymer films are chelated with multivalent ions like Fe^{3+} and Zr^{4+}, which is attributed to the steric hindrance caused by our polymer backbone structure. The chelated metals within the polymer film act as cross-linkers, which remarkably enhances the pH stability, thermal stability, and resistance against ion transfer of the original film. The feasibility of chelating metal ions from surface corrosion processes is demonstrated, which creates the opportunity for the utilization of these hydroxamic acid-modified films in corrosion detection.

Chapter VI describes another application of our compositionally versatile pNBDAC platform to produce pH-responsive, ester/carboxylic acid random copolymer films. This chapter demonstrates the ability of these compositionally versatile films to have multiple functionalities introduced. The studies in copolymer preparation show a significantly higher reactivity of ethanol than that of water within the film. The composition of the copolymer is controllable by employing a partial modification of the acyl chlorides with aqueous ethanol solutions of various concentrations for 15 min, followed by exposure of the film to pure water to modify the remaining acyl chlorides to carboxylic acids. This two-step modification yields a nearly linear relation between ester film composition and ethanol solution composition. The pH-responsive behavior of the films with different ester/acid compositions was investigated. The magnitude and range of the pH-responsive performance are highly dependent on the carboxylic acid content in the copolymer films, which demonstrates the effect of film hydrophilicity on the pH-responsive switching of ionic

barrier properties. The interactions of the copolymer films with water at different pH values were also explored. The results show that a 3x greater film thickness is obtained in high pH solution than in low pH solution due to ionically driven water swelling when the copolymer contains 34% carboxylic acid. The reversibility and reproducibility of the pH-responsive performance of these copolymer films is high based on the QCM-D measurements.

Chapter VII describes another compositionally versatile platform through the preparation of polymer/IL composites. Instead of chemically modifying the polymer films, the film properties can also be altered by the physical or electrostatic incorporation of other materials within the polymer framework. In this Chapter, I report the preparation of polymer/ionic liquid (IL) gels by incorporating ILs into surface-initiated poly(dicyclopentadiene) (pDCPD) films using a simple immersion method. In the method, a surface-initiated pDCPD film was exposed to a solution of 1-butyl-3-methylimidazolium hexafluorophosphate ([bmim][PF6]) in dichloromethane, which led to incorporation of the IL within the film. The volume ratio of the incorporated [bmim][PF6] to the original pDCPD film was adjusted as high as 0.5, and it is strongly dependent on the solvent, IL solution concentration, and the film immersion time. The maximum IL loading is affected by the swellability of pDCPD films in the solvent, the solubility of the IL in the solvent, and interactions between the IL and the polymer. The method is also proven to be feasible in preparing pDCPD-IL gels with different IL species. The incorporated ILs dramatically change the properties of the pDCPD films. The pDCPD-IL gel film has a higher shear loss modulus than that of the pure pDCPD film based on quartz crystal microbalance with dissipation. The resistance of the film against ion transfer is at least 4 orders of magnitude lower at high levels of IL incorporation than the resistance of pure pDCPD.

Chapter VIII concludes the major findings of the research work and proposes future work regarding the applications of the compositionally versatile platforms.

References

(1) Sioshansi, P. Surface Modification of Industrial Components by Ion Implantation. *Mater. Sci. Eng.* **1987**, *90*, 373–383.

(2) Belder, D.; Ludwig, M. Surface Modification in Microchip Electrophoresis. *Electrophoresis* **2003**, *24* (21), 3595–3606.

(3) Zheng, G.; Zhang, Q.; Cha, J. J.; Yang, Y.; Li, W.; Seh, Z. W.; Cui, Y. Amphiphilic Surface Modification of Hollow Carbon Nanofibers for Improved Cycle Life of Lithium Sulfur Batteries. *Nano Lett.* **2013**, *13* (3), 1265–1270.

(4) Ren, X.; Feng, Y.; Guo, J.; Wang, H.; Li, Q.; Yang, J.; Hao, X.; Lv, J.; Ma, N.; Li, W. Surface Modification and Endothelialization of Biomaterials as Potential Scaffolds for Vascular Tissue Engineering Applications. *Chem. Soc. Rev.* **2015**, *44*, 5680–5742.

(5) Yang, Y.; Qi, P.; Ding, Y.; Maitz, M. F.; Yang, Z.; Tu, Q.; Xiong, K.; Leng, Y.; Huang, N. A Biocompatible and Functional Adhesive Amine-Rich Coating Based on Dopamine Polymerization. *J. Mater. Chem. B* **2015**, *3* (1), 72–81.

(6) Kang, G.; Liu, M.; Lin, B.; Cao, Y.; Yuan, Q. A Novel Method of Surface Modification on Thin-Film Composite Reverse Osmosis Membrane by Grafting Poly(Ethylene Glycol). *Polymer (Guildf).* **2007**, *48* (5), 1165–1170.

(7) Pariona, M. M.; Teleginski, V.; Santos, K. dos; Machado, S.; Zara, A. J.; Zurba, N. K.; Riva, R. Yb-Fiber Laser Beam Effects on the Surface Modification of Al-Fe Aerospace Alloy Obtaining Weld Filet Structures, Low Fine Porosity and Corrosion Resistance. *Surf. Coatings Technol.* **2012**, *206*, 2293–2301.

(8) Zomorodian, A.; Garcia, M. P.; Moura E Silva, T.; Fernandes, J. C. S.; Fernandes, M. H.; Montemor, M. F. Corrosion Resistance of a Composite Polymeric Coating Applied on

Biodegradable AZ31 Magnesium Alloy. *Acta Biomater.* **2013**, *9* (10), 8660–8670.

(9) Beckford, S.; Zou, M. Wear Resistant PTFE Thin Film Enabled by a Polydopamine Adhesive Layer. *Appl. Surf. Sci.* **2014**, *292*, 350–356.

(10) Kobayashi, M.; Takahara, A. Tribological Properties of Hydrophilic Polymer Brushes under Wet Conditions. *Chem. Rec.* **2010**, *10* (4), 208–216.

(11) Kreer, T. Polymer-Brush Lubrication: A Review of Recent Theoretical Advances. *Soft Matter* **2016**, *12* (15), 3479–3501.

(12) Skarja, G. A.; Brown, A. L.; Ho, R. K.; May, M. H.; Sefton, M. V. Biomaterials The Effect of a Hydroxamic Acid-Containing Polymer on Active Matrix Metalloproteinases. *Biomaterials* **2009**, *30* (10), 1890–1897.

(13) Zhang, W.; Shi, Z.; Zhang, F.; Liu, X.; Jin, J.; Jiang, L. Superhydrophobic and Superoleophilic PVDF Membranes for Effective Separation of Water-in-Oil Emulsions with High Flux. *Adv. Mater.* **2013**, *25* (14), 2071–2076.

(14) Wei, Z.; Pan, Z.; Li, F.; Yu, J. Poly(Butylene Succinate-Co-Terephthalate) Nanofibrous Membrane Composited with Cyclodextrin Polymer for Superhydrophilic Property. *RSC Adv.* **2017**, *8*, 1378–1384.

(15) Chen, Y. C.; Xie, R.; Chu, L. Y. Stimuli-Responsive Gating Membranes Responding to Temperature, PH, Salt Concentration and Anion Species. *J. Memb. Sci.* **2013**, *442*, 206–215.

(16) Tokarev, I.; Minko, S. Stimuli-Responsive Hydrogel Thin Films. *Soft Matter* **2009**, *5* (3), 511–524.

(17) Li, W.; Roelofs, W. S. C.; Turbiez, M.; Wienk, M. M.; Janssen, R. A. J. Polymer Solar Cells with Diketopyrrolopyrrole Conjugated Polymers as the Electron Donor and Electron

Acceptor. *Adv. Mater.* **2014**, *26* (20), 3304–3309.

(18) Sundaram, H. S.; Han, X.; Nowinski, A. K.; Ella-Menye, J. R.; Wimbish, C.; Marek, P.; Senecal, K.; Jiang, S. One-Step Dip Coating of Zwitterionic Sulfobetaine Polymers on Hydrophobic and Hydrophilic Surfaces. *ACS Appl. Mater. Interfaces* **2014**, *6* (9), 6664–6671.

(19) Vaterrodt, A.; Thallinger, B.; Daumann, K.; Koch, D.; Guebitz, G. M.; Ulbricht, M. Antifouling and Antibacterial Multifunctional Polyzwitterion/Enzyme Coating on Silicone Catheter Material Prepared by Electrostatic Layer-by-Layer Assembly. *Langmuir* **2016**, *32* (5), 1347–1359.

(20) Lindemann, W. R.; Philiph, R. L.; Chan, D. W. W.; Ayers, C. T.; Perez, E. M.; Beckman, S. P.; Strzalka, J.; Chaudhary, S.; Vaknin, D. Oriented Polyvinylidene Fluoride–Trifluoroethylene (P(VDF–TrFE)) Films by Langmuir–Blodgett Deposition: A Synchrotron X-Ray Diffraction Study. *Phys. Chem. Chem. Phys.* **2015**, *17* (43), 29335–29339.

(21) Olivier, A.; Meyer, F.; Raquez, J. M.; Damman, P.; Dubois, P. Surface-Initiated Controlled Polymerization as a Convenient Method for Designing Functional Polymer Brushes: From Self-Assembled Monolayers to Patterned Surfaces. *Prog. Polym. Sci.* **2012**, *37* (1), 157–181.

(22) Edmondson, S.; Osborne, V. L. V.; Huck, W. T. S. W. Polymer Brushes via Surface-Initiated Polymerizations. *Chem. Soc. Rev.* **2004**, *33* (1), 14–22.

(23) Faulkner, C. J.; Fischer, R. E.; Jennings, G. K. Surface-Initiated Polymerization of 5-(Perfluoro-n-Alkyl)Norbornenes from Gold Substrates. *Macromolecules* **2010**, *43* (3), 1203–1209.

(24) Njoroge, I.; Kempler, P.; Deng, X.; Arnold, S.; Jennings, G. K. Surface-Initiated Ring-Opening Metathesis Polymerization of Dicyclopentadiene from the Vapor Phase. *Langmuir* **2017**.

(25) Escobar, C. a; Harl, R. R.; Maxwell, K. E.; Mahfuz, N. N.; Rogers, B. R.; Jennings, G. K. Amplification of Surface-Initiated Ring-Opening Metathesis Polymerization of 5-(Perfluoro-n-alkyl)Norbornenes by Macroinitiation. *Langmuir* **2013**, *29*, 12560–12571.

(26) Buchmeiser, M. R.; Sinner, F.; Mupa, M.; Wurst, K. Ring-Opening Metathesis Polymerization for the Preparation of Surface-Grafted Polymer Supports. *Macromolecules* **2000**, *33* (1), 32–39.

(27) Lerum, M. F. Z.; Chen, W. Surface-Initiated Ring-Opening Metathesis Polymerization in the Vapor Phase: An Efficient Method for Grafting Cyclic Olefins with Low Strain Energies. *Langmuir* **2011**, *27* (9), 5403–5409.

(28) Minet, I.; Delhalle, J.; Hevesi, L.; Mekhalif, Z. Surface-Initiated ATRP of PMMA, PS and Diblock PS-b-PMMA Copolymers from Stainless Steel Modified by 11-(2-Bromoisobutyrate)-Undecyl-1-Phosphonic Acid. *J. Colloid Interface Sci.* **2009**, *332* (2), 317–326.

(29) Bissadi, G.; Weberskirch, R. Formation of Polyoxazoline-Silica Nanoparticles: Via the Surface-Initiated Cationic Polymerization of 2-Methyl-2-Oxazoline. *Polym. Chem.* **2016**, *7* (32), 5157–5168.

(30) Min, J.; Lin, Y.; Zheng, J.; Tang, T. A Novel Strategy to Synthesize Well-Defined PS Brushes on Silica Particles by Combination of Lithium-Iodine Exchange (LIE) and Surface-Initiated Living Anionic Polymerization (SI-LAP). *Chem. Commun.* **2015**, *51* (27), 5921–5924.

(31) Balachandra, A. M.; Baker, G. L.; Bruening, M. L. Preparation of Composite Membranes by Atom Transfer Radical Polymerization Initiated from a Porous Support. *J. Memb. Sci.* **2003**, *227*, 1–14.

(32) Ulbricht, M. Advanced Functional Polymer Membranes. *Polymer (Guildf).* **2006**, *47* (7), 2217–2262.

(33) Leitgeb, A.; Wappel, J.; Slugovc, C. The ROMP Toolbox Upgraded. *Polymer (Guildf).* **2010**, *51* (14), 2927–2946.

(34) Bielawski, C. W.; Grubbs, R. H. Living Ring-Opening Metathesis Polymerization. *Prog. Polym. Sci.* **2007**, *32* (1), 1–29.

(35) Sutthasupa, S.; Shiotsuki, M.; Sanda, F. Recent Advances in Ring-Opening Metathesis Polymerization, and Application to Synthesis of Functional Materials. *Polym. J.* **2010**, *42* (12), 905–915.

(36) Montembault, V.; Desbrosses, J.; Campistron, I.; Reyx, D. Ring-Opening Metathesis Polymerization of 2-(S)-(-)-Endo-D-Pantolacton-O-Yl Norbornene-2-Carboxylate Using a Classical ROMP Catalyst. Synthesis and Characterization of Optically Active Poly(Norbornene-2-Carboxylic Acid). *Macromol. Chem. Phys.* **2000**, *201* (9), 973–979.

(37) Buchmeiser, M. R.; Atzl, N.; Bonn, G. K. Ring-Opening-Metathesis Polymerization for the Preparation of Carboxylic-Acid Functionalized, High-Capacity Polymers for Use in Separation Techniques. *J. Am. Chem. Soc.* **1997**, *119* (39), 9166–9174.

(38) Njoroge, I.; Matson, M. W.; Jennings, G. K. Dynamic Anion-Adaptive Poly(Ionic Liquid) Films via Surface-Initiated Ring-Opening Metathesis Polymerization. *J. Phys. Chem. C* **2017**, *121* (37), 20323–20334.

CHAPTER II

BACKGROUND

Surface-Initiated Polymerization (SIP)

SIP is an approach that offers many attractive advantages toward the fabrication of robust polymer films.[1–4] Surface-initiated polymerization (SIP) is unique in that the polymerization occurs during the formation of the film. SIP, also called the "grafting from" method, enables the growth of stable polymer films with tunable thicknesses ranging from tens of nanometers up to the micron level. The surface is first modified with initiator-terminated adsorbates, such as a reactive self-assembled monolayer (SAM), and then exposed to a monomer solution to grow polymer chains that are initiated from the surface. By contrast to conventional methods such as spin coating, dip coating, and drop casting, SIP offers key advantages in the preparation of polymer films. By using SIP, polymer films can be formed onto surfaces independent of the geometric shape and size of the substrate. Also, SIP provides stronger adhesion of the polymer film via either a chemisorbed or covalent linkage to the substrate than is achieved with typical spin coating or casting methods. SIP also enables improved control in grafting density and thickness of the polymer film than that of "grafting to" methods. Important for the work in this thesis, unreacted monomers are easily rinsed away after the polymerization is complete to simplify separations.[2–4] There are many types of SIP, categorized by their polymerization mechanism, including ring-opening metathesis polymerization (SiROMP)[3–6], atom-transfer radical polymerization (SiATRP)[7–10], anionic polymerization[11], cationic polymerization[12], etc. These SIPs are well

studied and utilized in functionalizing fine particles[12], membranes[7], biomaterials[13], and different substrates such as silicon[9], gold[3,4], and stainless steel.[8]

Surface-initiated Ring Opening Metathesis Polymerization (SiROMP)

Olefin metathesis was discovered in the mid-1950's by accident as an outgrowth of the study of Ziegler polymerization with alternative metal systems.[14,15] The name "olefin metathesis" means the change of position and was initially termed by Calderon and co-workers to describe this metal-catalyzed redistribution of carbon-carbon double bonds during reaction.[15,16] In 1970, Chauvin and He´risson proposed a generally accepted mechanism for olefin metathesis. The mechanism indicated that olefin metathesis mainly involves the coordination of olefin to a metal alkylidene via metallacyclobutane intermediates by alternating [2 + 2]-cycloadditions and cycloreversions.[15–17] After its discovery, olefin metathesis started to become a very powerful method in chemical synthesis in both industry and academia. Several subtypes of olefin metathesis have been developed including ring-opening metathesis polymerization (ROMP), ring-closing polymerization (RCM), cross metathesis (CM), and acyclic diene metathesis polymerization (ADMET).[14–17]

Applying olefin metathesis to polymer synthesis, ring-opening metathesis polymerization (ROMP) has become a powerful and broadly applicable method to synthesize macromolecules.[15,16,18] ROMP is a chain growth polymerization process where cyclic olefin monomers are converted into polymer. The unsaturation associated with the monomer is conserved in the resulting polymer in ROMP, which distinguishes it from conventional olefin addition polymerizations. Similar to other olefin metathesis reactions, ROMP is generally reversible. All the processes in the mechanism can also proceed in the opposite direction. However, the

equilibrium can be controlled and predicted by analyzing the thermodynamics of the polymerization. As a ring-opening process, the reaction from monomer to polymer is driven from the release of strain associated with cyclic olefin ("ring strain"), balanced by an entropic penalty. Generally, monomers with greater ring strains are more reactive in a ROMP.[6,15,17]

Norbornene (NB) is a cyclic seven-membered ring that exhibits high ring strain energy (27.2 kcal/mol) and superior reactivity in ROMP. During ROMP, both intermolecular and intramolecular chain transfer ("backbiting") can occur.[15] In those secondary metathesis reactions, one polymer chain containing an active metal alkylidene on its terminus can react with either olefin along the backbone of a different polymer chain or olefin on the same chain to release a cyclic species. Secondary metathesis reactions will not affect the total number of chains but influence the molecular weight distribution of the polymer. Therefore, the polydispersity of polymers obtained through ROMP can vary based on the degree of secondary metathesis reactions. The catalysts used in ROMP have been evolved for decades, and the discovery of Grubb's catalyst provides researchers the ability to reduce the chain transfer in ROMP and obtain nearly monodisperse polymers (PDI < 1.1). [6,17,19]

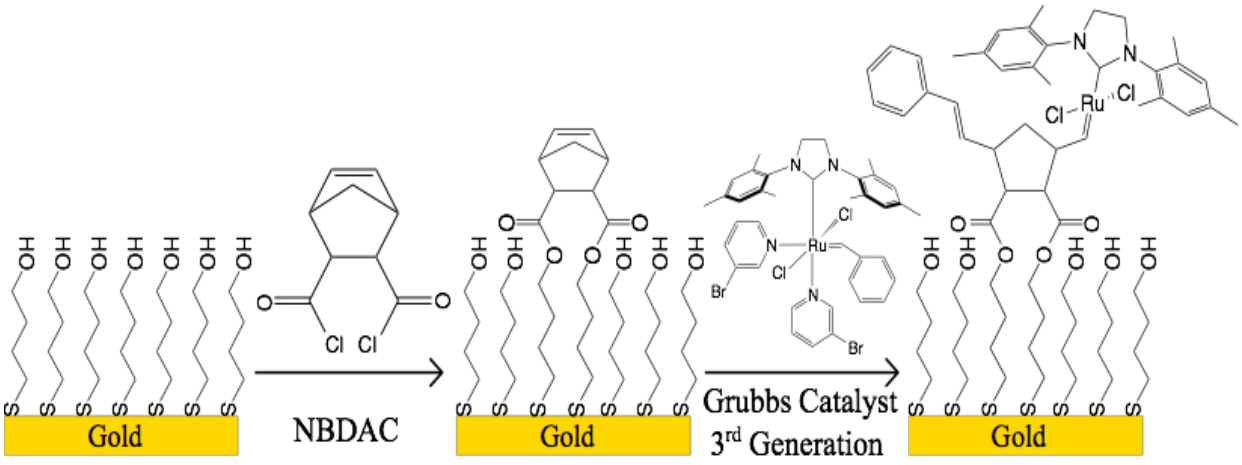

Figure 2.1. Initiator/catalyst immobilization on gold surface

Surface-initiated ring-opening metathesis polymerization (SiROMP) is the implementation of ROMP directly on the surface (Figure 2.1). SiROMP has emerged as a novel and versatile SIP technique over the past two decades. Compared to other types of SIP, SiROMP shows more rapid initiation and polymerization due to the continuously developed and improved SiROMP catalysts by Grubbs and others.[6,14–17,20] During SiROMP, either alkene functional groups or cyclic olefin functional derivatives are first immobilized on the surface, followed by the immobilization of the initiators on the surface to initiate the polymerization process.[3,4,21] SiROMP can provide high initiation rate and polymerization rate under mild condition compared to other SIPs.[3,4,21]

Hydroxamic Acid and Metal Chelation

Metal-chelating polymers are polymer compounds with multidentate functional groups, which can react with metal ions to form chelated materials. In the past few decades, research on metal-chelating polymers has developed rapidly and attracted attention from both academia and industry because of the important utilization of these polymers in various areas, such as environmental protection,[22–26] medical therapy,[27–29] and analytical separations.[30,31]

Among various chelating ligands, hydroxamic acid groups are widely utilized and known to effectively chelate many different metal ions. Hydroxamic acids have been widely applied in medical therapy because of their wide spectrum of biological activities.[32–34] For example, Krasavin et al.[35] utilized cyclic hydroxamic acids in the design of chelating agents for iron overload disease therapy. They also investigated the application of cyclic hydroxamic acids in antibiotic delivery across the bacterial cell wall due to the structural analogy of cyclic hydroxamic acids to bacterial siderophores (iron-binding compounds). Industrially, hydroxamic acids can also serve as anti-

oxidants, corrosion inhibitors, and extractors of toxic elements.[36] In addition, polymers with hydroxamic acid ligands are prevalent among those metal chelating polymers and have been well developed due to their straightforward preparation via post-modification from carboxylic acids, esters, or acyl chlorides.[26,37–41] The first successful preparation of hydroxamic acid polymers can be traced back to the 1950s. Kern & Schultz achieved 80 % hydroxamic acid conversion through a reaction of poly(methyl acrylate) with hydroxylamine.[37] Since then, hydroxamic acid modified polymers have been studied extensively and widely utilized in separation of metal ions and water treatments.[26,37–41] Abdullah et al. modified cellulose with hydroxamic acids and utilized them in the removal of transition metals such as Fe^{3+}, Cu^{2+}, Co^{2+}, Ni^{2+}, and $Cr^{3+}$from water.[25] Kumar et al. synthesized hydroxamic acid polymers from acyl amine and applied them in cartridges to determine the concentration of rare earth metals in sea water.[26] The salts in high concentration all pass through the cartridge, while rare earth metal ions become captured by chelation via the hydroxamic acid film. Then, these ions can be retrieved in acid solution, and their concentration can be determined.

In this thesis, I investigate a new type of hydroxamic acid-modified polymer film prepared by SiROMP, study the effect of the chelated metals on film properties, and explore the potential feasibility of utilizing our hydroxamic acid-modified film in corrosion detection.

pH-responsive Polymers

"Smart" polymers are a class of polymers that can undergo significant changes in physical or chemical properties responding to surrounding stimuli, such as temperature, pH, chemical agents, magnetic fields, electrical fields, etc.[42–44] pH-responsive polymers are a group of "smart" polymers that become ionized at a certain pH to greatly alter their film properties.[45–52] pH-

responsive polymers usually undergo changes in surface properties, barrier properties, and polymer structure when pH reversibly ionizes the film.[45–52] The special pH-responsive behavior of those polymers has impacted chemical sensors,[53] membrane separations,[47,48,50,51] drug delivery, [49,52] and dynamic surfaces.[51,54]

The pH-responsive properties are due to the ionizable moieties in the polymer.[46,55,56] The ionizable groups become protonated/deprotonated depending on pH change, and this change results in a hydrophobic/hydrophilic property switch of the polymer.[46,55,56] The change in polymer-water interaction can be easily applied in the tuning of surface properties such as wettability switching. For example, Cho et al.[51] designed a smart fabric with a copolymer film, poly[2-(diisopropylamino)ethylmethacrylate-co-3-(trimethoxysilyl)propyl methacrylate][poly(DPAEMA-co-TSPM)], which can switch between superhydrophobicity and superhydrophilicity between pH 2 and pH 12. By tuning the surface properties, Luo et al developed a pH-induced oil/water separation membrane with poly(methyl methacrylate)-block-poly(4-vinylpyridine) (PMMA-b-P4VP).[54] The copolymers demonstrate high hydrophilicity and high (under water) oleophobicity when pH ≤ 3 and vice versa, which offers a switchable hydrophilicity/oleophilicity for oil/water separation.

The change in water affinity also leads to structural changes of the polymer in aqueous solution. Polymers can undergo a swelling or collapsing process at different pH levels as the ionized film absorbs water and ions from solution.[46,47,49,52] The pH-responsive structural change can be utilized in pore size adjustments for membranes, microfluidic control, as well as drug encapsulation and release. For example, Sun et al.[52] developed pH-responsive drug delivery microdevices by embedding the pH-responsive poly(N-isopropylacrylamide-co- methacrylic acid)

nanoparticles into a composite membrane. The device they developed significantly increased the amount of drug release in acidic environments.

In this thesis, I report a unique approach to prepare a pH-responsive, random copolymer films via surface-initiated ROMP and post-polymerization modification, which provides fast film preparation plus sensitive, reversible, and repeatable pH-responsive performance with great controllability and a narrow range of pH stimulus.

Ionic Liquids (IL) and Polymer/IL Binary Systems

As molten organic salts at ambient temperature, ionic liquids possess a variety of unique properties such as chemical, thermal, and photocatalytic stability, negligible vapor pressure, nonflammability, and relatively high ionic conductivity, which has led to their investigation as solvents, catalysts, lubricants, electrolytes, and polymer plasticizers.[57–60] The beauty of ILs comes from their tunability of properties based on the molecular design of the cation and anion.[57–61] The IL structure and the resulting interactions between anions and large asymmetric cations determine its dielectric constant, conductivity, surface tension, and viscosity.[57–61] By interchanging the ionic components, researchers are able to achieve a large range of properties for the many applications of ILs.[57–61]

The utilization of ILs in polymer science has gained much attention because the utilization of pure ILs is limited by their liquid phase.[59,60] For applications such as membranes, lubricating coatings, and media for ion conduction, the unique properties of ILs are favorable, but the liquid phase lacks the requisite structural integrity.[61] Two main areas of investigation have been poly(ionic liquid)s (PILs)[58–61] and polymer-IL gels.[62–67] PILs are prepared from polymerization of IL-based monomers so that the anion or cation of the IL is chemically bound to the polymer

backbone,[58–61] while polymer-IL gels are binary systems in which ILs physically interact with the polymer matrix. The main advantage of polymer/IL gels is the higher mobility of these untethered ions as compared to that in PILs, where ions are stably bound to the backbone structure. The existence of the relatively free ILs in the polymer matrix also improves the liquid behavior of the film, which is relevant in applications where phase transition is critical, such as smart materials.[62] Polymer-IL compatible binary systems were first studied by Winterton et al.,[62] who combined imidazolium-based ILs with cross-linked polymer membranes for use in catalytic reactors. Polymer-IL binary systems gained attention after this first success, since they not only stabilized the ILs while maintaining their unique properties but also enhanced the thermal stability and ion conductivity of the polymer matrix.[63–65]

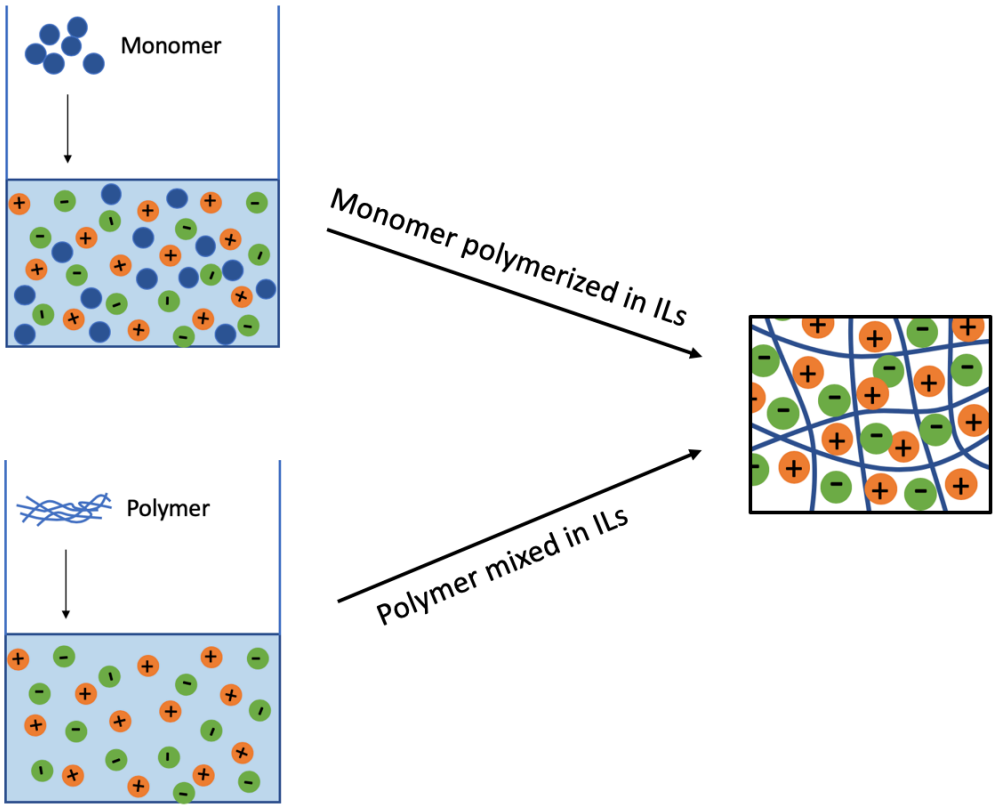

Figure 2.2. Preparation of ion gels by two common methods: polymerizing monomers in ILs and mixing pre-synthesized polymers in ILs.

Currently, polymer-IL systems are mainly prepared by two methods (Figure 2.2).[63–65] One method is direct in situ polymerization of monomers in the IL environment. Noda and Watanabe reported the preparation of polymer gels containing room temperature ILs for applications as polymer electrolytes. They observed that common vinyl monomers could be successfully polymerized in the IL.[68] Good compatibility of the resulting polymer film can be achieved in various polymer concentrations and over a wide range of temperatures. Watanabe and co-workers also showed that in certain cases, the glass transition temperature (T_g) of the polymer-IL gel will decrease with an increase in the mole fraction of IL.[68,69] Yu et al. also prepared a transparent [bmim][BF_4]/polystyrene membrane via microemulsion polymerization.[70] The second method of polymer-IL preparation is the direct mixing of the pre-synthesized polymer with an IL.[71,72] For instance, Tejwant and co-workers dissolved the biopolymer agarose into several imidazolium-based ionic liquids to create ion gel materials.[71] Vidinha et al. prepared transparent ion gels with gelatin dissolved in different ionic liquids and applied them in electrochemical devices.[72] These two methods have been widely used in polymer-IL gel preparations for many applications such as polymer electrolytes, gas separation membranes, and smart materials.

In this thesis, I provide a new method to prepare polymer/IL composite films on surfaces by swelling a surface-initiated polymer film in an appropriate organic solvent to enable ion liquid incorporation, which has great control on the polymer/IL composite composition and enables the incorporation of various ILs.

References

(1) Olivier, A.; Meyer, F.; Raquez, J. M.; Damman, P.; Dubois, P. Surface-Initiated Controlled Polymerization as a Convenient Method for Designing Functional Polymer Brushes: From Self-Assembled Monolayers to Patterned Surfaces. *Prog. Polym. Sci.* **2012**, *37* (1), 157–181.

(2) Edmondson, S.; Osborne, V. L. V.; Huck, W. T. S. W. Polymer Brushes via Surface-Initiated Polymerizations. *Chem. Soc. Rev.* **2004**, *33* (1), 14–22.

(3) Faulkner, C. J.; Fischer, R. E.; Jennings, G. K. Surface-Initiated Polymerization of 5-(Perfluoro-n-Alkyl)Norbornenes from Gold Substrates. *Macromolecules* **2010**, *43* (3), 1203–1209.

(4) Escobar, C. a; Harl, R. R.; Maxwell, K. E.; Mahfuz, N. N.; Rogers, B. R.; Jennings, G. K. Amplification of Surface-Initiated Ring-Opening Metathesis Polymerization of 5-(Perfluoro-n-alkyl)Norbornenes by Macroinitiation. *Langmuir* **2013**, *29*, 12560–12571.

(5) Buchmeiser, M. R.; Sinner, F.; Mupa, M.; Wurst, K. Ring-Opening Metathesis Polymerization for the Preparation of Surface-Grafted Polymer Supports. *Macromolecules* **2000**, *33* (1), 32–39.

(6) Lerum, M. F. Z.; Chen, W. Surface-Initiated Ring-Opening Metathesis Polymerization in the Vapor Phase: An Efficient Method for Grafting Cyclic Olefins with Low Strain Energies. *Langmuir* **2011**, *27* (9), 5403–5409.

(7) Xu, F. J.; Zhao, J. P.; Kang, E. T.; Neoh, K. G.; Li, J. Functionalization of Nylon Membranes via Surface-Initiated Atom-Transfer Radical Polymerization. *Langmuir* **2007**, *23* (16), 8585–8592.

(8) Minet, I.; Delhalle, J.; Hevesi, L.; Mekhalif, Z. Surface-Initiated ATRP of PMMA, PS and

Diblock PS-b-PMMA Copolymers from Stainless Steel Modified by 11-(2-Bromoisobutyrate)-Undecyl-1-Phosphonic Acid. *J. Colloid Interface Sci.* **2009**, *332* (2), 317–326.

(9) Wu, Z.; Chen, H.; Liu, X.; Zhang, Y.; Li, D.; Huang, H. Protein Adsorption on Poly(N-Vinylpyrrolidone)-Modified Silicon Surfaces Prepared by Surface-Initiated Atom Transfer Radical Polymerization. *Langmuir* **2009**, *25* (5), 2900–2906.

(10) Vaterrodt, A.; Thallinger, B.; Daumann, K.; Koch, D.; Guebitz, G. M.; Ulbricht, M. Antifouling and Antibacterial Multifunctional Polyzwitterion/Enzyme Coating on Silicone Catheter Material Prepared by Electrostatic Layer-by-Layer Assembly. *Langmuir* **2016**, *32* (5), 1347–1359.

(11) Min, J.; Lin, Y.; Zheng, J.; Tang, T. A Novel Strategy to Synthesize Well-Defined PS Brushes on Silica Particles by Combination of Lithium-Iodine Exchange (LIE) and Surface-Initiated Living Anionic Polymerization (SI-LAP). *Chem. Commun.* **2015**, *51* (27), 5921–5924.

(12) Bissadi, G.; Weberskirch, R. Formation of Polyoxazoline-Silica Nanoparticles: Via the Surface-Initiated Cationic Polymerization of 2-Methyl-2-Oxazoline. *Polym. Chem.* **2016**, *7* (32), 5157–5168.

(13) Lindqvist, J.; Nyström, D.; Östmark, E.; Antoni, P.; Carlmark, A.; Johansson, M.; Hult, A.; Malmström, E. Intelligent Dual-Responsive Cellulose Surfaces via Surface-Initiated ATRP. *Biomacromolecules* **2008**, *9* (8), 2139–2145.

(14) Grubbs, R. H. Olefin Metathesis. *Tetrahedron* **2004**, *60* (34), 7117–7140.

(15) Bielawski, C. W.; Grubbs, R. H. Living Ring-Opening Metathesis Polymerization. *Prog. Polym. Sci.* **2007**, *32* (1), 1–29.

(16) Vougioukalakis, G. C.; Grubbs, R. H. Ruthenium-Based Heterocyclic Carbene-Coordinated Olefin Metathesis Catalysts. *Chem. Rev.* **2010**, *110* (3), 1746–1787.

(17) Sutthasupa, S.; Shiotsuki, M.; Sanda, F. Recent Advances in Ring-Opening Metathesis Polymerization, and Application to Synthesis of Functional Materials. *Polym. J.* **2010**, *42* (12), 905–915.

(18) Leitgeb, A.; Wappel, J.; Slugovc, C. The ROMP Toolbox Upgraded. *Polymer (Guildf).* **2010**, *51* (14), 2927–2946.

(19) Bielawski, C. W.; Grubbs, R. H. Highly Efficient Ring-Opening Metathesis Polymerization (ROMP) Using New Ruthenium Catalysts Containing N-Heterocyclic Carbene Ligands. *Angew. Chemie - Int. Ed.* **2000**, *39* (16), 2903–2906.

(20) Love, J. A.; Sanford, M. S.; Day, M. W.; Grubbs, R. H. Synthesis, Structure, and Activity of Enhanced Initiators for Olefin Metathesis. *J. Am. Chem. Soc.* **2003**, *125* (33), 10103–10109.

(21) Njoroge, I.; Kempler, P.; Deng, X.; Arnold, S.; Jennings, G. K. Surface-Initiated Ring-Opening Metathesis Polymerization of Dicyclopentadiene from the Vapor Phase. *Langmuir* **2017**.

(22) Tian, F.; Roman, M. J.; Decker, E. A.; Goddard, J. M. Biomimetic Design of Chelating Interfaces. *J. APPL. POLYM. SCI.* **2015**, *41231*, 2–9.

(23) Duran, A.; Soylak, M.; Tuncel, S. A. Poly(Vinyl Pyridine-Poly Ethylene Glycol Methacrylate-Ethylene Glycol Dimethacrylate) Beads for Heavy Metal Removal. *J. Hazard. Mater.* **2008**, *155*, 114–120.

(24) Zhang, Z.; Li, J.; Song, X.; Ma, J.; Chen, L. Hg2+ Ion-Imprinted Polymers Sorbents Based on Dithizone–Hg2+ Chelation for Mercury Speciation Analysis in Environmental

and Biological Samples. *RSC Adv.* **2014**, *4*, 46444–46453.

(25) Rahman, L.; Sarkar, S. M.; Mohd, M.; Abdullah, M. H. Optical Detection and Efficient Removal of Transition Metal Ions from Water Using Poly (Hydroxamic Acid) Ligand. *Sensors Actuators B. Chem.* **2017**, *242*, 595–608.

(26) Rahman, L.; Kumar, T.; Sarkar, S. M.; Yusoff, M. M.; Sani, M.; Arshad, S. E.; Musta, B. Adsorption of Rare Earth Metals from Water Using a Kenaf Cellulose-Based Poly (Hydroxamic Acid) Ligand. *J. Mol. Liq.* **2017**, *243*, 616–623.

(27) Liu, Z.; Lin, T.; Purro, M.; Xiong, M. P. Enzymatically Biodegradable Polyrotaxane-Deferoxamine Conjugates for Iron Chelation. *ACS Appl Mater Interfaces.* **2017**, *8* (39), 25788–25797.

(28) Qian, J.; Sullivan, B. P.; Peterson, S. J.; Berkland, C. Nonabsorbable Iron Binding Polymers Prevent Dietary Iron Absorption for the Treatment of Iron Overload. *ACS Macro Lett.* **2017**, *6*, 350–353.

(29) Liu, Z.; Max, P.; Qiao, J.; Xiong, M. P. Multifunctional Polymeric Micelles for Combining Chelation and Detection of Iron in Living Cells. *Adv Heal. Mater.* **2017**, *6* (17).

(30) White, B. Supermacroporous PolyHIPE and Cryogel Monolithic Materials as Stationary Phases in Separation Science: A Review. *Anal. Methods* **2015**, *7* (17), 6967–6982.

(31) Moyna, Á.; Connolly, D.; Nesterenko, E.; Nesterenko, P. N.; Paull, B. Separation of Selected Transition Metals by Capillary Chelation Ion Chromatography Using Acetyl-Iminodiacetic Acid Modified Capillary Polymer Monoliths. *J. Chromatogr. A* **2012**, *1249*, 155–163.

(32) Ai, T.; Qiu, L.; Xie, J.; Geraghty, R. J.; Chen, L. Design and Synthesis of an Activity-

Based Protein Profiling Probe Derived from Cinnamic Hydroxamic Acid. *Bioorg. Med. Chem.* **2016**, *24* (4), 686–692.

(33) Angibaud, P.; Arts, J.; Emelen, K. Van; Poncelet, V.; Pilatte, I.; Roux, B.; Brandt, S. Van; Verdonck, M.; Winter, H. De; Ten, P.; Marien, A.; Floren, W.; Janssens, B.; Dun, J. Van; Aerts, A. Discovery of Pyrimidyl-5-Hydroxamic Acids as New Potent Histone Deacetylase Inhibitors. *Eur. J. Med. Chem. 40* **2005**, *40*, 597–606.

(34) Zhang, S.; Wu, K.; Feng, J.; Wu, Z.; Deng, Q.; Guo, C.; Xia, B.; Zhang, J.; Huang, H.; Zhu, L.; Zhang, K. Epigenetic Therapy Potential of Suberoylanilide Hydroxamic Acid on Invasive Human Non-Small Cell Lung Cancer Cells. *Oncotarget 7* (42), 68768–68780.

(35) Bakulina, O.; Bannykh, A.; Dar'in, D.; Krasavin, M. Cyclic Hydroxamic Acid Analogues of Bacterial Siderophores as Iron-Complexing Agents Prepared through the Castagnoli–Cushman Reaction of Unprotected Oximes. *Chem. - A Eur. J.* **2017**, *23* (70), 17667–17673.

(36) Hull, R.; Jagadish, C.; Kawazoe, Y.; Osgood, R. M.; Pohl, U. W.; Seong, T.; Uchida, S.; Wang, Z. M. Chemistry of Polymeric Metal Chelates: General Introduction. In *Chemistry of Polymeric Metal Chelates*; 2018; pp 1–9.

(37) Winston, A.; Mazza, E. T.; Virginia, W. Hydroxamic Acid Polymers. *J. Polym. Sci.* **1975**, *13*, 2019–2030.

(38) Winston, A.; Mclaughlin, G. R.; Virginia, W. Hydroxamic Acid Polymers . II. Design of a Polymeric Chelating Agent for Iron *. *J. Polym. Sci.* **1976**, *14*, 2155–2165.

(39) Kumar, S. A.; Pandey, S. P.; Shenoy, N. S.; Kumar, S. D. Matrix Separation and Preconcentration of Rare Earth Elements from Seawater by Poly Hydroxamic Acid Cartridge Followed by Determination Using ICP-MS. *Desalination* **2011**, *281*, 49–54.

(40) Roman, M. J.; Decker, E. A.; Goddard, J. M. Fourier Transform Infrared Studies on the Dissociation Behavior of Metal-Chelating Polyelectrolyte Brushes. *ACS Appl. Mater. Interfaces* **2014**, *6*, 5383–5387.

(41) Agrawal, Y. K.; Kaur, H.; Menon, S. K. Poly (Styrene- p -Hydroxamic Acids): Synthesis , and Ion Exchange Separation of Rare Earths. *React. Funct. Polym.* **1999**, *39*, 155–164.

(42) Chen, J. K.; Chang, C. J. Fabrications and Applications of Stimulus-Responsive Polymer Films and Patterns on Surfaces: A Review. *Materials (Basel)*. **2014**, *7* (2), 805–875.

(43) Chen, Y. C.; Xie, R.; Chu, L. Y. Stimuli-Responsive Gating Membranes Responding to Temperature, PH, Salt Concentration and Anion Species. *J. Memb. Sci.* **2013**, *442*, 206–215.

(44) Tokarev, I.; Minko, S. Stimuli-Responsive Hydrogel Thin Films. *Soft Matter* **2009**, *5* (3), 511–524.

(45) Kocak, G.; Tuncer, C.; Bütün, V. PH-Responsive Polymers. *Polym. Chem.* **2017**, *8* (1), 144–176.

(46) Bai, D.; Habersberger, B.; Jennings, G. K. PH-Responsive Copolymer Films by Surface-Catalyzed Growth. *J. Am. Chem. Soc.* **2005**, *1527*, 16486–16493.

(47) Jin, X.; Hsieh, Y. Lo. PH-Responsive Swelling Behavior of Poly(Vinyl Alcohol)/Poly(Acrylic Acid) Bi-Component Fibrous Hydrogel Membranes. *Polymer (Guildf)*. **2005**, *46* (14), 5149–5160.

(48) Luo, T.; Lin, S.; Xie, R.; Ju, X. J.; Liu, Z.; Wang, W.; Mou, C. L.; Zhao, C.; Chen, Q.; Chu, L. Y. PH-Responsive Poly(Ether Sulfone) Composite Membranes Blended with Amphiphilic Polystyrene-Block-Poly(Acrylic Acid) Copolymers. *J. Memb. Sci.* **2014**, *450*, 162–173.

(49) Schmaljohann, D. Thermo- and PH-Responsive Polymers in Drug Delivery. *Adv. Drug Deliv. Rev.* **2006**, *58* (15), 1655–1670.

(50) Han, Z.; Cheng, C.; Zhang, L.; Luo, C.; Nie, C.; Deng, J.; Xiang, T.; Zhao, C. Toward Robust PH-Responsive and Anti-Fouling Composite Membranes via One-Pot in-Situ Cross-Linked Copolymerization. *Desalination* **2014**, *349*, 80–93.

(51) Lee, C. H.; Kang, S. K.; Lim, J. A.; Lim, H. S.; Cho, J. H. Electrospun Smart Fabrics That Display PH-Responsive Tunable Wettability. *Soft Matter* **2012**, *8* (40), 10238–10240.

(52) Chen, J.; Chu, M.; Koulajian, K.; Wu, X. Y.; Giacca, A.; Sun, Y. A Monolithic Polymeric Microdevice for PH-Responsive Drug Delivery. *Biomed. Microdevices* **2009**, *11* (6), 1251–1257.

(53) Richter, A.; Paschew, G.; Klatt, S.; Lienig, J.; Arndt, K. F.; Adler, H. J. P. Review on Hydrogel-Based PH Sensors and Microsensors. *Sensors* **2008**, *8* (1), 561–581.

(54) Li, J. J.; Zhou, Y. N.; Luo, Z. H. Smart Fiber Membrane for PH-Induced Oil/Water Separation. *ACS Appl. Mater. Interfaces* **2015**, *7* (35), 19643–19650.

(55) Amalvy, J. I.; Wanless, E. J.; Li, Y.; Michailidou, V.; Armes, S. P.; Duccini, Y. Synthesis and Characterization of Novel PH-Responsive Microgels Based on Tertiary Amine Methacrylates. *Langmuir* **2004**, *20* (21), 8992–8999.

(56) Zhu, L.; Powell, S.; Boyes, S. G. Synthesis of Tertiary Amine-Based PH-Responsive Polymers by RAFT Polymerization. *J. Polym. Sci. Part A Polym. Chem.* **2015**, *53* (8), 1010–1022.

(57) Marsh, K. N.; Boxall, J. A.; Lichtenthaler, R. Room Temperature Ionic Liquids and Their Mixtures - A Review. *Fluid Phase Equilib.* **2004**, *219* (1), 93–98.

(58) Qian, W.; Texter, J.; Yan, F. Frontiers in Poly(Ionic Liquid)s: Syntheses and Applications.

Chem. Soc. Rev. **2017**, *46* (4), 1124–1159.

(59) Yuan, J.; Mecerreyes, D.; Antonietti, M. Poly(Ionic Liquid)s: An Update. *Prog. Polym. Sci.* **2013**, *38* (7), 1009–1036.

(60) Mecerreyes, D. Polymeric Ionic Liquids: Broadening the Properties and Applications of Polyelectrolytes. *Prog. Polym. Sci.* **2011**, *36* (12), 1629–1648.

(61) Marr, P. C.; Marr, A. C. Ionic Liquid Gel Materials: Applications in Green and Sustainable Chemistry. *Green Chem.* **2015**, *18*, 105–128.

(62) Snedden, P.; Cooper, A. I.; Scott, K.; Winterton, N. Cross-Linked Polymer - Ionic Liquid Composite Materials. *Macromolecules* **2003**, 4549–4556.

(63) Kokorin, A. *Ionic Liquids: Applications and Perspectives*; InTech: Rijeka, 2011.

(64) Lu, J.; Yan, F.; Texter, J. Advanced Applications of Ionic Liquids in Polymer Science. *Prog. Polym. Sci.* **2009**, *34* (5), 431–448.

(65) Ueki, T.; Watanabe, M. Macromolecules in Ionic Liquids: Progress, Challenges, and Opportunities. *Macromolecules* **2008**, *41* (11), 3739–3749.

(66) Xie, Z. L.; Huang, X.; Taubert, A. Dyeionogels: Proton-Responsive Ionogels Based on a Dye-Ionic Liquid Exhibiting Reversible Color Change. *Adv. Funct. Mater.* **2014**, *24* (19), 2837–2843.

(67) Terasawa, N. High-Performance Transparent Actuator Made from Poly(Dimethylsiloxane)/Ionic Liquid Gel. *Sensors Actuators B Chem.* **2018**, *257*, 815–819.

(68) Noda, A.; Watanabe, M. Highly Conductive Polymer Electrolytes Prepared by in Situ Polymerization of Vinyl Monomers in Room Temperature Molten Salts. *Electrochim. Acta* **2000**, *45* (8), 1265–1270.

(69) Susan, M. A. B. H.; Kaneko, T.; Noda, A.; Watanabe, M. Ion Gels Prepared by in Situ Radical Polymerization of Vinyl Monomers in an Ionic Liquid and Their Characterization as Polymer Electrolytes. *J. Am. Chem. Soc.* **2005**, *127* (13), 4976–4983.

(70) Yu, S.; Yan, F.; Zhang, X.; You, J.; Wu, P.; Lu, J.; Xu, Q.; Xia, X.; Ma, G. Polymerization of Ionic Liquid-Based Microemulsions : A Versatile Method for the Synthesis of Polymer Electrolytes. *ChemPhysChem* **2008**, *41* (10), 3389–3392.

(71) Singh, T.; Trivedi, T. J.; Kumar, A. Dissolution, Regeneration and Ion-Gel Formation of Agarose in Room-Temperature Ionic Liquids. *Green Chem.* **2010**, *12* (6), 1029.

(72) Vidinha, P.; Lourenço, N. M. T.; Pinheiro, C.; Brás, A. R.; Carvalho, T.; Santos-Silva, T.; Mukhopadhyay, A.; Romão, M. J.; Parola, J.; Dionisio, M.; Cabral, J. M. S.; Afonso, C. a M.; Barreiros, S. Ion Jelly: A Tailor-Made Conducting Material for Smart Electrochemical Devices. *Chem. Commun. (Camb).* **2008**, No. 44, 5842–5844.

CHAPTER III

EXPERIMENTAL PROCEDURES AND CHARACTERIZATION METHODS

Experimental Procedures

Materials

Gold shot (99.99%) was obtained from J&J Materials, and chromium-coated tungsten rods were obtained from R.D. Mathis. Silicon wafers (100%) were obtained from WRS materials. Deionized water (10 MΩ) was purified by using a Millipore Elix filtration system.

The following chemicals were obtained and used as received from Sigma-Aldrich: 4-mercapto-1-butanol (95%), Grubbs catalyst 2nd generation [$(H_2IMes)(PCy_3)(Cl)_2Ru{=}CHPh$], 3-bromopyridine, dicyclopentadiene (98%), ethylamine solution (2M) in THF, and 1-butyl-3-methylimidazolium hexafluorophosphate ([bmim][PF_6]).

The following chemicals were obtained and used as received from Fisher Scientific: dichloromethane (DCM), chloroform, toluene, N,N-dimethylformamide, ethanol (200 Proof), methanol, 1-propanol, 1-butanol, 1-octanol, 1-dodecanol, 1-hexadecanol, dimethylethanolamine, aniline, fluorescein, pentane, hexadecane, hydroxylamine hydrochloride, iron (II) sulfate heptahydrate, copper (II) sulfate pentahydrate, cobalt (II) sulfate heptahydrate, nickel (II) sulfate hexahydrate, zinc (II) chloride, iron (III) chloride anhydrous, zirconium (IV) chloride, potassium hydroxide, copper foil (0.025 mm thick), 0.1 M hydrochloric acid, 0.1 M sodium hydroxide, sodium bicarbonate, sodium carbonate, potassium hydrogen phthalate, sodium phosphate monobasic, hydrochloric acid, lithium perchlorate ($LiClO_4$), potassium hexafluorophosphate (KPF_6), and premium plain microscope slides.

The following chemicals were obtained and used as received from IoLiTec Ionic Liquids Technologies, Inc: 1-hexyl-3-methylimidazolium hexafluorophosphate ([hmim][PF_6]), 1-butyl-3-methylimidazolium tetrafluoroborate ([bmim][BF_4]), 1-butyl-3-methylimidazolium bis(trifluoromethylsulfonyl)imide ([bmim][NTf_2]), and 1-butyl-3 methylimidazolium trifluoromethanesulfonate ([bmim][OTf]).

Quartz crystal microbalance with dissipation (QCM-D) sensor crystals (quartz, 4.95 MHz, 14 mm diameter, polished, AT-cut with gold electrodes) were obtained from Biolin Scientific. Ag/AgCl reference electrodes were obtained from CH Instruments, Inc.

Preparation of Gold Substrates

Silicon wafers were rinsed with deionized water and ethanol and then dried in a nitrogen stream. Chromium (100 Å) and gold (1250 Å) were evaporated onto the cleaned silicon wafers at a rate $\leqslant$ 2 Å/s in a diffusion pumped chamber at a base pressure of 4×10^{-6} torr. The wafers then were typically cut into 1.2 cm x 4 cm samples after evaporation.

Synthesis of [(H2IMes)(3-Brpy)2(Cl)2Ru=CHPh] (Grubbs Catalyst 3rd Generation)

[(H_2IMes)(3-Brpy)$_2$(Cl)$_2$Ru=CHPh] (Grubbs catalyst 3rd generation) was synthesized as described by Love et al.[1] Grubbs second generation catalyst (0.5 g, 0.59 mmol) and 3-bromopyridine (0.94g, 5.9 mmol) were added to a 20 mL vial. The reaction was stirred for 5 min, with a color change from scarlet red to bright green. Pentane (20 mL) was added into the vial to remove the extra 3-bromopyridine, with the precipitation of a green solid. The vial was capped under air and placed in the freezer overnight. The green precipitate was vacuum filtered, washed with pentane (4 × 10 mL), and dried under vacuum to yield Grubbs 3rd generation catalyst as a green powder.

Preparation of Grubbs Catalyst-Modified Surface

The gold-coated wafers were placed into 1 mM ethanolic solution of 4-mercapto-1-butanol for at least 1 h to yield a hydroxyl-terminated self-assembled monolayer (SAM) on the gold surface. The films were subsequently rinsed with ethanol, water, and ethanol and dried in a stream of nitrogen, followed by exposure to a 5 mM solution of NBDAC in DCM for at least 30 min to yield the acylation product of a surface-tethered norbornenyl group.[2] The norbornenyl-modified substrates were rinsed with DCM, ethanol, water, and ethanol and dried in a stream of nitrogen. Then the substrates were exposed to a 5 mM solution of Grubbs 3rd generation catalyst ([$(H_2IMes)(3\text{-}Brpy)_2(Cl)_2Ru{=}CHPh$]) in DCM for 12 min.

Characterization Methods

Polarization Modulation-Infrared Reflection-Absorption Spectroscopy (PM-IRRAS)

Infrared (IR) spectroscopy is a technique that measures the vibrational behavior of different molecular groups at different wavelengths.[3–5] Reflectance adsorption infrared spectroscopy (RAIRS) is one of the reflection IR techniques that involves a single external reflection of IR radiation at a reflective surface that is coated by an organic layer/film. The reflected radiation is measured, and the vibrational spectrum depends on the optical constants of the coated layer/film and the substrate and the angle of incidence and the polarization of the incident IR radiation. However, regular RAIRS has several drawbacks, such as signal interference caused by water vapor and carbon dioxide in the surrounding environment, aberrant spectra due to low signal-to-noise ratio, and long acquisition times. The use of PM-IRRAS can overcome the disadvantages of

regular RAIRS. In PM-IRRAS, the differential absorption spectrum of a sample can be obtained as $\Delta R/R$[4,6,7]

$$\frac{\Delta R}{R} = \frac{I_p - I_s}{I_p + I_s} \tag{3.1}$$

where I_p is the intensity of the parallel polarized radiation component with respect to the plane of incidence (*p*-polarized), I_s is the intensity of the perpendicularly polarized radiation component (*s*-polarized). In PM-IRRAS, only *p*-polarized light interacts with the surface of sample so that the differential reflectance spectrum provides a direct measurement of the vibrational spectrum of the molecular structures in the film without a background reference.[4,7] At the same time, the effect of the water and carbon dioxide vapor to the spectrum is eliminated by using PM-IRRAS. In addition, PM-IRRAS provides a higher surface absorption sensitivity than does RAIRS since the spectrometer and background fluctuations are taken into account during each mirror scan.[4,6,7]

In this thesis, PM-IRRAS is used to investigate the composition and crystallinity of the many obtained polymer films (Chapter IV, V, VI) and to study the incorporation of ionic liquids (ILs) in polydicyclopentadiene (pDCPD) to prepare ionogel films. Polarization modulation-infrared reflectance-absorption spectroscopy (PM-IRRAS) was performed using a Bruker Tensor 27 Fourier transform infrared spectrometer equipped with a PEM-90 photoelastic modulator (Hinds Instruments) and a liquid-nitrogen cooled mercury-cadmium-telluride (MCT) detector with a non-dichroic BaF_2 window. The source beam employed a half-wavelength ($\lambda/2$) retardation modulated at a frequency of 50 kHz and was set at an 85° angle of incidence to the sample surface. Spectra were collected over 5 min (360 scans) at a resolution of 4 cm^{-1}.

Contact Angles

Contact angle measurement is a method that describes the hydrophobic and hydrophilic behavior of material surfaces. When a liquid drop is resting on a flat, horizontal solid surface, the drop forms a contact angle, θ, which is defined as the angle formed by the intersection of the liquid-solid interface and the liquid-vapor interface as Figure 3.1 shows.[8] A small contact angle is achieved when the liquid drop spreads on the surface, while a large contact angle is achieved if the liquid beads up on the surface. The shape of the liquid drop on the surface is determined by the surface tensions of the solid-liquid system. Thomas Young first described the contact angle θ in terms of three interfacial tensions as shown in Equation 3.2:

$$\cos\theta_Y = \frac{\gamma_{SV} - \gamma_{SL}}{\gamma_{LV}} \tag{3.2}$$

where γ_{SV}, γ_{SL}, γ_{LV} represents the solid-vapor, solid-liquid, liquid-vapor interfacial tensions, and θ_Y is referred as Young's contact angle.[8,9]

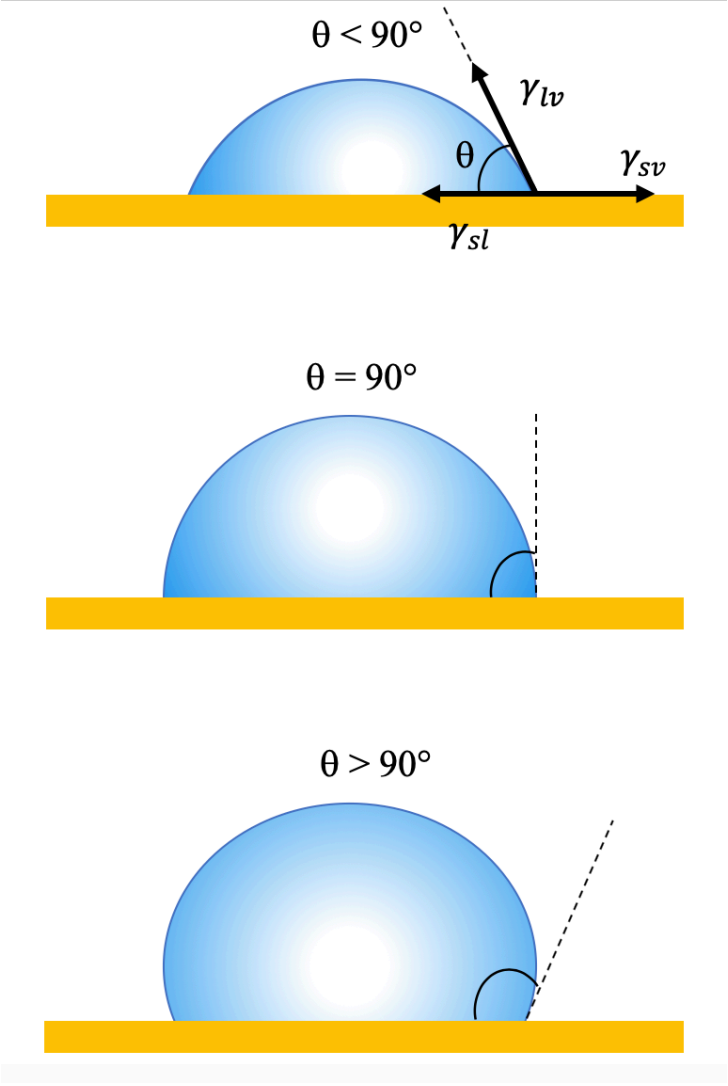

Figure 3.1 Illustration of contact angles formed by liquid drops on a smooth solid surface.

However, in practice, the static contact angle is not adequate to represent the wetting behavior of the surface since there exist many metastable states of a liquid droplet on a solid. Thus, dynamic contact angles are often measured for characterization. The contact angle formed by expanding the three-phase contact line is referred as the advancing contact angle θ_a, while that formed by contracting the line is referred as the receding contact angle, θ_r, and the difference between the advancing and receding contact angles is called hysteresis (H), which is mainly

affected by surface roughness and chemical heterogeneity. If the films surface is rough or compositionally heterogeneous, the hysteresis will increase:[8,9]

$$H = \theta_a - \theta_r \tag{3.3}$$

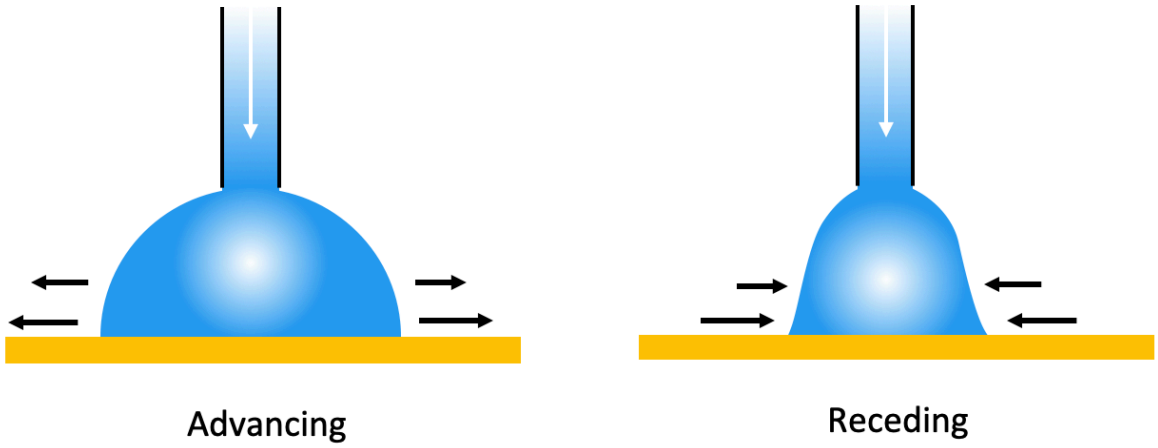

Figure 3.2 Illustration of advancing and receding contact angle measurements

In Chapter IV, water contact angles were obtained to quanlitatively assess the wetting properties of the polymer film surfaces. A Rame-Hart manual contact angle goniometer with a microliter syringe was used to measure the advancing and receding contact angles of static drops of water on the film surfaces. The contact angle measurements were taken on both sides of approximately 5 μL drops. The needle tip of the syringe remained inside the probe droplet during measurements. The reported values and ranges represent the averages and standard deviations from three independently prepared samples with three measurements per sample.

Electrochemical Impedance Spectroscopy (EIS)

EIS is a non-destructive method that can be used to determine the ionic barrier properties of thin films. In EIS, a small frequency-alternating sinusoidal potential perturbation is applied, and

the current corresponding to the perturbation is collected at each frequency.[10] The overall impedance (Z) at each frequency can be determined by using the following equation:

$$Z = \frac{E(t)}{I(t)} = \frac{E_0 \cos(\omega t)}{I_0 \cos(\omega t - \phi)} = Z_0 \frac{\cos(\omega t)}{\cos(\omega t - \phi)} \tag{3.4}$$

where $E(t)$ is the applied perturbation potential at time t, $I(t)$ is the corresponding current at that time, E_0 is the amplitude of the sinusoidal potential, I_0 is the amplitude of the corresponding current, ω is the radial frequency (equals to $2\pi f$, where f is the frequency in Hz), ϕ is the phase angle, and Z_0 is the magnitude of the impedance.

The magnitude of Z can be expressed as:

$$|Z|^2 = (Z_{RE})^2 + (Z_{IM})^2 \tag{3.5}$$

where Z_{RE} is the real part of the impedance and is expressed as the resistance:

$$Z_{RE} = R \tag{3.6}$$

and Z_{IM} is the imaginary part of the impedance and can be expressed as:

$$Z_{IM} = \frac{1}{j\omega C} \tag{3.7}$$

where C is capacitance, and j is the imaginary unit.

EIS spectra can be presented in a Bode magnitude plot in which impedance (in logarithm scale) and phase angle are plotted as a function of log frequency. The impedance behavior of the film can be fully demonstrated by the Bode plot. If the Bode plot shows a straight line with a slope of -1, and the phase angle is at -90°, then the layer/thin film demonstrates perfect capacitance behavior to separate the ions in solution from the underlying electrode surface. If an impedance plateau is achieved in the Bode plot and the phase angle is 0°, the layer/thin film behaves as a pure resistor to the transfer of ions. The results of the EIS measurements can be fit with an equivalent circuit of resistors and capacitors to obtain physical and quantitative meaning of the data. The two main equivalent circuits used in this thesis are shown in Figure 3.3 and Figure 3.4. In Figure 3.3, the impedance response at low frequency comes from the interface, the impedance response at high frequency comes from the electrolyte solution, while that at middle frequency is from the coated polymer film and corresponds to the combination of resistance and capacitance effects of the film. The Bode plot can also demonstrate the time required for ionic transport through the polymer film.

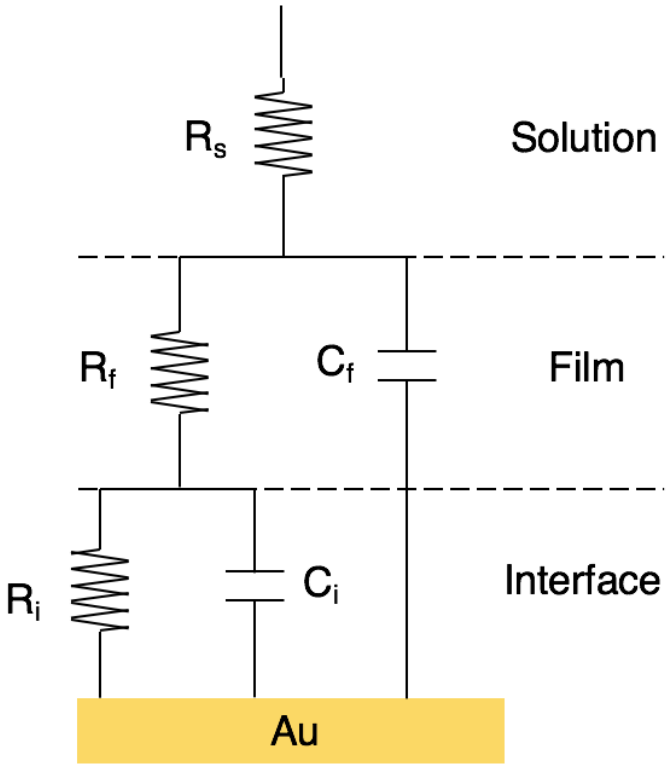

Figure 3.3 Equivalent circuit model used to model a surface-tethered polymer thin film on an electrode surface. The two-time-constant circuit model consists of a solution resistance (R_s), film capacitance (C_f), film resistance (R_f), interfacial capacitance (C_i), and interfacial resistance (R_i)

If the polymer films possess high impedance against ion transfer such that ions cannot penetrate the film to reach the interface even at the lowest frequency, the effects of the interface do not appear in the spectrum and therefore, these items can be removed from the equivalent circuit. The simplified equivalent circuit is shown as Figure 3.4.

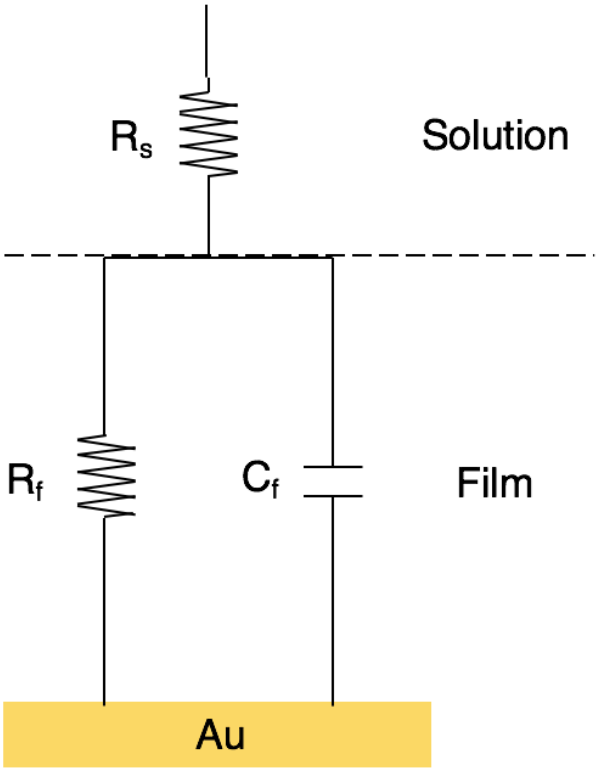

Figure 3.4: Equivalent circuit model used to model a surface-tethered polymer thin film when the film resistance is significantly higher than the interfacial impedance so that the latter is not present in the spectrum. The model consists of a solution resistance (R_s), a film capacitance (C_f), and a film resistance (R_f)

In Chapter IV, V, VI, and VII, EIS was performed with a Gamry Instruments Reference 600 potentiostat interfaced to a computer. Measurements were conducted in an electrochemical cell to limit the testing area to 1 cm^2 of each sample. The experiment set up is demonstrated in Figure 3.5 In Chapter IV and V, the electrochemical cell consisted of an aqueous solution of 0.1 M KCl with a Ag/AgCl/KCl (3 M) reference electrode, a gold-coated silicon substrate that was coated with the polymer film as the working electrode, and a gold-coated silicon substrate as the counter electrode. In Chapter VI, pH buffer solutions (pH 4 – 11) (buffer preparation included in

Chapter VI) were used as the electrolytes. A 5 mV AC voltage was applied to perturb the cell. The frequency of the AC voltage was varied from 100 kHz to 0.1 Hz with 10 points per decade.

In Chapter VII, the electrochemical cell consisted of an ionic liquid, [bmim][PF6], as electrolyte in a two-electrode cell. The gold substrate with the pDCPD-IL gel film served as the working electrode, while a clean gold substrate on top served as the counter electrode. A 5 mV AC voltage was applied to perturb the cell. The frequency of the AC voltage was varied from 100 kHz to 1 Hz with 10 points per decade. Equivalent circuits shown in Figure 3.3 and Figure 3.4 were employed to fit the spectra to determine the electrochemical parameters of the films.

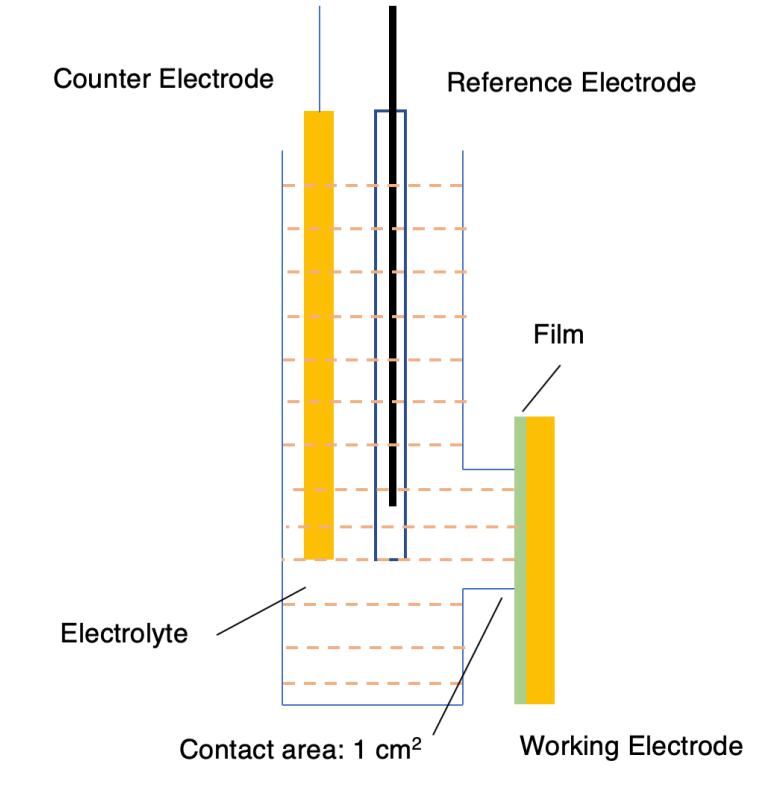

Figure 3.5: Demonstration of an electrochemical cell and the three-electrode system used in EIS measurements

Profilometry

Surface roughness and film thickness can be determined via various methods, such as stylus profiler (SP), AFM, and non-contact optical profiler. Compared to a non-contact optical profiler such as an ellipsometer, the contact methods like SP and AFM also provide the scanning contour profile, which can demonstrate the surface roughness and basic topography. SP and AFM are both contact techniques, while SP collects the data on the larger order of mm and requires much less experimental time consumption as compared to AFM.[11] A stylus profiler consists of a tip on the end of a cartilever, and surface measurements are performed as the stylus moves across the surface at a constant velocity, following its contour, to obtain the surface height variation. The vertical displacement of the stylus is translated into a transducer voltage so that the surface contour data can be collected after appropriate calibration.[12]

In this thesis, a SP is used to measure polymer thin film thickness (Chapter IV and Chapter VII) and roughness (Chapter VII and Appendix). The surface contour data of the surface-tethered films were collected, with film thickness reported as the mean height variation for the film from the baseline and film roughness as the root mean square roughness (R_q) of the contour. Profilometric thickness and roughness were determined using a Veeco Dektak 150 profiler with a stylus of 12.5 μm radius and 3 mg of force with a 0.28 μm/sample data collection rate. Thickness was estimated by scratching the film surface down to the metal, scanning 1 mm across the scratch, and plane-fitting the scan results using the instrument software. Reported values represent the averages and standard deviations of at least three independent samples.

Quartz Crystal Microbalance with Dissipation (QCM-D)

QCM-D is a technique that measures the frequency shifts and energy dissipation of a quartz crystal sensor in a precise way and allows the calculation of added mass, water interaction, and viscoelastic properties of materials deposited onto the sensor by applying models related to the change of frequency and dissipation.[13] In a QCM-D measurement, an alternating current (AC) voltage is applied to excite the crystal to oscillation at its fundamental resonant frequency. By periodically connecting and disconnecting the crystal from the AC voltage, frequency (f) and dissipation (D) can be determined by fitting the decay of the oscillation.[14,15]

In this thesis, QCM-D was used to determine the water interaction and viscoelastic properties of the surface-initiated films. Polymer films were grown on the gold electrodes of the quartz crystal sensor via SiROMP. In Chapter V and VI, QCM-D was performed with a Biolin Scientific Q-Sense E4 interfaced to a computer and an ISMATEC IPC pump. The QCM-D measurements were performed at 25 °C. In Chpater V, all f and D measurements were collected at a rate of 200 times per second in ultrapure water or 5 mM $FeSO_4$ solution at a flow rate of 100 μL/min. In Chapter VI, different pH buffer solutions (pH 4-11) at a flow rate of 100 μL/min were used. A clean, pretreated quartz crystal was first analyzed by QCM-D with ultrapure (18.2 MΩ·cm) water at a flow rate of 100 μL/min, and the collected measurements were used as the reference baseline for the data analysis.

In Chapter VII, QCM-D was performed at 25 °C in air with a Biolin Scientific Q-Sense E4 interfaced to a computer . All f and D measurements are collected at a rate of 200 times per second. A clean, pretreated quartz crystal was first analyzed by QCM-D in air, and the collected measurements were used as the reference baseline for the data analysis.

References

(1) Love, J. A.; Morgan, J. P.; Trnka, T. M.; Grubbs, R. H. A Practical and Highly Active Ruthenium-Based Catalyst That Effects the Cross Metathesis of Acrylonitrile. *Angew. Chemie - Int. Ed.* **2002**, *41* (21), 4035–4037.

(2) Njoroge, I.; Kempler, P.; Deng, X.; Arnold, S.; Jennings, G. K. Surface-Initiated Ring-Opening Metathesis Polymerization of Dicyclopentadiene from the Vapor Phase. *Langmuir* **2017**.

(3) Stuart, B. H. *Infrared Spectroscopy: Fundamentals and Applications*; Wiley: Chichester, England, 2004.

(4) Golden, W. G.; Saperstein, D. D.; Severson, M. W.; Overend, J. Infrared Reflection-Absorption Spectroscopy of Surface Species: A Comparison of Fourier Transform and Dispersion Methods. *J. Phys. Chem.* **1984**, *88* (3), 574–580.

(5) Barner, B. J.; Green, M. J.; Saez, E. I.; Corn, R. M. Polarization Modulation Fourier Transform Infrared Reflectance Measurements of Thin Films and Monolayers at Metal Surfaces Utilizing Real-Time Sampling Electronics. *Anal. Chem.* **1991**, *63*, 55–69.

(6) Buffeteau, T.; Desbat, B.; Turlet, J. M. Polarization Modulation FT-IR Spectroscopy of Surfaces and Ultra-Thin Films: Experimental Procedure and Quantitative. *Appl. Spectrosc.* **1991**, *45* (3), 380–389.

(7) Green, M. J.; Barner, B. J.; Corn, R. M. Real-Time Sampling Electronics for Double Modulation Experiments with Fourier Transform Infrared Spectrometers. *Rev. Sci. Instrum* **1991**, *62* (6), 1426–1430.

(8) Yuan, Y.; Lee, T. R. Contact Angle and Wetting Properties. In *Surface Science Techniques*; Bracco, G., Holst, B., Eds.; Springer-Verlag Berlin Heidelberg, 2013.

(9) Zismann, W. A. Relation of the Equilibrium Contact Angle to Liquid and Solid Constitution. In *Adv. Chem. Ser.*; American Chemical Society: Washington, DC, 1964; pp 1–51.

(10) Bard, A. J.; Faulkner, L. R. *Electrochemical Methods: Fundamentals and Applications*, 2nd Editio.; Wiley, 2000.

(11) Poon, C. Y.; Bhushan, B. Comparison of Surface Roughness Measurements by Stylus Profiler, AFM and Non-Contact Optical Profiler. *Wear* **1995**, *190* (1), 76–88.

(12) Wood, J. W.; Redin, R. D. A Simple Profilometer for Film Thickness Measurement. *Rev. Sci. Instrum.* **1993**, *64* (8), 2405–2406.

(13) Hook, F.; Rodahl, M.; Brzezinski, P.; Kasemo, B. Energy Dissipation Kinetics for Protein and Antibody-Antigen Adsorption under Shear Oscillation on a Quartz Crystal Microbalance. *Langmuir* **1998**, *14*, 729–734.

(14) Rodahl, M.; Kasemo, B. A Simple Setup to Simultaneously Measure the Resonant Frequency and the Absolute Dissipation Factor of a Quartz Crystal Microbalance. *Rev. Sci. Instrum.* **1996**, *67* (9), 3238–3241.

(15) Reviakine, I.; Johannsmann, D.; Richter, R. P. Hearing What You Cannot See and Visualizing What You Hear: Interpreting Quartz Crystal Microbalance Data from Solvated Interfaces. *Anal. Chem.* **2011**, *83* (23), 8838–8848.

CHAPTER IV

SURFACE-INITIATED POLYMERIZATION OF TRANS-5-NORBORNENE-2,3-DICARBONYL CHLORIDE: A VERSATILE PLATFORM FOR TAILORED POLYMER FILM COMPOSITIONS

Introduction

Functional polymer films attract substantial attention from both industry and academia due to their ability to tailor the properties of surfaces[1,2] such as corrosion resistance,[3] wear resistance,[4] lubrication,[5,6] biocompatibility.[7,8] Many film preparation techniques have been developed onver last decades, such as spin coating,[9] dip coating,[10] layer-by-layer assembly,[11] and Langmuir–Blodgett deposition.[12] Surface-initiated polymerization (SIP) is a bottom-up technique for the preparation of robust polymer thin films that offers many attractive advantages, such as high stability, dense grafting, thickness controllability, geometric adaptiveness, and simple separations.[13–15] Among the several polymerization methods of SIP, surface-initiated ring opening metathesis polymerization (SiROMP) is unique because of the rapid initiation and polymerization under mild conditions and good control over film thickness from tens to thousands of nanometers.[15–18] However, preparation of functional polymer films using SiROMP is still limited due to the low availability of functional polymerizable monomers. Finding a method that can impart various functionalities to polymer films prepared by SiROMP is necessary to exploit its many advantages toward applications.

In this Chapter, I report a method to prepare thin polymer films with various functionalities by Si-ROMP followed by simple modifications that are driven to completion. Acyl chloride groups

are highly reactive toward water, alcohols, and amines at room temperature.[19] Therefore, if polymers with acyl chloride groups can be prepared, the simple modification of polymer films to introduce versatile compositions can be achieved. A few polymer scientists have synthesized acyl chloride-containing polymers in solution and esterified the reactive pendant groups to prepare functionalized polymers.[20–22] In fact, Hanson et al. reported polymerizations of NBDAC from both solution and surfaces,[23,24] but they only utilized the obtained pNBDAC as scavengers, not in a platform to introduce other functionalities. Also, they achieved the SIP on nanoparticles, which do not require a significant film growth to alter surface properties. Employing a similar approach on flat surfaces, as we have performed herein, does not produce sufficient polymer growth for detection with IR spectroscopy (vide infra). Beyond the limits of these investigations, polymers with acyl chloride groups have not gained much attention and are not well established in studies of polymer thin films.

In this chapter, I report the preparation of poly(trans-5-norbornene-2,3-dicarbonyl chloride) (pNBDAC)) by surface-initiated ring-opening metathesis polymerization (SiROMP) of the monomer from the vapor phase. SIPs in vapor phase not only allow for a reduction of solvent consumption and high purity of monomer, but also reduce occurrence of secondary metathesis reactions with a reduced polymer chain mobility at the vapor/solid interface. We prepare the pNBDAC films and use them as reactive intermediates to introduce various functionalities by simple acylation reactions to produce ester and amide linkages in high yield. We show that this modification method can routinely prepare many types of polymer films, all from a common base film of pNBDAC, with distinct functionalities to generate a wide range of film and surface properties.

Polymerization and Post-polymerization Modification

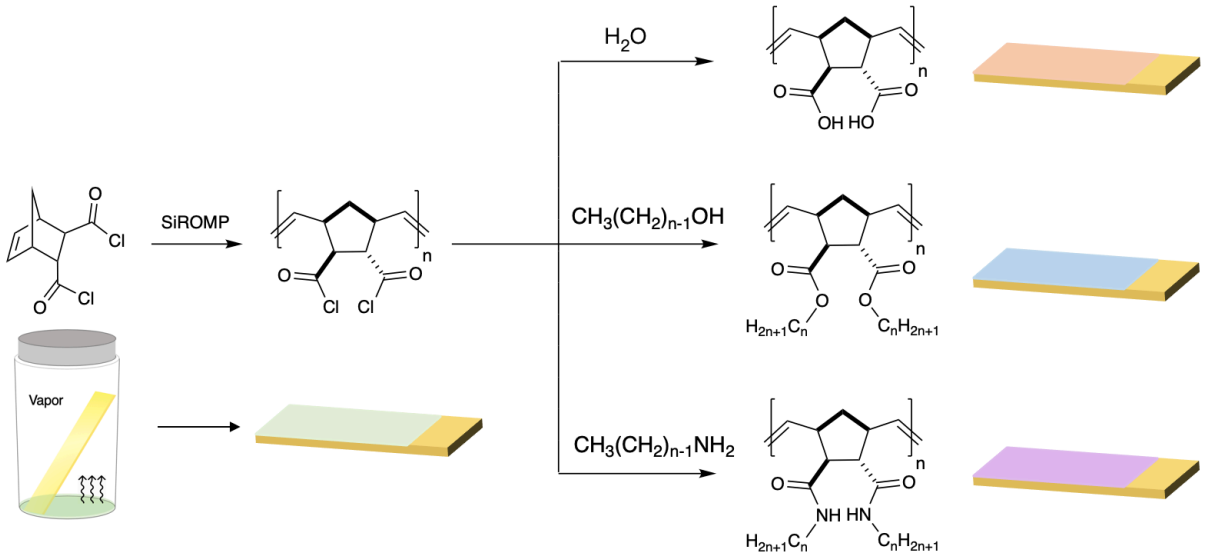

Figure 4.1. Polymerization of NBDAC and its modification with water, n-alcohols, or n-amines.

Polymerization of pNBDAC was accomplished in the vapor phase. The ROMP-active substrates removed from the Grubbs 3rd generation catalyst solution were quickly rinsed with DCM, dried in a stream of nitrogen, and immediately placed into a pre-heated reaction vial (65 °C) containing pure liquid NBDAC monomer (Figure 4.1a). NBDAC monomers from the vapor phase were then polymerized from the catalyst-modified surface to form a smooth thin film. After the surface-initiated polymerization in the vial, the substrates were quickly rinsed with DCM to remove any additional monomer on the film surface and then the pNBDAC-coated gold substrates were immediately rinsed with DCM, dried, and then exposed to water, ethanol, or a 0.2 M

ethylamine solution in THF for 30 min. The substrates were then dried in a stream of nitrogen. Figure 4.1 shows the polymerization and basic modification of pNBDAC.

Results and Discussion

Preparation of pNBDAC Films on Gold Surfaces

Exposure of gold substrates modified with Grubbs third-generation catalyst [$(H_2IMes)(3\text{-}Brpy)_2(Cl)_2Ru{=}CHPh$] to solutions of NBDAC in DCM or to neat NBDAC liquid monomer result in little growth of polymer from the surface. However, exposure of the same substrates to the vapor of NBDAC rapidly yielded robust polymer films on the surface. PM-IRRAS was used to confirm the successful preparation of the pNBDAC films on the surface and identify the functional groups in the film after modification. Figure 4.2 shows the PM-IRRAS of the pNBDAC film prepared by polymerization from the vapor phase. Considering that the chloride groups in the film may react with the water molecules in the ambient air, the obtained pNBDAC films were stored in DCM solution before the IR measurements. The spectrum of the pNBDAC films shows absorption bands due to C=O stretching of the acyl chloride (1794 cm^{-1}), C_{sp3}-H in-plane bending (1430-1500 cm^{-1}), C_{sp3}-H out-of-plane bending (1300-1400 cm^{-1}), and C_{sp2}-H out of plane bending (900-1100 cm^{-1}). The spectrum indicates the successful SiROMP of NBDAC from the vapor phase.

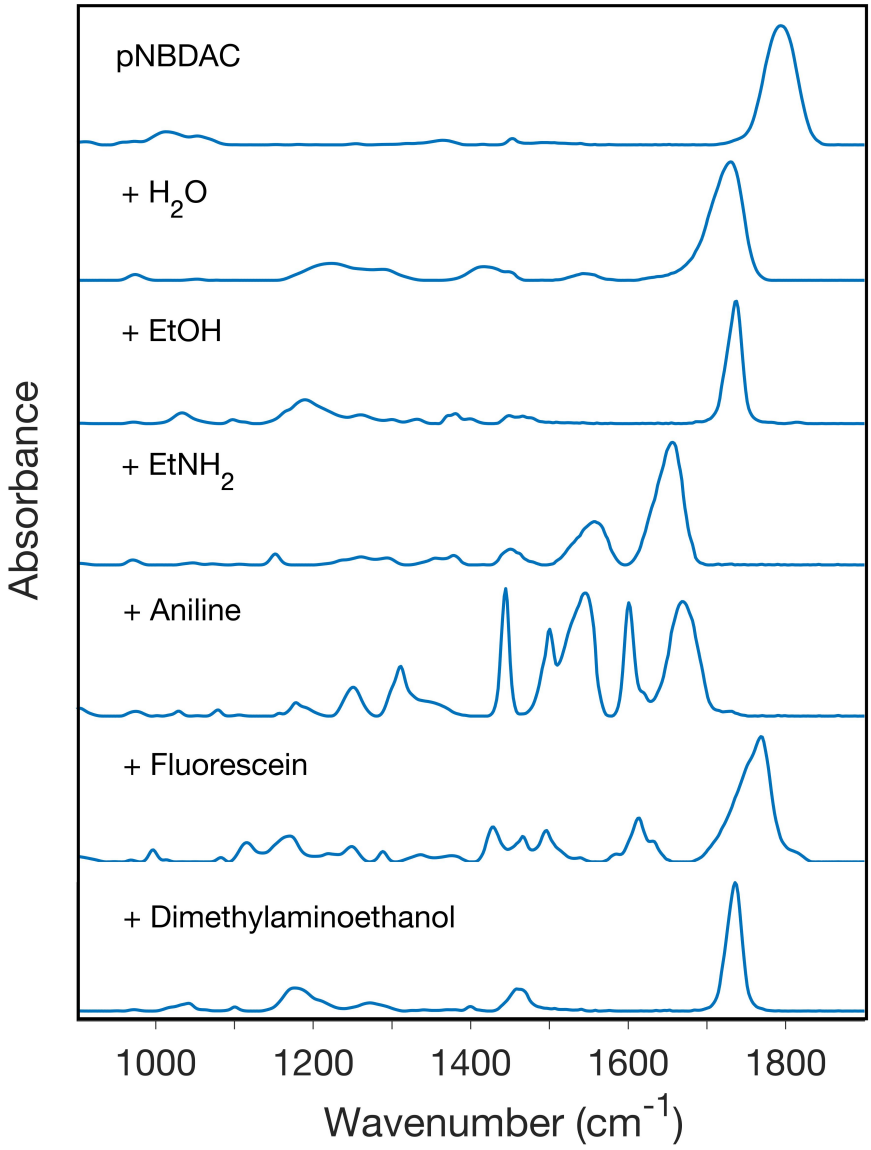

Figure 4.2. FTIR spectra of pNBDAC and polymer films obtained by modifying pNBDAC with water, ethanol, and ethyl amine to create pendant –COOH, -COOEt, and -CONHEt functionality within the film. FTIR spectra of pNBDAC films after exposure to aniline, fluorescein, and dimethylethanolamine demonstrate that larger and more diverse molecular groups can be introduced as pendant side chains by this approach.

Kinetics of Film Growth

To investigate the SiROMP of NBDAC in the vapor phase and examine the control over film growth, the kinetics of pNBDAC film growth was examined. Polymer films were grown for different polymerization times ranging from 1 to 10 min. Since pNBDAC is not stable long-term in the ambient air, we modified all the samples with water to produce stable, pendant $-CO_2H$ groups before measuring the thicknesses. To model the data, the film thickness as a function of time can be given as

$$d = \left(\frac{KMm_0}{k_t\rho}\right)(1 - e^{-k_t t}) \qquad (4.1)$$

where K is a rate constant that expresses both the initiation and propagation of the polymerization process, M is the concentration of the monomer, m_0 is the mass of the monomer unit, k_t is the termination rate constant, and ρ is the density of the polymer film.[17,18] The approximate monomer concentration in the vapor phase can be calculated as 4.3 mM using the Clausius Clapeyron equation.[17] The density of the polymer film was assumed to be approximately the density of the monomer (1.35 g/cm^3). The rate constants were calculated by fitting the experimental data with Eq 4.1. The fitted propagation rate constant K is $3.8 \times 10^{-6} \pm 0.3 \times 10^{-6}$ m/s and the fitted termination rate constant k_t is $6.7 \times 10^{-3} \pm 1.2 \times 10^{-3}$ s^{-1}. The kinetics investigation shows that the rapid polymerization of NBDAC occurs from the vapor phase and that film thickness can be controlled up to 370 nm based on polymerization time under these conditions. As a comparison, our group has studied the SiROMP of polydicyclopentadiene from the vapor phase in previous work,[17] which has an even faster propagation with K of $1.5 \times 10^{-4} \pm 0.5 \times 10^{-4}$ m/s and k_t of 0.04 ± 0.01 s^{-1}.

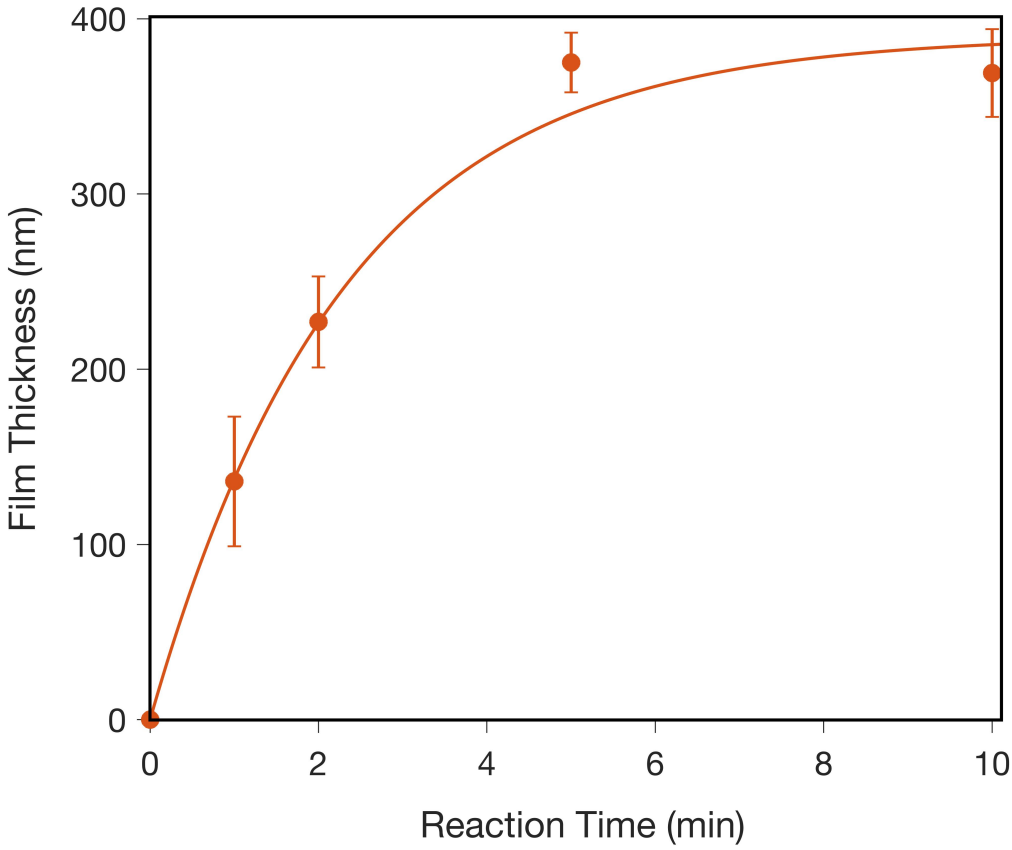

Figure 4.3. Kinetics plot of pNBDAC film growth via Si-ROMP of NBDAC from the vapor phase at 65 °C. Thicknesses were determined by profilometry. The approximate vapor-phase concentration of NBDAC was 4.3 mM. The data were fit with Equation 4.1 to determine propagation and termination rate constants.

Post-polymerization Modification of pNBDAC Films

Although pNBDAC is too unstable to be utilized as a polymer film long term, it is a very effective intermediate to produce stable polymer films with other functional groups via post-polymerization modification due to the fast and versatile reactions between pendant acyl chlorides and other reagents. Therefore, we investigated the feasibility of modifying pNBDAC films to

obtain polymer films with pendant carboxylic acids (-COOH), ethyl esters (-COOEt,) and ethyl amides (-CONHEt) by reacting the polymer film with water, ethanol, and ethylamine, respectively. The IR spectra of polymer films containing pendant -CO_2H, -CO_2Et, and –CONHEt side groups are shown in Figure 4.2, together with the IR spectrum of pNBDAC. The spectrum of the CO_2H-modified film shows absorption bands due to the stretching of C=O (1726 cm^{-1}) and C-O (1200-1350 cm^{-1}) in carboxylic acids. The spectrum of the EtO_2C-modified film shows absorption bands due to the stretching of C=O (1738 cm^{-1}) and C-O (1130-1300 cm^{-1}) of esters. The spectrum of the –CONHEt modified film shows absorption bands due to C=O stretching (1657 cm^{-1}) and N-H bending (1557 cm^{-1}) in amides. Importantly, these spectra also show the complete diminution of the C=O stretching at 1794 cm^{-1} due to the acyl chloride functionality to signal complete modification of the original pNBDAC film with these three different pendant functional groups. These results confirm the feasibility of utilizing pNBDAC films as the intermediate to prepare other functional groups. By extending the modification agent to any type of alcohol, phenol, amine, or any other molecule with functional groups that react with acyl chlorides, we can prepare an unlimited array of surface-attached polymer films using this pNBDAC modification method.

We also examined the modification of pNBDAC with larger molecular reagents and those beyond simple alcohols and amines to confirm the versatility of the modification method. The grown pNBDAC films were exposed overnight to (1) aniline, (2) 0.01 M fluorescein in acetone, and (3) dimethylethanolamine, and PM-IRRAS measurements were taken after the modification process. The modification of the pNBDAC film with aniline demonstrates that the aromatic groups can also be introduced quantitatively into the film. The IR spectrum of the formed anilide shows absorption bands due to C=O stretching (1668 cm^{-1}), aromatic C=C ring stretching (1500-1610 cm^{-1}), and C-N stretching (1250 cm^{-1} and 1310 cm^{-1}). The IR spectra of fluorescein modified film

shows a shift of C=O stretching absorption band from 1794 cm^{-1} to 1769 cm^{-1}, which signals the successful incorporation of large functional group fluorescein into the film. The C=O stretching absorption band is much broader due to the introduced carboxylic acid and phenyl ester groups in fluorescein. A small absorption band is still observed around 1794 cm^{-1}, which means that a small portion of the acyl chloride groups in the film are not modified. The two acyl chloride groups at the repeating unit are proximal, which may result in a steric limitation for the complete modification with larger functionality. Quantitative modification of pNBDAC with dimethylethanolamine, as further supported by new absorption bands due to C=O stretching of the ester (1736 cm^{-1}) and C-N stretching (1270 cm^{-1}), indicates that the method is tolerant of more diverse functional groups than those imparted by unsubstituted n-alcohols or n-amines.

Modification of Film Properties

The feasibility of adding various functional groups to the pNBDAC films provides an extremely powerful way to easily develop polymer films for targeted properties. Here, we modified pNBDAC with various reagents and briefly characterized the introduced properties after the modification.

As shown in Figure 4.2, pNBDAC films can react with water and dimethylaminoethanol to obtain carboxylic acid-modified and tertiary amine-modified films. Carboxylic acids and tertiary amines are commonly utilized in pH-responsive materials due to their ionization with changes in solution pH, which result in a significant changes in the hydrophilicity and related properties of the materials. We obtained both carboxylic acid-modified and tertiary amine-modified films and measured their water contact angles at both pH 4 and pH 8 (Table 4.1). Films

were placed in pH 4/8 solutions for 2 min and dried. A 2μL droplet of corresponding pH solution was dropped on the surface and contact angles were measured.

Table 4.1 Sessile drop contact angles of carboxylic acid-modified and tertiary amine-modified films measured at pH 4 and pH 8 environments.

Films	θ at pH 4	θ at pH 8
Carboxylic Acid-Modified	67 ± 2	14 ± 1
Tertiary Amine-Modified	46 ± 2	67 ± 3

Results in Table 4.1 show pH-driven changes in the contact angles of the modified polymer films. Carboxylic acid-modified films demonstrate a remarkable increase in wettability (decrease in θ) at higher pH because the acids are deprotonated to charged carboxylates to enhance their interactions with water, while the tertiary amine-modified films show an opposite pH-responsive behavior in that low pH results in a decrease in contact angle due to the ionization of tertiary amines in the acidic environment. Both carboxylic acid-modified and tertiary amine-modified groups demonstrate pH-responsive surface properties, which shows that simple modification of pNBDAC is a versatile route to responsive film property design.

We also modified pNBDAC with n-alcohols with different alkyl chain lengths to incrementally increase film hydrophobicity and examine its effect on film properties. Water, methanol, ethanol, propanol, 1-butanol, and 1-octanol were used to modify the pNBDAC films via overnight exposure. To achieve longer side chains, 0.1 M solutions of 1-dodecanol and 1-

hexadecanol in DCM were used to modify the pNBDAC films after a one-week exposure. Longer exposure times were needed to approach complete modification for larger molecular groups.

Film Thicknesses. With increasing carbon chain lengths introduced by the reaction of pNBDAC with n-alcohols, the film thicknesses were expected to increase as the film expands to accommodate the larger side chains. Profilometric thickness changes of the films modified with 1-butanol (n = 4), 1-octanol (n = 8), 1-dodecanol (n = 12), and 1-hexadecanol (n = 16) were investigated. Film thicknesses both before and after each ester modification were measured by profilometry, and the ratios of the film thicknesses after modification to those before modification were determined to assess the expansion of the film. As a basis for comparison, the thickness ratios were also calculated based on the change of the molecular weight of the repeating unit. Figure 4.4 shows that the thickness ratios increase with the hydrocarbon chain length, and the trend of thickness increase follows the calculated predictions based on molecular weight. The measured thickness ratios are slightly greater than the predicted ones. Considering that the prediction is based solely on molecular weight and not molecular volume, the difference of the measured and predicted values are noted as minimal. Since four carbons were added to the side chain for each modification, the increase in thickness ratio across each interval should be nearly constant. From 4 to 12, a linear increase in the thickness ratio is observed. However, when n changes from 12 to 16, the increase in thickness ratio corresponds to the prediction but deviates from the trend. The result suggests that the modification of pNBDAC with 1-hexadecanol is not complete, as is supported by the IR spectrum in Figure 4.4, which shows that 22% of the acyl chlorides remain in the film after week-long exposure to 1-hexadecanol. Diffusion of the long-chain alcohol into the film becomes constrained at high conversions, and the diminishing concentration of acyl chlorides greatly slows the rate of modification.

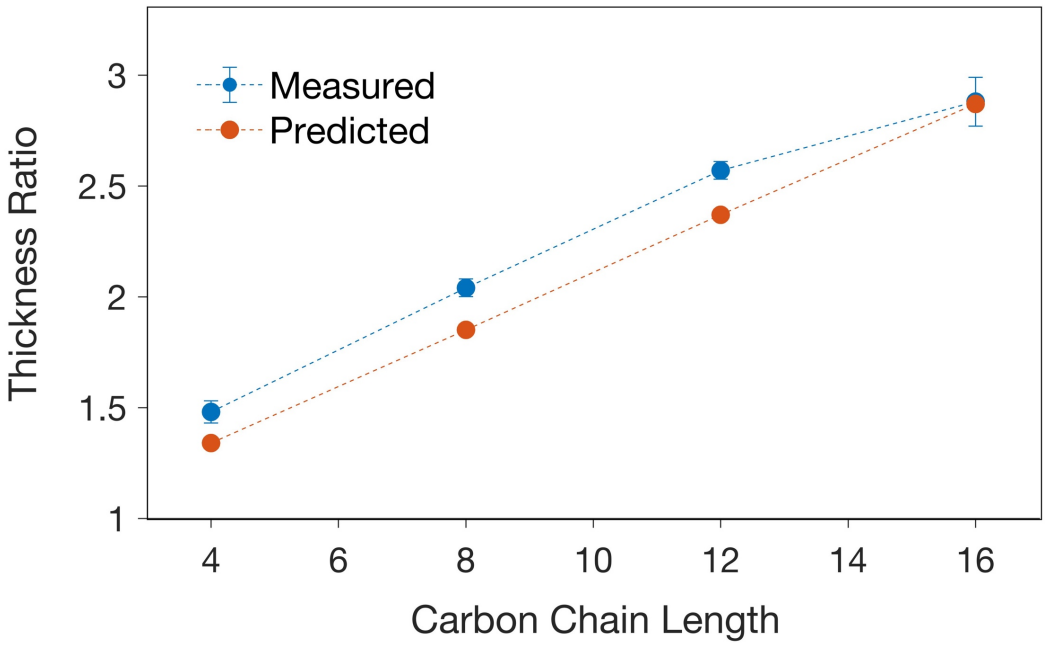

Figure 4.4. Measured and predicted thickness ratios of ester-modified films with different carbon chain length. The predicted values are based on changes in molecular weight of the repeat unit.

To examine the structure and conversion of the resulting ester films, IR spectra were collected for the films with different hydrocarbon chain lengths (n = 2, 4, 8, 12, and 16) (Figure 4.5). The absorption bands due to C=O stretching in the ester (1739 cm^{-1}) are narrow and symmetric for n = 2 to 12, and combined with the complete disappearance of the C=O stretching due to the acyl chlorides, these results are consistent with full modification of the film with pendant ester side chains throughout. When n is increased to 16, a fraction (22%) of the original absorption band due to C=O stretching in the acyl chloride remains at 1810 cm^{-1}, which demonstrates an incomplete modification. The results are consistant with the thickness ratio investigation discussed above, suggesting that a chain with 16 carbons is too large to overcome the steric hindrance to fully modify the pNBDAC film. An obvious change as we increase the chain length from 2 to 16

is the significant increase in methylene stretching from 2920 cm^{-1} to 2950^{-1} as the polymethylene groups comprise a greater volume fraction of the repeat unit. The methylene stretching peak position also shifts from 2947 cm^{-1} when n = 2 , to 2935 cm^{-1} when n = 4, to 2928 cm^{-1} when n = 8, 12, and to 2925 cm^{-1} when n = 16. These peak positions are not indicative of highly crystalline, trans-extended hydrocarbon chains and suggest that the side chains predominately exist in strained, high gauche conformations. Another noticable change in the IR spectra from C_2 to C_{16} is at 1460-1470 cm^{-1}, where the absoption band due to $-CH_2$ bending is shown[25,26]. A sharp peak appears at this position when a longer hydrocarbon chain (n = 12, 16) is introduced, which suggests that these films do exhibit a higher methylene crystallinity than those with shorter hydrocarbon side chains.

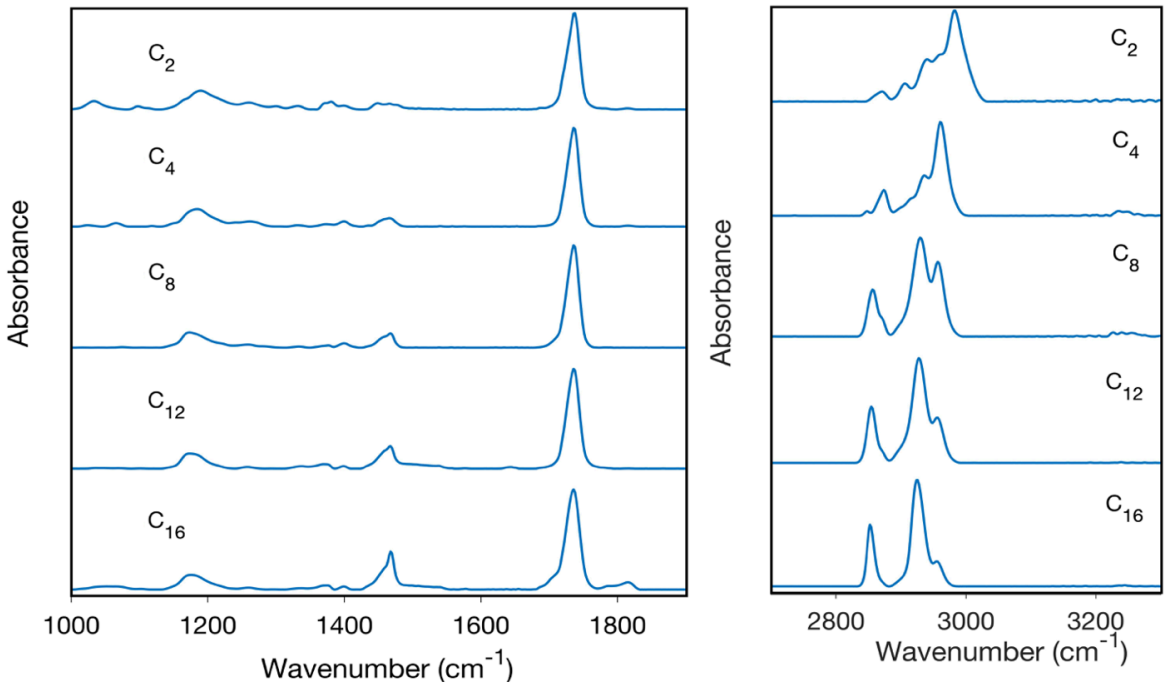

Figure 4.5. IR spectra of ester-modified films with different hydrocarbon chain lengths.

Surface Properties. The effect of hydrocarbon chain length on the measured water contact angles of n-alcohol-modified pNBDAC is shown below in Table 4.2.

Table 4.2. Advancing and Receding Contact Angle Measurements of Water on Polymer Films Modified with Water and n-Alcohols.

Functional Group	θ_a (°)	θ_r (°)
$-CO_2H$	39 ± 2	20 ± 1
$-CO_2CH_3$	67 ± 1	44 ± 2
$-CO_2C_2H_5$	80 ± 1	56 ± 3
$-CO_2C_3H_7$	89 ± 1	64 ± 3
$-CO_2C_4H_9$	99 ± 1	53 ± 3
$-CO_2C_8H_{17}$	116 ± 1	49 ± 2
$-CO_2C_{12}H_{25}$	117 ± 1	47 ± 4
$-CO_2C_{16}H_{33}$	112 ± 1	101 ± 1

The carboxylic acid modified films have the lowest contact angle due to the hydrophilicity of the carboxylic acid group. The pH of the deionized water used here is 6.6, which may partially deprotonate carboxylic acids to carboxylates and result in the lower advancing contact angle in Table 4.2 as compared to the higher sessile contact angle at pH 4 in Table 4.1. As compared to the pendant carboxylic acid groups, the use of n-alcohols to generate various alkyl esters causes the film surface to become more hydrophobic. The films with methyl ester groups still result in a

comparatively low contact angle because the more polar ester groups are expected to occupy a portion of the surface. The table shows that the advancing contact angles generally increase as the hydrocarbon chain length (n) increases from 1 to 8. As n increases, more hydrocarbon content is introduced into the film, and the film surface is progressively dominated by the $CH_3(CH_2)_n$ moiety. Accordingly, the volume fraction of the ester group is reduced, decreasing its likelihood to be present on the surface and resulting in lower surface energy and increased hydrophobicity of the polymer film. The advancing contact angles for n = 16 are generally consistent with values reported for dense methyl surfaces, implying that the alkyl chains are oriented more vertically at the interface to expose the low energy methyl groups. The hysteresis is the difference between advancing contact angle and the receding contact angle. For n = 16, the hysteresis dramatically decreases, which demonstrates the chemical homogeneity and smoothness of the surface. When n = 8 or 12, instead, the contact angles are slightly higher than the values expected for a dense methyl surface and high hystereses are obtained, suggesting the existence of surface heterogeneity and roughness. To gain greater insight on these more hydrophobic films, contact angles with hexadecane were measured for the films modified with 1-octanol, 1-dedecanol, and 1-hexadecanol. Hexadecane has a greater sensitivity in distinguishing hydrocarbon structure, as a surface dominated by $-CH_3$ groups will exhibit a hexadecane contact angle value of >40° whereas $-CH_2-$ surfaces are nearly wet by hexadecane.[27] The measured contact angles for the long carbon chain ester-modified films are 20 ± 1° (n = 8), 31 ± 1° (n = 12), and 44 ± 1° (n = 16). The hexadecane contact angles show the chemical heterogeneity of the films when n = 8 and 12 and support the view of a dense methyl surface of the film when n = 16.

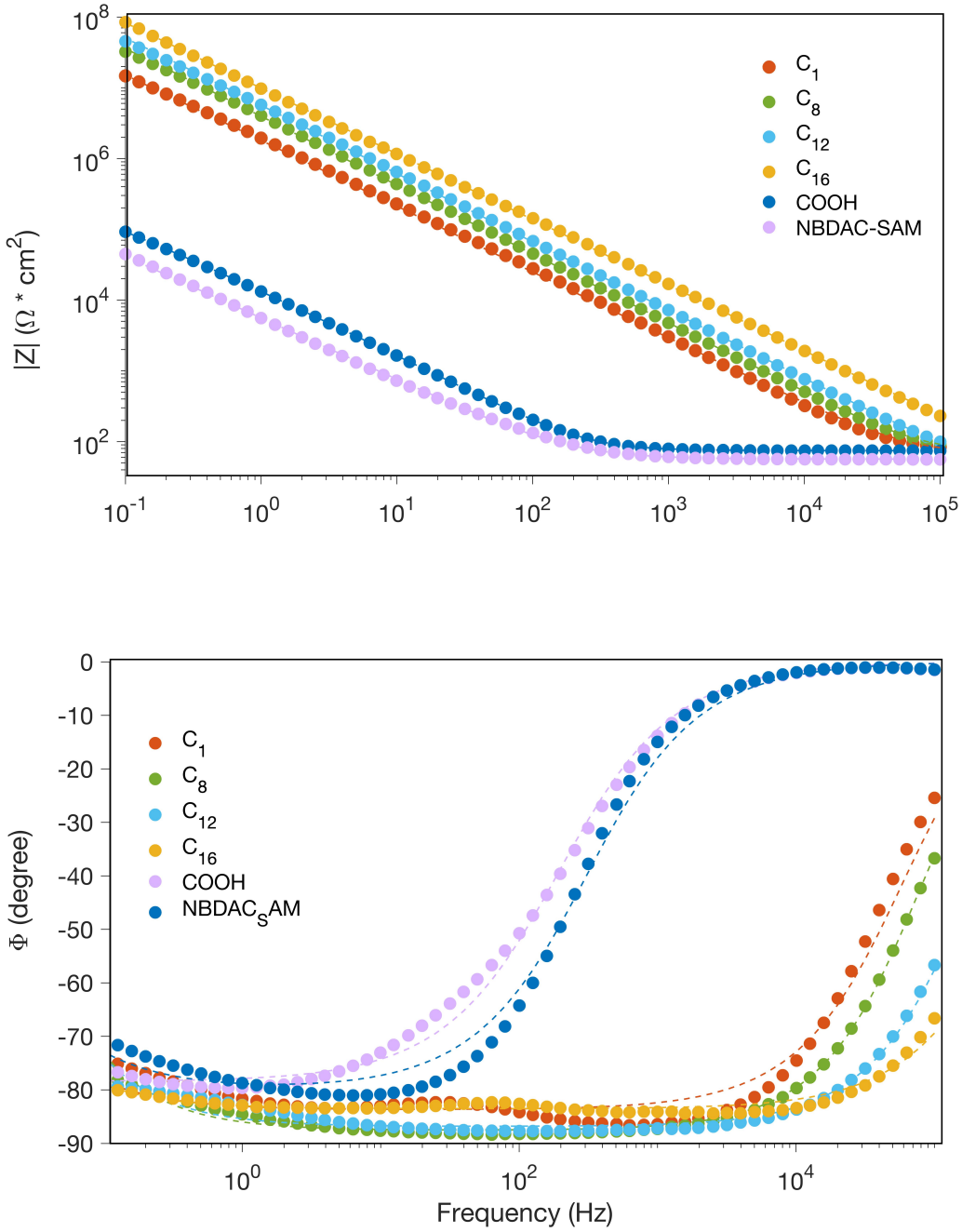

Figure 4.6. The EIS spectra in Bode magnitude (top) and phase angle (bottom) format of ester-modified films with different carbon chain lengths, with those of the norbornene-terminated SAM (NBDAC-SAM) and carboxylate-modified film as the controls.

Ion Transport in Polymer Films. The barrier properties of the modified polymer films to ion transport in an aqueous medium were characterized by utilizing electrochemical impedance spectroscopy (EIS) in the presence of a 0.1M KCl solution. To examine the effect of hydrophobic chain length on the barrier properties, EIS measurements for the films modified with -CO_2H, -CO_2C_1, -CO_2C_8, -CO_2C_{12}, and -CO_2C_{16} groups were obtained, along with a control film consisting of a hydroxyl-terminated SAM exposed to NBDAC. The EIS spectra show frequency response data of the system from 100 kHz to 0.1 Hz, and the results are plotted in a format of Bode magnitude and phase angle plots in Figure 4.6. The magnitude and phase spectra of the CO_2H-modified film shows similar barrier behavior as that of the NBDAC-terminated SAM, which demonstrates that almost no barrier to ion transport is observed for the –CO_2H-modified film. The results are due to relatively high hydrophilicity of –CO_2H groups, many of which are deprotonated to charged carboxylates in the aqueous solution, which contributes to the swelling of the film with electrolyte. The EIS spectra of the films with hydrocarbon ester side chains show highly capacitive behavior, as evidenced by straight lines with slopes of nearly -1 in the Bode magnitude plots and phase angles > 70° over most of the frequency range, and much higher impedances, demonstrating the importance of replacing of CO_2H groups with hydrophobically capped ester functionality to create a more hydrophobic volume fraction and dramatically enhance the barrier to ion transport. Different chain lengths (from n = 1 to 16) result in increases in the EIS spectra, which are due to an increase in the effective thickness of the film with increasing hydrocarbon chain length. Thus, as n is varied from 1 to 16, greater film hydrophobicity and increased film thicknesses result in higher impedances against water and ion transfer.

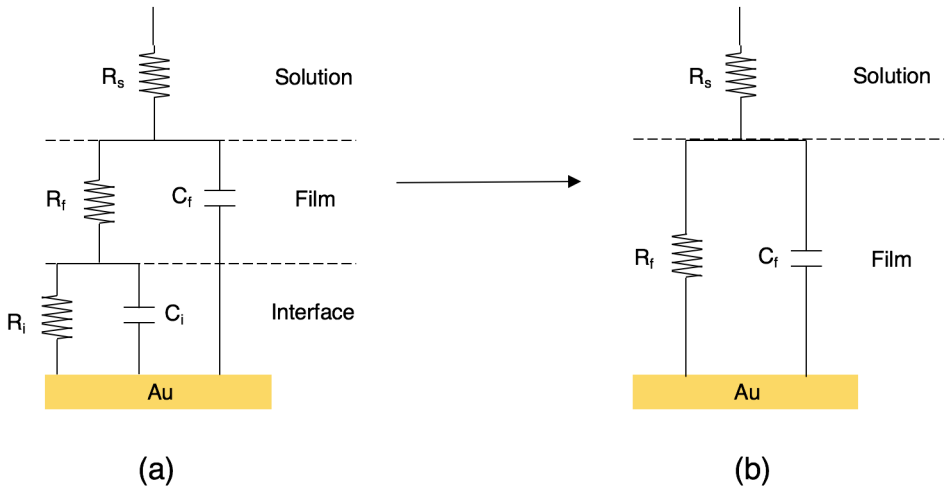

Figure 4.7. (a) The common equivalent circuit model used to fit the EIS spectra for surface initiated polymer films on substrates. The circuit model consists of a solution resistance (R_s), film capacitance (C_f), film resistance (R_f), interfacial capacitance (C_i), and interfacial resistance (R_i). (b) The simplified equivalent circuit model used to fit the EIS spectra of the ester-modified films, as their R_f values are significantly higher than the interfacial impedances. Constant phase elements (CPEs) were used in lieu of capacitors to obtain the best fit of the EIS spectra.

Table 4.3. Film resistance and film capacitance values of the ester-modified films obtained from a fit of EIS spectra of Figure 4.7 with the equivalent circuit shown in Figure 4.7(b).

	Impedance at 0.1 Hz ($M\Omega \bullet cm^2$)	Y_0 ($nS^{\alpha}/\Omega \bullet cm^2$)	α
CO_2C_1	56	59.96 ± 0.41	0.98
CO_2C_8	116	11.84 ± 0.08	0.97
CO_2C_{12}	162	8.41 ± 0.05	0.96
CO_2C_{16}	301	5.15 ± 0.03	0.93

A quantitative analysis was performed by fitting the EIS spectra with an equivalent circuit model. Figure 4.7(a) shows a common equivalent circuit used in EIS spectral fitting for surface-initiated polymer films, where both film and interfacial resistances and capacitances play important roles. Since the film resistances of our ester-modified films are orders of magnitude greater than the interfacial impedance, we have simplified the equivalent circuit for those films to the one shown in Figure 4.7(b). The fitted electrochemical parameters are listed in Table 4.3.

Since none of the ester-modified films behave as perfect capacitors, we used constant phase elements (CPEs) in lieu of capacitors to fit the experimental data. The impedance of the CPE is given by Eq. S1,

$$Z_{CPE} = \frac{1}{Y_0(j\omega)^{\alpha}} \tag{S1}$$

where Y is a constant with units of $S^{\alpha}/\Omega \bullet cm^2$ and α is a dimensionless constant between 0 and 1 to represent the deviation from the perfect capacitor.[28]

Comparing the fitted results, the increase of the hydrocarbon content in the film generally results in an increase in the film resistance and a decrease in the Y_0 constant. The higher resistance is due to the greater hydrophobic volume fraction within the film that eliminates contiguous pathways for electrolyte transfer. The decrease in Y_0 with n is attributed to both a thicker film due to the addition of the longer chain hydrocarbons, as well as a reduced dielectric permittivity because of the greater volume fraction of the nonpolar hydrocarbon and reduced volume fraction of the polar ester. These combined effects result in greater impedances against electrolyte penetration into the film as hydrocarbon volume fraction is increased. In total, these impedance

results show the ability to transform a base pNBDAC film across a wide range of barrier properties through a simple one-step modification.

Conclusions

PNBDAC films were successfully prepared via SiROMP of NBDAC from the vapor phase. This method ensures rapid kinetics of film growth with film thicknesses reaching near 400 nm. Via the exposure of the pNBDAC to compounds such as water, alcohols, and amines, the post-polymerization modification can be easily achieved to produce various pendant functionalities. The introduction of aromatic rings, pH-responsive tertiary amines, fluorescein, and long hydrocarbon chains to the polymer film has been examined. Small molecules can easily react with the acyl chloride groups to modify the film composition, while complete modification with large molecules like fluorescein and 1-hexadecanol is challenging to achieve due to the combined slow rates of diffusion and steric hindrances. Post-polymerization modification of pNBDAC was also used to fine tune film properties. pH-responsive wettability can be introduced by modifying the film with carboxylic acid or tertiary amine side groups. The tunability of film properties is also achieved by employing a series of n-alcohols with different hydrocarbon chain lengths (n). Longer side chains result in a greater volumetric expansion of the film to increase thicknesses linearly in a manner slightly greater than that predicted based on molecular weight. An increase of side chain from 0 to 8 results in advancing water contact angles that increase from 40° to 117°, with little effect of longer chains beyond 8 carbons. For n = 16, the surface of the film is dominated by low-energy methyl groups, suggesting that these long chains orient nearly vertically at the outer surface. A dramatic increase in the impedance of ion transfer occurs when carboxylic acid groups in the film are replaced with esters—even simple methyl esters. As the carbon chain length

appended to the ester is increased, a gradual increase in impedance accompanies the increasingly hydrophobic film. The modification of the pNBDAC film can be easily achieved with different reagents by a simple exposure. We expect that this versatile modification strategy can be extended to the preparation of many other functional polymer and copolymer films.

References

(1) Zhang, W.; Shi, Z.; Zhang, F.; Liu, X.; Jin, J.; Jiang, L. Superhydrophobic and Superoleophilic PVDF Membranes for Effective Separation of Water-in-Oil Emulsions with High Flux. *Adv. Mater.* **2013**, *25* (14), 2071–2076.

(2) Wei, Z.; Pan, Z.; Li, F.; Yu, J. Poly(Butylene Succinate-Co-Terephthalate) Nanofibrous Membrane Composited with Cyclodextrin Polymer for Superhydrophilic Property. *RSC Adv.* **2017**, *8*, 1378–1384.

(3) Zomorodian, A.; Garcia, M. P.; Moura E Silva, T.; Fernandes, J. C. S.; Fernandes, M. H.; Montemor, M. F. Corrosion Resistance of a Composite Polymeric Coating Applied on Biodegradable AZ31 Magnesium Alloy. *Acta Biomater.* **2013**, *9* (10), 8660–8670.

(4) Beckford, S.; Zou, M. Wear Resistant PTFE Thin Film Enabled by a Polydopamine Adhesive Layer. *Appl. Surf. Sci.* **2014**, *292*, 350–356.

(5) Kobayashi, M.; Takahara, A. Tribological Properties of Hydrophilic Polymer Brushes under Wet Conditions. *Chem. Rec.* **2010**, *10* (4), 208–216.

(6) Kreer, T. Polymer-Brush Lubrication: A Review of Recent Theoretical Advances. *Soft Matter* **2016**, *12* (15), 3479–3501.

(7) Yang, Y.; Qi, P.; Ding, Y.; Maitz, M. F.; Yang, Z.; Tu, Q.; Xiong, K.; Leng, Y.; Huang, N. A Biocompatible and Functional Adhesive Amine-Rich Coating Based on Dopamine Polymerization. *J. Mater. Chem. B* **2015**, *3* (1), 72–81.

(8) Skarja, G. A.; Brown, A. L.; Ho, R. K.; May, M. H.; Sefton, M. V. Biomaterials The Effect of a Hydroxamic Acid-Containing Polymer on Active Matrix Metalloproteinases. *Biomaterials* **2009**, *30* (10), 1890–1897.

(9) Li, W.; Roelofs, W. S. C.; Turbiez, M.; Wienk, M. M.; Janssen, R. A. J. Polymer Solar Cells with Diketopyrrolopyrrole Conjugated Polymers as the Electron Donor and Electron Acceptor. *Adv. Mater.* **2014**, *26* (20), 3304–3309.

(10) Sundaram, H. S.; Han, X.; Nowinski, A. K.; Ella-Menye, J. R.; Wimbish, C.; Marek, P.; Senecal, K.; Jiang, S. One-Step Dip Coating of Zwitterionic Sulfobetaine Polymers on Hydrophobic and Hydrophilic Surfaces. *ACS Appl. Mater. Interfaces* **2014**, *6* (9), 6664–6671.

(11) Vaterrodt, A.; Thallinger, B.; Daumann, K.; Koch, D.; Guebitz, G. M.; Ulbricht, M. Antifouling and Antibacterial Multifunctional Polyzwitterion/Enzyme Coating on Silicone Catheter Material Prepared by Electrostatic Layer-by-Layer Assembly. *Langmuir* **2016**, *32* (5), 1347–1359.

(12) Lindemann, W. R.; Philiph, R. L.; Chan, D. W. W.; Ayers, C. T.; Perez, E. M.; Beckman, S. P.; Strzalka, J.; Chaudhary, S.; Vaknin, D. Oriented Polyvinylidene Fluoride–Trifluoroethylene (P(VDF–TrFE)) Films by Langmuir–Blodgett Deposition: A Synchrotron X-Ray Diffraction Study. *Phys. Chem. Chem. Phys.* **2015**, *17* (43), 29335–29339.

(13) Olivier, A.; Meyer, F.; Raquez, J. M.; Damman, P.; Dubois, P. Surface-Initiated Controlled Polymerization as a Convenient Method for Designing Functional Polymer Brushes: From Self-Assembled Monolayers to Patterned Surfaces. *Prog. Polym. Sci.* **2012**, *37* (1), 157–181.

(14) Zoppe, J. O.; Ataman, N. C.; Mocny, P.; Wang, J.; Moraes, J.; Klok, H. A. Surface-Initiated Controlled Radical Polymerization: State-of-the-Art, Opportunities, and

Challenges in Surface and Interface Engineering with Polymer Brushes. *Chem. Rev.* **2017**, *117* (3), 1105–1318.

(15) Lerum, M. F. Z.; Chen, W. Surface-Initiated Ring-Opening Metathesis Polymerization in the Vapor Phase: An Efficient Method for Grafting Cyclic Olefins with Low Strain Energies. *Langmuir* **2011**, *27* (9), 5403–5409.

(16) Faulkner, C. J.; Fischer, R. E.; Jennings, G. K. Surface-Initiated Polymerization of 5-(Perfluoro-n-Alkyl)Norbornenes from Gold Substrates. *Macromolecules* **2010**, *43* (3), 1203–1209.

(17) Njoroge, I.; Kempler, P.; Deng, X.; Arnold, S.; Jennings, G. K. Surface-Initiated Ring-Opening Metathesis Polymerization of Dicyclopentadiene from the Vapor Phase. *Langmuir* **2017**.

(18) Escobar, C. a; Harl, R. R.; Maxwell, K. E.; Mahfuz, N. N.; Rogers, B. R.; Jennings, G. K. Amplification of Surface-Initiated Ring-Opening Metathesis Polymerization of 5-(Perfluoro-n-alkyl)Norbornenes by Macroinitiation. *Langmuir* **2013**, *29*, 12560–12571.

(19) Morrison, R. T.; Boyd, R. N. *Organic Chemistry*; Prentice Hall, 1992.

(20) Yang, Y. S.; Qi, G. R.; Qian, J. W.; Yang, S. L. Acryloyl Chloride Polymer. *J. Appl. Polym. Sci* **1997**, *68* (April), 665–670.

(21) Buruiana, E. C.; Buruiana, T.; Hahui, L. Preparation and Characterization of New Optically Active Poly (N -Acryloyl Chloride) Functionalized with (S) -Phenylalanine and Pendant Pyrene. *J. Photochem. Photobiol. A* **2007**, *189*, 65–72.

(22) Wang, X.; Zhang, C.; Du, Z.; Li, H.; Zou, W. Synthesis of Non-Destructive Amido Group Functionalized Multi-Walled Carbon Nanotubes and Their Application in Antistatic and

Thermal Conductive Polyetherimide Matrix Nanocomposites. *Polym. Adv. Technol.* **2017**, *28* (November 2016), 791–796.

(23) Moore, J. D.; Byrne, R. J.; Vedantham, P.; Flynn, D. L.; Hanson, P. R. High-Load, ROMP-Generated Oligomeric Bis-Acid Chlorides: Design of Soluble and Insoluble Nucleophile Scavengers. *Org. Lett.* **2003**, *5* (23), 4241–4244.

(24) Rolfe, A.; Loh, J. K.; Maity, P. K.; Hanson, P. R. High-Load , Hybrid Si-ROMP Reagents. *Org. Lett.* **2011**, *13* (1), 4–7.

(25) Hagemam, H.; Snyder, R. G. Quantitative Infrared Methods for the Measurement of Crystallinity and Its Temperature Dependence : Polyethylene. *Macromolecules* **1989**, *22*, 3600–3606.

(26) Yan, C.; Zhang, Y.; Hu, Y.; Ozaki, Y.; Shen, D.; Gan, Z. Melt Crystallization and Crystal Transition of Poly (Butylene Adipate) Revealed by Infrared Spectroscopy. *J. Phys. Chem. B* **2008**, *112*, 3311–3314.

(27) Bain, C. D.; Troughton, E. B.; Tao, Y.-T.; Evall, J.; Whitesides, G. M.; Nuzzo, R. G. Formation of Monolayer Films by the Spontaneous Assembly of Organic Thiols from Solution onto Gold. *J. Am. Chem. Soc.* **1989**, *111* (1), 321–335.

(28) Hsu, C. H.; Mansfeld, F. Technical Note: Concerning the Conversion of the Constant Phase Element Parameter Y0 into a Capacitance. *Corrosion* **2001**, *57* (9), 747–748.

CHAPTER V

SYNTHESIS AND PROPERTIES OF METAL-CHELATED POLYMER FILMS BY SURFACE-INITIATED POLYMERIZATION

Introduction

Metal chelating polymers attract great attention because of their important utilization in various areas, such as environmental protection,[1–5] medical therapy,[6–8] and analytical separations.[9,10] Among various chelating ligands, hydroxamic acid is one of the most widely utilized ligands as it is known to effectively chelate many different metal ions.[5,11–15] Polymers with hydroxamic acid functionality have been widely investigated in the past decades. However, most of the research on hydroxamic acid-modified polymers focuses on bulk polymers[5,13–15] For example, Menon et al. prepared poly(styrene-p-hydroxamic acids) and utilized them in the removal of transition metals from water.[15] Kumar et al. synthesized hydroxamic acid polymers from acyl amines and applied them in cartridges to determine the concentration of rare earth metals in sea water.[5] Fewer studies have been performed on polymer thin films.[4,5,14] Rahman et al. modified a PMA-grafted kenaf cellulose with hydroxamic acid groups and utilized them water treatment.[4,5] Polymer thin films are one of the most important areas of polymer science and provide a means to transfer advances in solution polymerization to the design of interfaces with controlled thicknesses and compositions to tailor surface properties.[16–20] If the metal chelating ability of hydroxamic acid groups can be applied to polymer thin films, the application of hydroxamic acid-modified polymers can be further extended to applications where a thin film on an underlying surface is critical, such as high surface area chelating materials and corrosion detection.

Furthermore, the previous research on chelating polymers has focused more on the chelation activity and the selectivity or capacity of the chelating ligands but rarely on the effect of metal chelation on polymer film properties. Also, most chelation studies have investigated the chelation with metal ions that already exist in the environment whereas only a very few pay attention to the chelation of ions released into the environment, such as in the case of a corroded metal. Therefore, although metal chelating polymers and hydroxamic acids have been extensively studied, a unified research study on chelating polymer thin films coupled with the associated changes in polymer properties, including the examination of metal sources of chelation, is needed to expand the applications of these materials.

Here, I report a new route to the preparation of hydroxamic acid-modified (PHA) thin films, and I investigate their chelating behaviors, the effect of metal loading on film properties, and their potential application in corrosion detection. I utilize SiROMP of NBDAC and the straightforward modification of acyl chloride groups to hydroxamic acids. SiROMP offers rapid film growth under mild conditions, high controllability over film thickness, dense grafting, stable adhesion, and independence of geometry.[16,21–23]

Experimental Section

Polymerization of NBDAC and Modification to PHA

Polymerization of pNBDAC was accomplished from the vapor phase as reported in Chapter 4 After the surface-initiated polymerization in the vial, the substrates were quickly rinsed with DCM to remove extra monomers from the film and then directly exposed to 0.1 M hydroxylamine aqueous solution to obtain hydroxamic acid modified films (Figure 5.1).

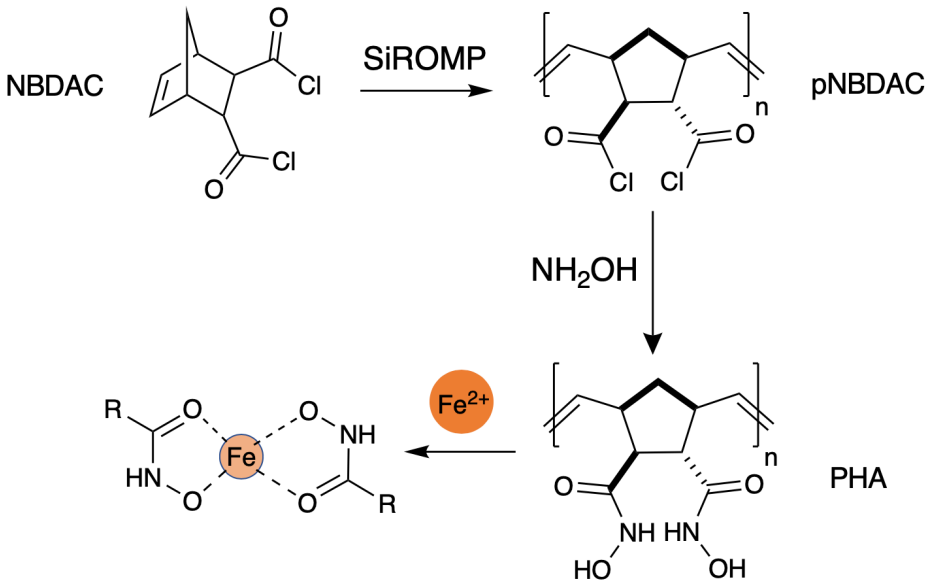

Figure 5.1. SiROMP of pNBDAC, its modification to PHA, and an example of an Fe-chelation structure.

Results and Discussion

Preparation of Poly(hydroxamic acid) (PHA) Films on Gold Substrates

PNBDAC films were first prepared by SiROMP of NBDAC from the vapor phase on initiator-modified gold substrates to achieve smooth films with thickness of ~300 nm and roughnesses of less than 10 nm. The pNBDAC films were then soaked overnight in a 0.1 M hydroxylamine aqueous solution to modify the acyl chloride groups to hydroxamic acids. The substrates were then rinsed with water to remove the extra hydroxylamine and dried with N_2 to obtain the film. PM-IRRAS was used to determine the successful preparation of PHA films. IR

spectra of the films were collected both before and after hydroxylamine modification and are shown in Figure 5.2. The spectrum of the pNBDAC film shows a strong absorption band due to C=O stretching in acyl chloride (1794 cm^{-1}), along with weaker bands due to C_{sp3}-H in-plane bending (1430-1500 cm^{-1}), C_{sp3}-H out-of-plane bending (1300-1400 cm^{-1}), and C_{sp2}-H out-of-plane bending (900-1100 cm^{-1}). Compared to the spectrum of pNBDAC, the IR spectrum of the film after hydroxylamine shows strong absorption bands due to C=O stretching (1666 cm^{-1}) and N-O stretching (1500 – 1550 cm^{-1}) in the hydroxamic acid, which demonstrate the successful film modification to PHA. In addition, an absorption band due to C=O stretching for ester (1739 cm^{-1}) is also observed. The small percentage of ester found in the film can be explained by the use of the modification reagent hydroxylamine. Hydroxylamine contains both an amine group and a hydroxyl group. During the modification process, the amine group shows much higher reactivity, but a very small portion of the acyl chlorides are reacted with the hydroxyl group of hydroxylamine to form the ester.

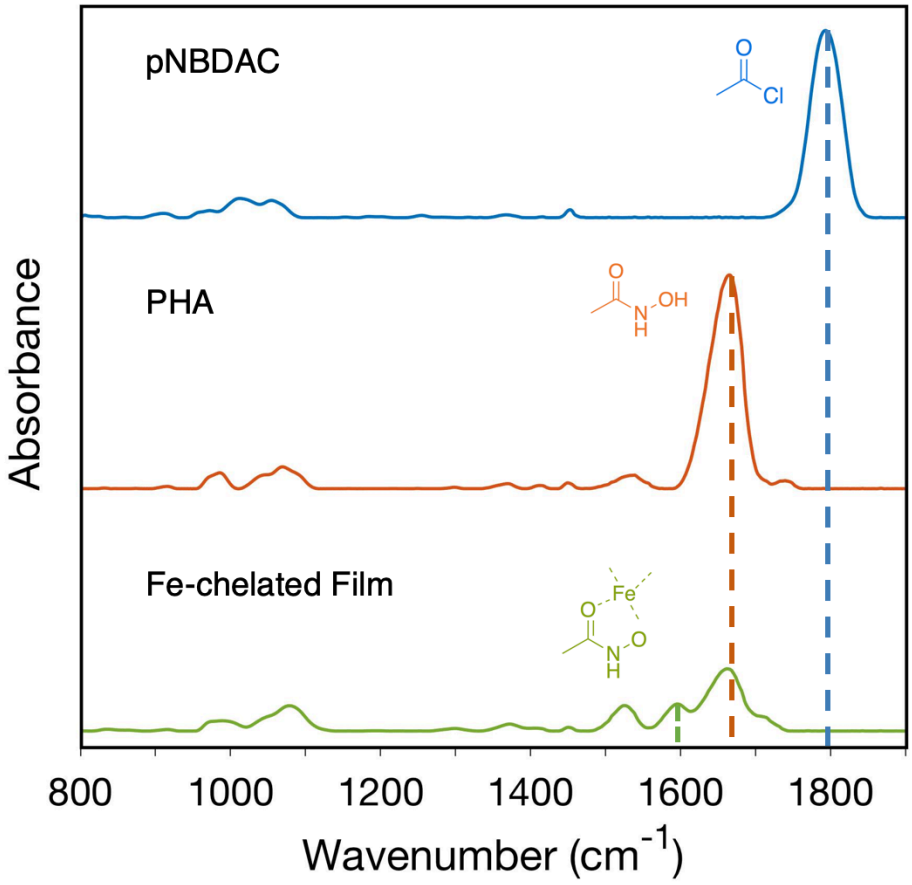

Figure 5.2. IR spectra of the original pNBDAC film, hydroxamic acid-modified film (PHA), and the PHA film after exposure to an Fe^{2+} salt to yield the Fe-chelated film.

Chelation of Transition Metal Ions with the PHA Films

Chelation of Fe^{2+} with the PHA Films. The chelation ability of the prepared PHA films was tested with the divalent ion Fe^{2+}. The obtained PHA film was exposed to 0.03 M $FeSO_4$ aqueous solution for 30 min, and the IR spectrum of the resulting film is shown in Figure 5.2. Two significant changes in the IR spectrum of the Fe^{2+} chelated film as compared to that of the PHA film are the dramatically reduced intensity of the absorption band due to C=O stretching in hydroxamic acid (1666 cm^{-1}) and the appearance of an absorption band at 1597 cm^{-1} due to C=O stretching in the chelated structure, which signals the existence of the Fe^{2+}-PHA chelation in the

resulting film.[14] However, the IR spectrum also shows that not all the hydroxamic acid groups in the film are chelated with the Fe^{2+}. The incomplete conversion is consistent with previous literature on chelation. Considering that two center-symmetric hydroxamic acid groups are required to chelate Fe^{2+} as Figure 5.1 shows, not all the hydroxamic acid groups would be positioned or oriented to form such a center-symmetric structure, and thus, a portion of unchelated hydroxamic acid groups remain after the exposure to iron(ii) salt solution. By peak deconvolution (shown in Figure 5.3), the area of the unchelated PHA in the film can be obtained, and the molar percentage of the chelation can be calculated as

$$\text{chelation percentage} = \left(1 - \frac{area\ of\ unchelated\ PHA}{area\ of\ original\ PHA}\right) \times 100 \qquad (5.1)$$

Other noticeable changes are the disappearance of the absorption band due to C=O stretching (1739 cm^{-1}) and newly formed absorption band at 1710 cm^{-1} due to C=O stretching in carboxylic acid. The C=O stretching shifting from 1739 to 1710 cm^{-1} is due to the hydrolysis of the ester. Some divalent metal ions can be used as the catalyst for the hydrolysis of esters with amino groups.[24,25]

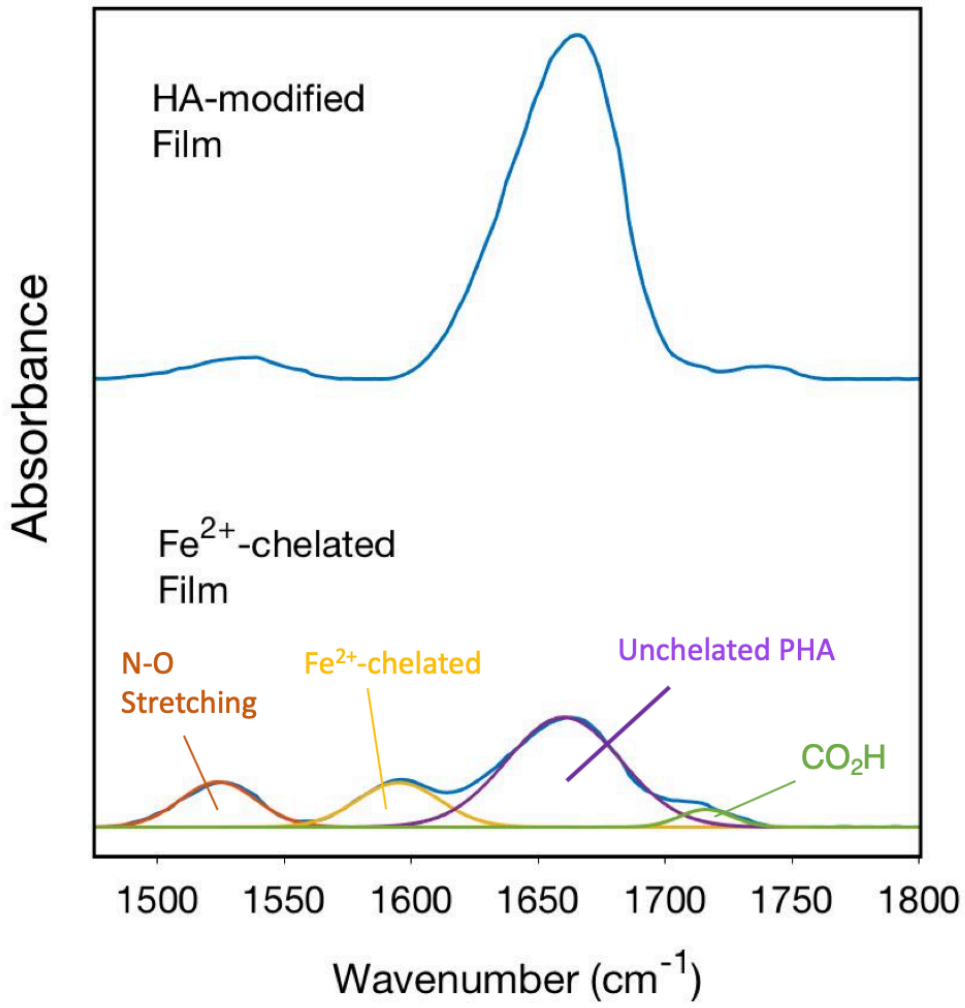

Figure 5.3. Illustration of the peak deconvolution used to calculate peak areas of the original PHA film and the chelated PHA film. The yellow, purple and green deconvoluted peaks demonstrate C=O stretching absorption bands in different molecular structures.

Chelation of Transition Metal Ions with the PHA Films. The chelation ability of the prepared PHA films with several other transition metal ions beyond Fe^{2+} was also tested and compared. The PHA films were exposed overnight separately to 0.03 M solutions of Cu^{2+}, Co^{2+},

Zn^{2+} and Ni^{2+}. The IR spectra of the PHA films before and after exposure to metal ion solutions are shown in Figure 5.4. All IR spectra show significant decrease of the carbonyl intensity for the hydroxamic acid group after exposure to the metal ion solutions, indicating successful chelation of divalent metal ions. In contrast, a low percentage of chelation (< 30%) was observed for Fe^{3+} and Zr^{4+}. The lack of chelation is likely due to the special structure of the repeating unit in our PHA films. Two hydroxamic groups are located on adjacent carbons in a trans conformation, which results in conformational limitations for these hydroxamic acid groups to chelate within the same repeat unit. With divalent metal ions, only two chelating ligands are required so chelation can occur between either of these HA groups and nearby HA groups from another repeat unit along the same chain or another polymer chain. In contrast, for Fe^{3+} and Zr^{4+}, three and four chelating ligands are required to achieve the chelation, which would require the unlikely presence of additional chelating ligands in the same localized area.

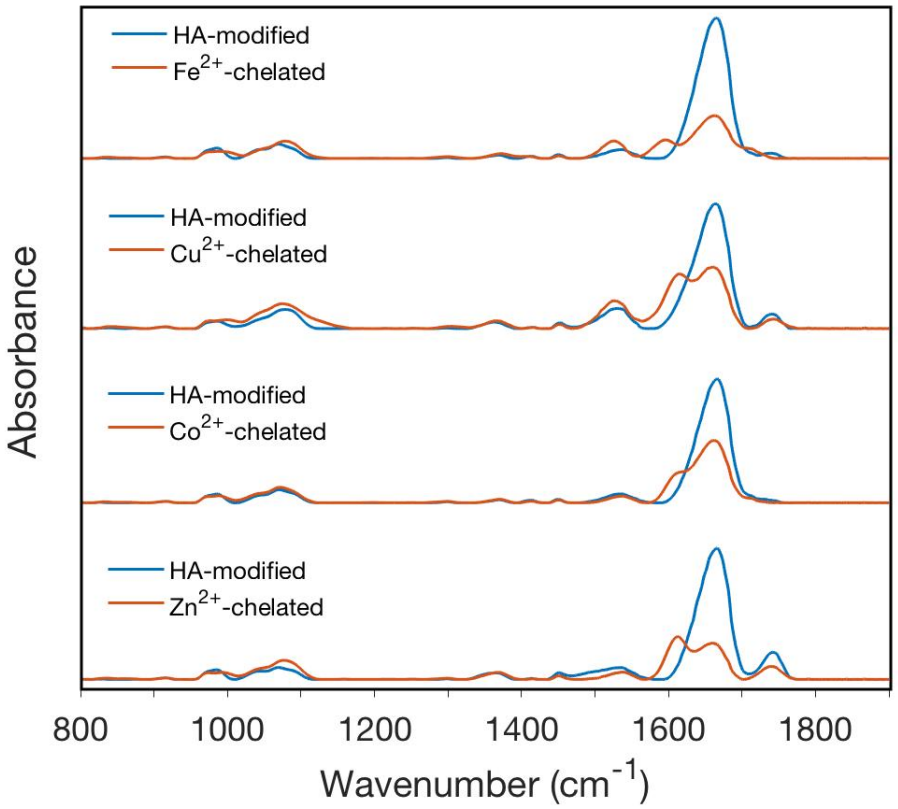

Figure 5.4. The IR spectra of PHA films before and after chelation of various divalent metal ions.

Stability of Fe Chelation at Different pH Levels. Chelated bonds are generally stable and metal-chelated polymers usually exhibit high stability to environmental changes.[26] However, in many chelation applications, such as heavy metal removal, the polymer matrices are expected to be reusable for many cycles, even after repeated liberation of ions from the bound metals. In addition, the stability of metal-chelated polymers is important if the chelated film is actually the final product. Acid treatment is a feasible method to break the ligand-metal bond and remove the chelated metal ion from the polymer. Therefore, we soaked the PHA films in pH 4 standard buffer solution, 0.1 M HCl (pH 1), and pH 0 for 1 h and recorded IR spectra both before and after the

acid treatment (Figure 5.5). The IR spectra after treatment at pH 4 and pH 1 are almost the same as in the chelated polymer film, which shows that the ligand-metal chelation exhibits a high stability even in pH 1 acidic solutions. When we further increase the acidity of the solution to pH 0 (1 M HCl), the IR spectrum shows dramatic change, as the absorption band due to C=O (1666 cm^{-1}) stretching in the chelated structure disappears and the absorption band due to C=O stretching in the hydroxamic acid is reobtained. Upon comparing the spectrum of the pH 0 treated film to that of the original unchelated PHA film, the intensity of the hydroxamic acid peak slightly decreases and a peak due to carboxylic acid C=O stretching (1710 cm^{-1}) appears. The appearance of carboxylic acid groups are possibly due to the hydrolysis of a small portion of hydroxamic acid. When we apply strong acid to regenerate the PHA from the chelated polymer, the strong acid also may not only break the chelation bond but may also catalyze the hydrolysis of hydroxamic acids in the aqueous solution.

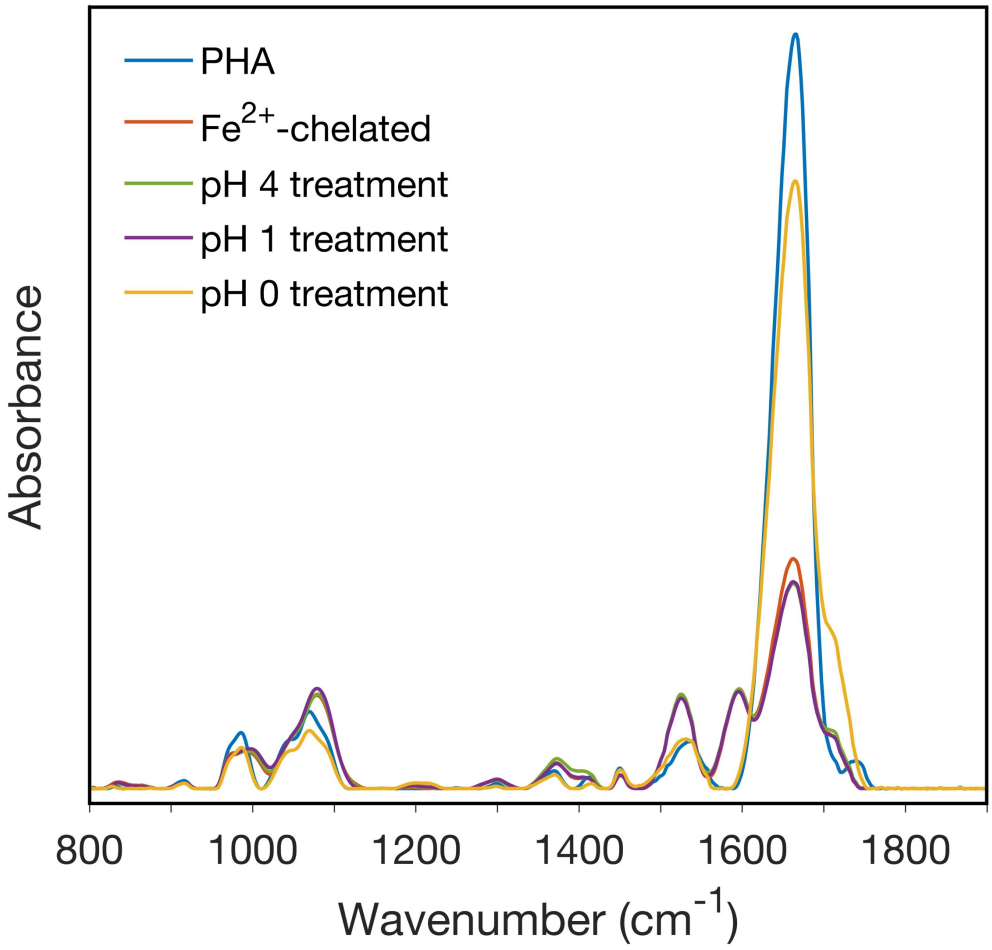

Figure 5.5. IR spectra of a PHA film, an Fe-chelated film, and resulting films after different pH treatments

To examine the film stability in basic solutions, the metal-chelated film was placed in pH 10 and pH 13 solutions. The IR spectra of the original PHA film, the film after chelation, and chelated films after pH 10 and pH 13 treatments are shown in Figure 5.6. The IR spectra of the films after basic solution treatments show the same peak positions but different peak shapes as compared with the spectrum after chelation. The overall intensities of the spectra remain the same, which indicates that there is no film loss after the basic solution treatment. The slight change in

peak shapes is due to the deprotonation of the carboxylic acid groups in the chelated film. In high pH solution, those carboxylic acid groups become deprotonated to carboxylate, which will result in a new absorption band due to C=O stretching in carboxylate (1600 to 1650 cm^{-1}). The existence of the new absorption band results in the changes in peak shape in the region from 1500 to 1700 cm^{-1}. The same peak positions and spectral intensity demonstrate that the metal-chelated film is stable to these basic conditions.

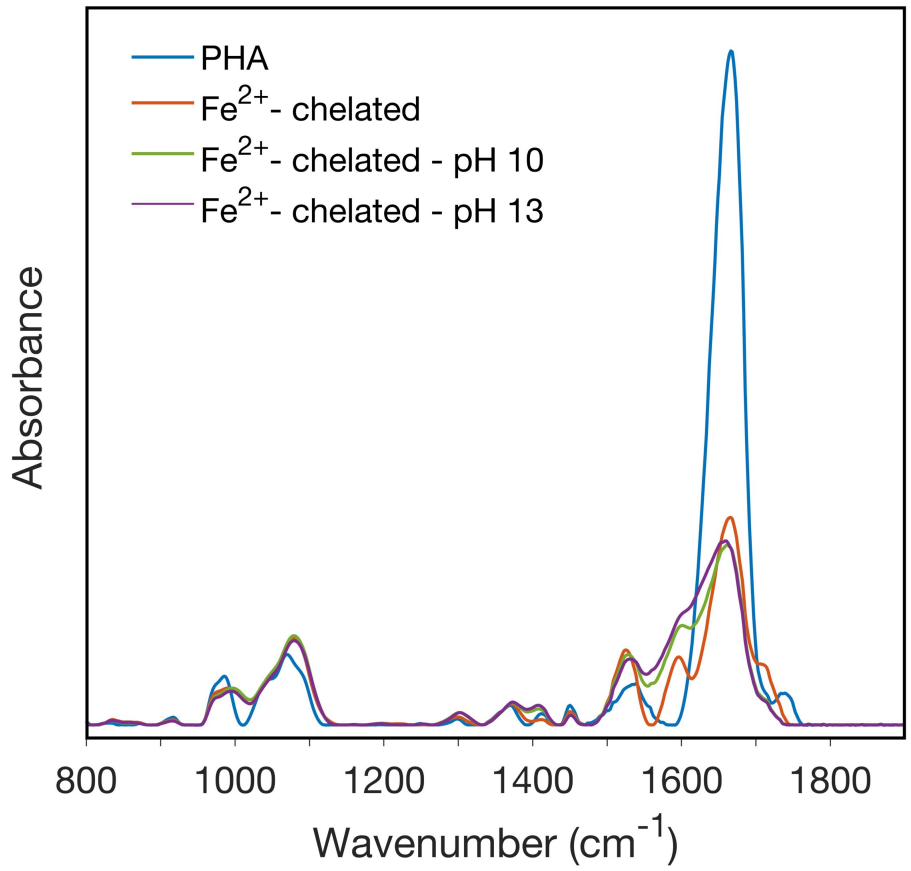

Figure 5.6. IR spectra of the original PHA film and Fe-chelated films before and after exposure to basic environments.

Effect of Fe Chelation on Film Properties

The chelation of metals plays an important role in altering the film properties. Two center-symmetric hydroxamic acids are required to chelate a ferrous ion, which means that the metal chelation does not occur within the monomer unit of these films but occurs between different units or even different polymer chains. In this case, chelated metal ions also function as cross-linkers, changing the structure and properties of the film.

Polymer Film Stability Change. Film stability is important for surface-initiated polymer thin films as they are utilized in applications. The prepared PHA films show stability in air and in water at room temperature. However, the film can be easily detached from the gold surface when placed in water at 80 °C (Figure 5.7). The decrease in stability is mainly due to the stronger interaction of the polymer chain with the aqueous environment. At high temperature, the polymer chains have sufficient energy of motion to overcome the thiol-Au bond that affixes the film to the substrate. In this case, the chelated metal ions can behave as crosslinkers, which would make the structure less swellable in solution and increase the film stability. Film stability investigations were performed for both the PHA film and Fe^{2+} chelated film.

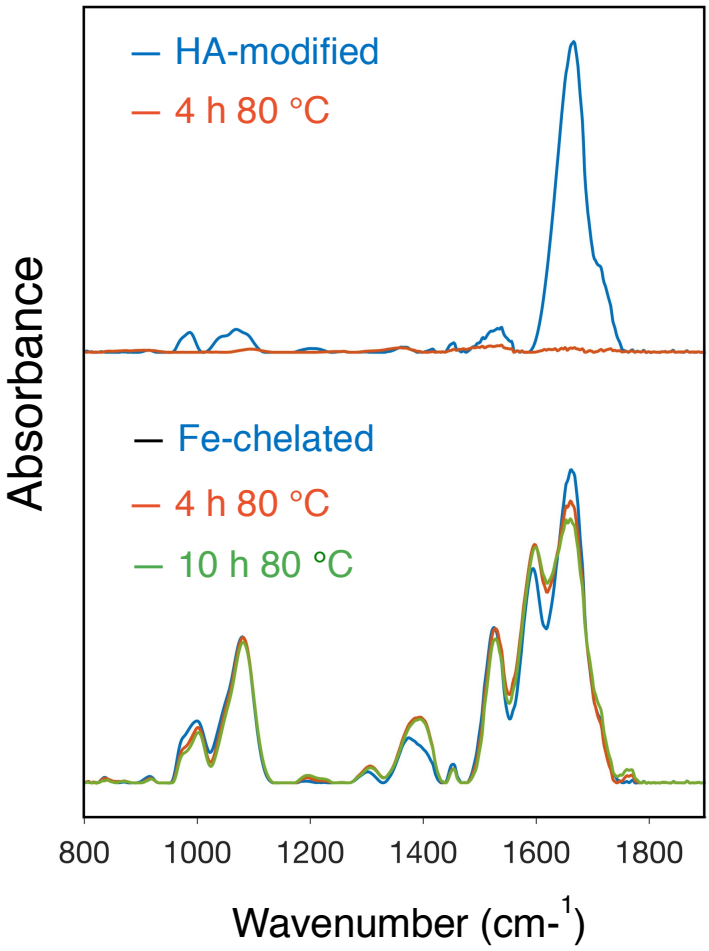

Figure 5.7. IR spectra of a PHA film and an Fe-chelated film, both before and after exposure to 80°C water for 4 and 10 h.

To investigate the film stability in solution at high temperature, the PHA film and Fe^{2+} chelated film were placed in 80 °C deionized water for 4 h. The PHA film was eventually removed from the surface while the chelated film was stable on the surface. The chelated film was then placed back in the 80 °C deionized water for an additional 6 h to examine the long-term stability. The result shows that the film is still stable after soaking in high temperature water for 10 h. The IR spectra of the thermal stability investigation are shown in Figure 5.7. We also tested the stability of the films with different chelation percentages. Table 5.1 demonstrates that even a low

percentage of partial chelation (e.g. 27 %) is enough to stabilize the films in a cross-linked structure that reduces chain motion and is less swellable in solution to enhance the thermal stability of the film.

Table 5.1. Thermal Stability of the Film with Different Chelation Percentages

Chelation Percentage (%)	Stability in 80°C water
0	Unstable
27	Stable
60	Stable
69	Stable

Effect of Fe Chelation on Water Interaction and Mechanical Properties. The effect of Fe chelation on the interaction of the film with water can be characterized by employing QCM-D. QCM-D is a technique that provides precise measurements of resonant frequency shifts and energy dissipation factor of a QCM crystal upon loading by a film or coating. The addition of film mass on the quartz crystal will result in a decrease in the frequency of oscillations, while varying the viscoelastic properties of the film can be related to the energy dissipation of the coated crystal. The interaction of the polymer film with water can be directly demonstrated by the change in energy dissipation, with the mechanical properties indicating the phase state of the film in the solution. We collected the frequency and dissipation values for a clean quartz crystal sensor with flowing water and used those as the baseline. The changes in frequency (Δf) and energy dissipation (ΔD) as we deposited the PHA film and chelated Fe^{2+} into the film on the crystal are shown in Figure 5.8. Both the

addition of the PHA film on the crystal and the chelation of Fe^{2+} into the PHA film result in a decrease in frequency, which shows that masses have been deposited onto the crystal. A mass ratio of the chelated Fe^{2+} film to the original PHA film (0.15) is obtained by applying the Kelvin-Voigt model. Then, based on the molecular weights of Fe^{2+} and the repeat unit, we estimated that 56% percent of the hydroxamic acid groups are chelated with Fe^{2+}. The chelation degree is lower than the chelation degree of 69% estimated based on the IR spectra. One reason for the difference is that some PHA film grew on the backside of the crystal, where the ferrous ions have no accessibility during the QCM-D experiment. The area of gold surface on the backside of the crystal is ¼ of that on the frontside. Assuming that same thickness is achieved on both sides of the crystal during the polymerization, the actual mass increase from Fe chelation for the front side of the crystal is an additional 20%, and the adjusted chelation degree derived from the mass ratio is 74%, which is close to the chelation degree of 69% based on the IR measurements.

QCM can also be used to evaluate the viscoelastic properties of the coated crystal in the aqueous solution by analyzing the change in dissipation (ΔD). In the Kelvin-Voigt model, a complex shear modulus is used to present the viscoelastic properties of the film,

$$\mathrm{G} = \mathrm{G}' + jG'' \tag{5.2}$$

where G' is the shear storage modulus that describes the solid behavior of the material, and G'' is the shear loss modulus that describes the liquid behavior of the material. In our experiments, after the chelation of Fe^{2+}, the shear storage modulus increased by 65% and the shear loss modulus decreased by 47%, which shows that the existence of chelated Fe^{2+} results in a more solid-like and

less liquid-like behavior of the material in the aqueous solution. Therefore, the changes in complex shear moduli are consistent with Fe-chelated cross-linking in the polymer film.

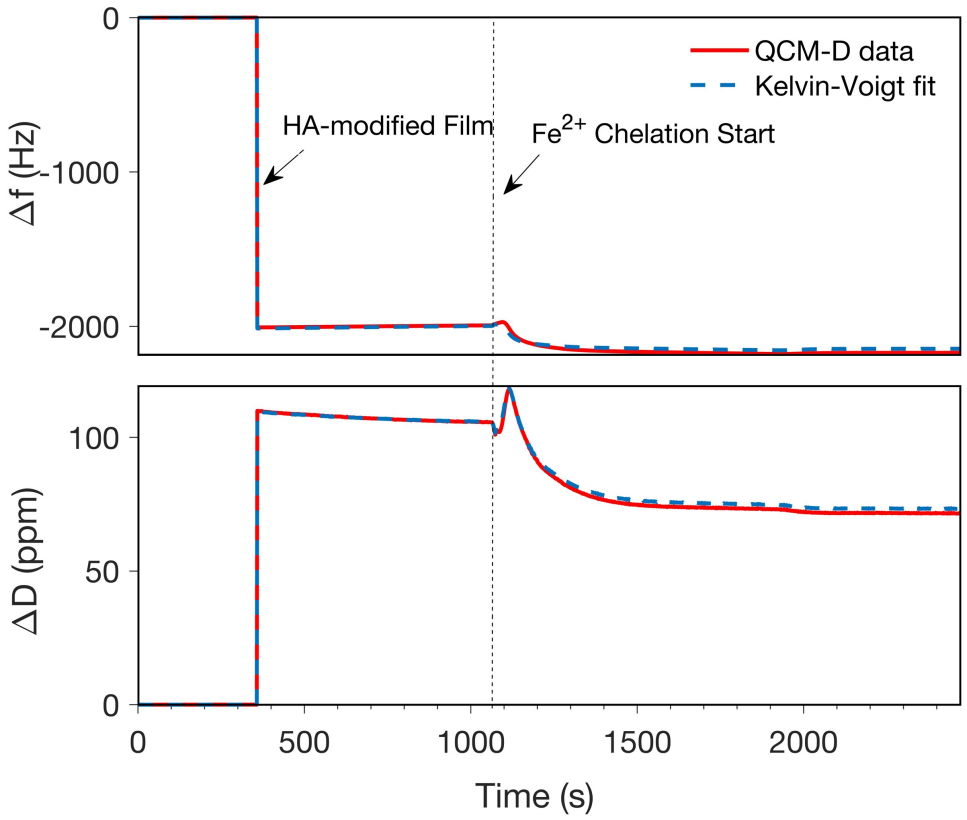

Figure 5.8. QCM analysis of the bare crystal and the PHA film (grown ex situ on the QCM crystal) before and after exposure to 0.05 M Fe^{2+}(aq) to achieve the Fe-chelated film.

Effect of Fe Chelation on Ion Transport in the Chelated Film. Ion transport through the PHA and Fe-chelated films was investigated with EIS by using a gold substrate with the film attached as the working electrode. The frequency response of the system was recorded by applying a frequency-varied AC potential of 5 mV and plotted in the format of a Bode magnitude plot (Figure 5.9). In the Bode plots, the EIS spectra of the PHA film provides a slightly higher

capacitive impedance from 0.01 – 200 Hz than does the norbornene tethered SAM, which we attribute to the much greater thickness of the PHA film. The modest increase observed here suggests that PHA films are swollen in the aqueous solution, and the absence of a resistive plateau at higher frequencies indicates that they provide no measurable film resistance against ion transfer. For the EIS spectrum of the Fe^{2+} chelated film, there is substantial change in the frequency range of 100-20,000 Hz. The near plateau shown in the spectrum represents the resistance that the chelated film provides against ion migration, which results from the cross-linked structure upon Fe^{2+} chelation. This resistance of 1.42 ± 0.05 k$\Omega \cdot cm^2$ is at least 15 times greater than any resistance provided by the PHA film.

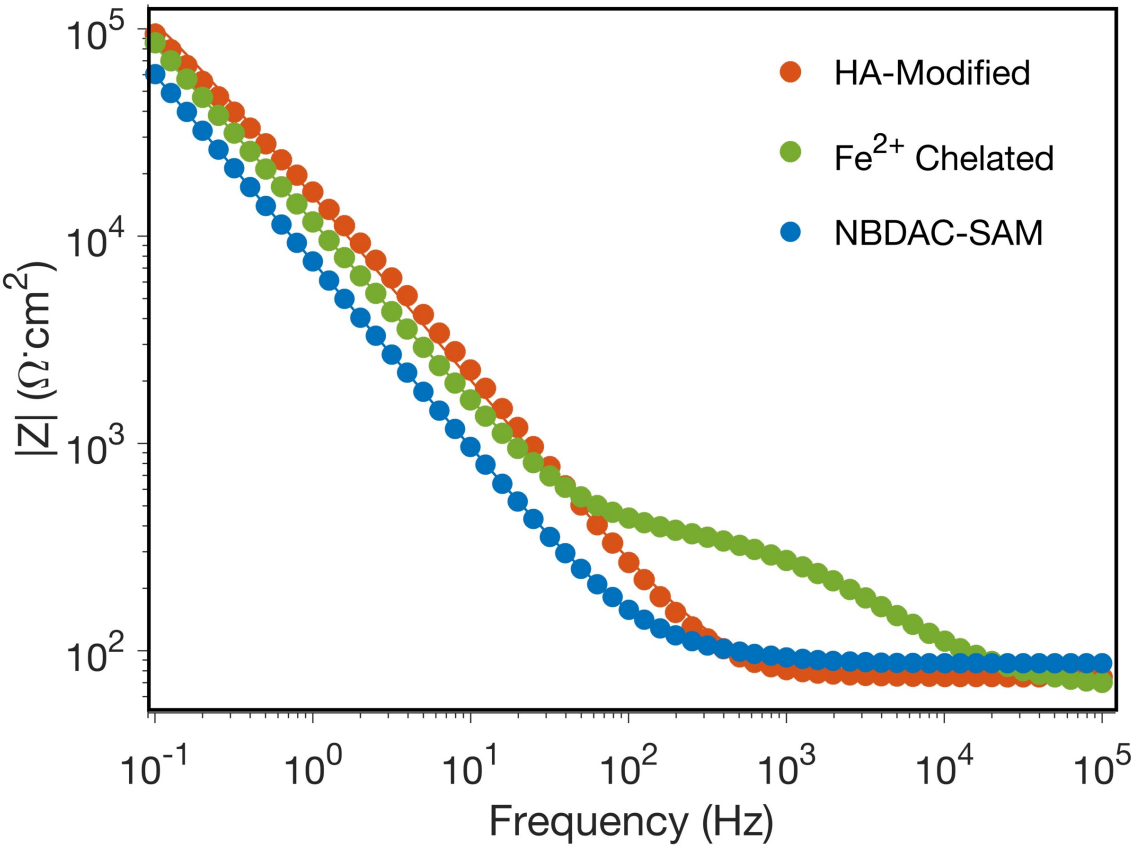

Figure 5.9. Impedance spectra in the form of Bode magnitude plots of PHA and Fe^{2+} chelated films, with the spectrum of the NBDAC-modified SAM as a control.

Metal Ion Capture with Surface Corrosion

The chelation by PHA films has been widely utilized in many applications, especially in the removal of heavy metal ions.[4,5] The chelation of metal ions in aqueous solution by PHA has been studied extensively, while the capture of metal ions released from a metal surface due to, for example, a corrosion process has gained much less attention. A few research groups utilized the hydroxamic acids as the corrosion inhibitor by forming a SAM via the reaction of hydroxamic acids and metal oxides.[27,28] However, none of them utilize the chelation property of hydroxamic acids in detection. If the metal ions liberated from surface corrosion can be easily captured by PHA films, such chelation can lead to changes in various film properties and thus, lead to detection of the corrosion process at a very early stage. Therefore, we investigated the feasibility of PHA film chelation with ions generated from a nearby corroding surface.

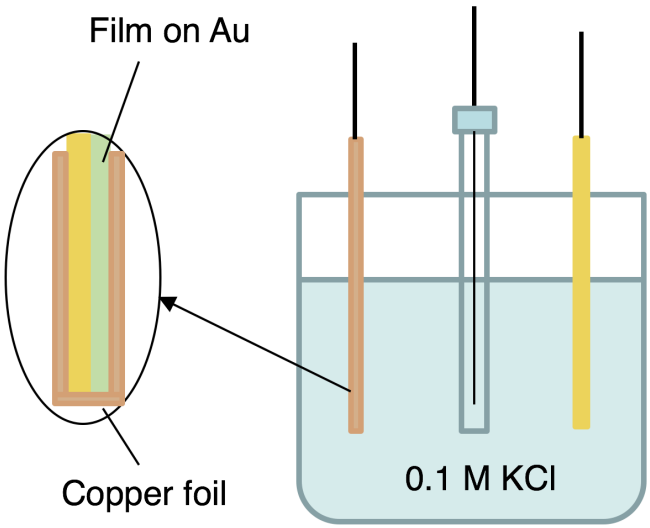

Figure 5.10. Experimental set up to investigate the chelation of local metal ions resulting from corrosion.

The experimental set up is shown in Figure 5.10. A copper foil was positioned in direct contact with the PHA film grown on a gold substrate, and this copper foil-wrapped gold substrate served as the working electrode. Constant potentials (100 mV and 300 mV) were applied for 5 min to corrode the copper at a constant rate. IR spectra of the film before and after the corrosion experiments were obtained and are shown in Figure 5.11. Changes in the carbonyl IR peaks indicate that some chelation (54%) occurs with a 5 min corrosion at 100 mV potential and additional chelation (74%) occurs with a 5 min corrosion at 300 mV. The Cu^{2+} concentration in the solution after corrosion was calculated to be 23 μM and 221μM based on the electrons transferred in the corrosion process. The 5 min chelation of PHA films in 20 μM and 200 μM copper ion solutions were also investigated as controls. No remarkable difference has been found in the IR spectra of the films before and after the 5 min copper solution soaking, which means that little to no chelation is achieved in 20 μM and 200 μM with 5 min soaking time. This solution control demonstrates that in the corrosion experiments, the ions are much more concentrated near the surface so that PHA films can capture the metal ions from the surface process easily. These results demonstrate that the PHA films in this work are sensitive to copper corrosion at the earliest stage.

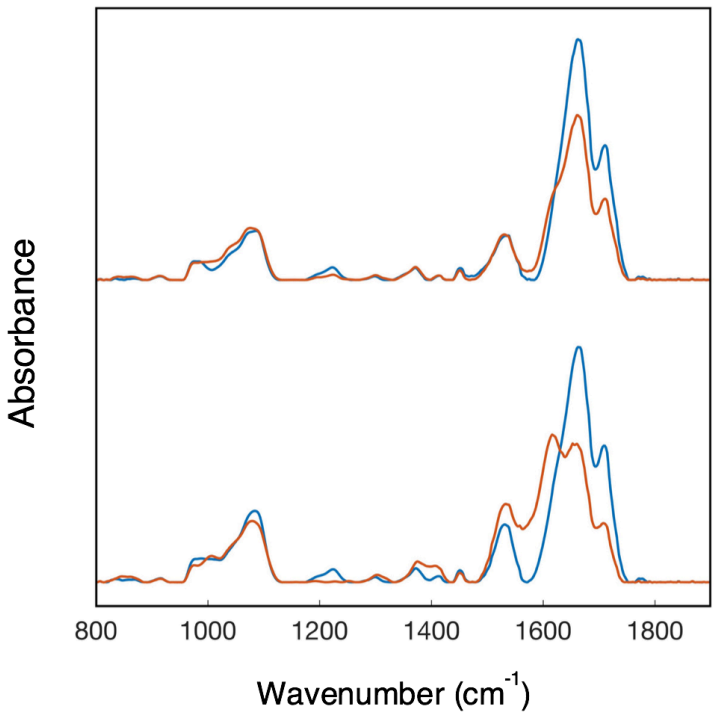

Figure 5.11. FTIR spectra of PHA films before (blue) and after (red) a 5 min exposure to a corroding copper surface at either 100 mV (top) or 300 mV (bottom) overpotentials.

Conclusions

In the Chapter, I report the successful preparation of polynorbornene films that contain pendant hydroxamic acid groups by post-polymerization modification of pNBDAC. The hydroxamic acid-modified film is prepared by the reaction of acyl chloride groups in the pNBDAC films with hydroxylamine. The chelation ability of our hydroxamic acid-modified film was investigated to show that the polymer film can chelate most divalent ions such as Fe^{2+}, Cu^{2+}, Ni^{2+}, Co^{2+}, and Zn^{2+}, with a 70% chelation degree. Lower extents of chelation (< 30 %) are achieved when the hydroxamic acid-modified polymer films are chelated with multivalent ions like Fe^{3+} and Zr^{4+}, which is attributed to the steric hindrance caused by our polymer backbone structure. The chelated structure demonstrates high stability at various pH environment from pH 1 to pH 13.

1 M HCl solution (pH 0) is able to retrieve the metal ions from the chelated film. The chelated metals within the polymer film act as cross-linkers, which remarkably enhances the pH stability, thermal stability, and resistance against ion transfer of the original film. The feasibility of chelating metal ions from surface corrosion processes is demonstrated, which creates the opportunity for the utilization of these hydroxamic acid-modified films in corrosion detection.

References

(1) Tian, F.; Roman, M. J.; Decker, E. A.; Goddard, J. M. Biomimetic Design of Chelating Interfaces. *J. APPL. POLYM. SCI.* **2015**, *41231*, 2–9.

(2) Duran, A.; Soylak, M.; Tuncel, S. A. Poly(Vinyl Pyridine-Poly Ethylene Glycol Methacrylate-Ethylene Glycol Dimethacrylate) Beads for Heavy Metal Removal. *J. Hazard. Mater.* **2008**, *155*, 114–120.

(3) Zhang, Z.; Li, J.; Song, X.; Ma, J.; Chen, L. Hg2+ Ion-Imprinted Polymers Sorbents Based on Dithizone–Hg2+ Chelation for Mercury Speciation Analysis in Environmental and Biological Samples. *RSC Adv.* **2014**, *4*, 46444–46453.

(4) Rahman, L.; Sarkar, S. M.; Mohd, M.; Abdullah, M. H. Optical Detection and Efficient Removal of Transition Metal Ions from Water Using Poly (Hydroxamic Acid) Ligand. *Sensors Actuators B. Chem.* **2017**, *242*, 595–608.

(5) Rahman, L.; Kumar, T.; Sarkar, S. M.; Yusoff, M. M.; Sani, M.; Arshad, S. E.; Musta, B. Adsorption of Rare Earth Metals from Water Using a Kenaf Cellulose-Based Poly (Hydroxamic Acid) Ligand. *J. Mol. Liq.* **2017**, *243*, 616–623.

(6) Liu, Z.; Lin, T.; Purro, M.; Xiong, M. P. Enzymatically Biodegradable Polyrotaxane-Deferoxamine Conjugates for Iron Chelation. *ACS Appl Mater Interfaces.* **2017**, *8* (39), 25788–25797.

(7) Qian, J.; Sullivan, B. P.; Peterson, S. J.; Berkland, C. Nonabsorbable Iron Binding Polymers Prevent Dietary Iron Absorption for the Treatment of Iron Overload. *ACS Macro Lett.* **2017**, *6*, 350–353.

(8) Liu, Z.; Max, P.; Qiao, J.; Xiong, M. P. Multifunctional Polymeric Micelles for Combining Chelation and Detection of Iron in Living Cells. *Adv Heal. Mater.* **2017**, *6*

(17).

(9) White, B. Supermacroporous PolyHIPE and Cryogel Monolithic Materials as Stationary Phases in Separation Science: A Review. *Anal. Methods* **2015**, *7* (17), 6967–6982.

(10) Moyna, Á.; Connolly, D.; Nesterenko, E.; Nesterenko, P. N.; Paull, B. Separation of Selected Transition Metals by Capillary Chelation Ion Chromatography Using Acetyl-Iminodiacetic Acid Modified Capillary Polymer Monoliths. *J. Chromatogr. A* **2012**, *1249*, 155–163.

(11) Winston, A.; Mazza, E. T.; Virginia, W. Hydroxamic Acid Polymers. *J. Polym. Sci.* **1975**, *13*, 2019–2030.

(12) Winston, A.; Mclaughlin, G. R.; Virginia, W. Hydroxamic Acid Polymers . II. Design of a Polymeric Chelating Agent for Iron *. *J. Polym. Sci.* **1976**, *14*, 2155–2165.

(13) Kumar, S. A.; Pandey, S. P.; Shenoy, N. S.; Kumar, S. D. Matrix Separation and Preconcentration of Rare Earth Elements from Seawater by Poly Hydroxamic Acid Cartridge Followed by Determination Using ICP-MS. *Desalination* **2011**, *281*, 49–54.

(14) Roman, M. J.; Decker, E. A.; Goddard, J. M. Fourier Transform Infrared Studies on the Dissociation Behavior of Metal-Chelating Polyelectrolyte Brushes. *ACS Appl. Mater. Interfaces* **2014**, *6*, 5383–5387.

(15) Agrawal, Y. K.; Kaur, H.; Menon, S. K. Poly (Styrene- p -Hydroxamic Acids): Synthesis , and Ion Exchange Separation of Rare Earths. *React. Funct. Polym.* **1999**, *39*, 155–164.

(16) Escobar, C. a; Harl, R. R.; Maxwell, K. E.; Mahfuz, N. N.; Rogers, B. R.; Jennings, G. K. Amplification of Surface-Initiated Ring-Opening Metathesis Polymerization of 5-(Perfluoro-n-alkyl)Norbornenes by Macroinitiation. *Langmuir* **2013**, *29*, 12560–12571.

(17) Njoroge, I.; Kempler, P.; Deng, X.; Arnold, S.; Jennings, G. K. Surface-Initiated Ring-

Opening Metathesis Polymerization of Dicyclopentadiene from the Vapor Phase. *Langmuir* **2017**.

(18) Deng, X.; Njoroge, I.; Kane Jennings, G. Surface-Initiated Polymer/Ionic Liquid Gel Films. *J. Phys. Chem. C* **2018**, *122* (11), 6033–6040.

(19) Kobayashi, M.; Takahara, A. Tribological Properties of Hydrophilic Polymer Brushes under Wet Conditions. *Chem. Rec.* **2010**, *10* (4), 208–216.

(20) Zomorodian, A.; Garcia, M. P.; Moura E Silva, T.; Fernandes, J. C. S.; Fernandes, M. H.; Montemor, M. F. Corrosion Resistance of a Composite Polymeric Coating Applied on Biodegradable AZ31 Magnesium Alloy. *Acta Biomater.* **2013**, *9* (10), 8660–8670.

(21) Faulkner, C. J.; Fischer, R. E.; Jennings, G. K. Surface-Initiated Polymerization of 5-(Perfluoro-n-Alkyl)Norbornenes from Gold Substrates. *Macromolecules* **2010**, *43* (3), 1203–1209.

(22) Edmondson, S.; Osborne, V. L. V.; Huck, W. T. S. W. Polymer Brushes via Surface-Initiated Polymerizations. *Chem. Soc. Rev.* **2004**, *33* (1), 14–22.

(23) Olivier, A.; Meyer, F.; Raquez, J. M.; Damman, P.; Dubois, P. Surface-Initiated Controlled Polymerization as a Convenient Method for Designing Functional Polymer Brushes: From Self-Assembled Monolayers to Patterned Surfaces. *Prog. Polym. Sci.* **2012**, *37* (1), 157–181.

(24) Sutton, P. A.; Buckingham, D. A. Cobalt (III) -Promoted Hydrolysis of Amino Acid Esters and Peptides and the Synthesis of Small Peptides. *Acc. Chem. Res.* **1987**, *20* (10), 357–364.

(25) Fife, T. H.; Przystas, T. J. Divalent Metal Ion Catalysis in the Hydrolysis of Esters of Picolinic Acid . Metal Ion Promoted Hydroxide Ion and Water Catalyzed Reactions. *J.*

Am. Chem. Soc. 1985, **1985**, *9* (14), 1041–1047.

(26) Martell, A. E. CHELATION: STABILITY AND SELECTIVITY. *Ann. N. Y. Acad. Sci.* **1960**, *88* (2), 284–292.

(27) Alagta, A.; Felhösi, I.; Bertoti, I.; Kálmán, E. Corrosion Protection Properties of Hydroxamic Acid Self-Assembled Monolayer on Carbon Steel. *Corros. Sci.* **2008**, *50* (6), 1644–1649.

(28) Shaban, A.; Kálmán, E.; Telegdi, J. An Investigation of Copper Corrosion Inhibition in Chloride Solutions by Benzo-Hydroxamic Acids. *Electrochim. Acta* **1998**, *43* (1–2), 159–163.

CHAPTER VI

PH-RESPONSIVE CARBOXYLIC ACID/ESTER COPOLYMER FILMS PREPARED BY SIMPLE MODIFICATION OF POLY(NORBORNENE DIACYL CHLORIDE)

Introduction

Polymer films that undergo significant physical or chemical property changes in response to surrounding stimuli, such as temperature, pH, chemical agents, magnetic fields, or electrical fields, have gained abundant attention from the scientific world.[1–3] Among them, pH-responsive polymer films have been largely studied due to their wide applications in biomedicine,[4,5] membranes,[6–9] dynamic surfaces,[10] and chemical sensors.[11] pH-responsive behavior is generally achieved by the ionization/deionization of certain groups at various pH levels through protonation or deprotonation.[1,12,13]

The majority of preparations of pH-responsive films is by direct deposition of premade hydrogel polymers, which are typically prepared by either mixing appropriate polymers or synthesizing block copolymers.[14–17] Several groups also have made achievements in the preparation of pH-responsive films with surface-initiated polymerization, such as surface-initiated atom transfer radical polymerization (SiATRP),[18–20] surface-initiated reversible addition-fragmentation chain transfer polymerization (SiRAFT),[21] and surface-initiated nitroxide mediated polymerization (SiNMP).[22] ATRP is applied by many groups due to the wide variety of commercially available monomers to tailor film compositions. However, another highly controllable polymerization method with rapid polymerization rate, ring-opening metathesis polymerization (ROMP),[23–25] has not been utilized for the preparation of pH-responsive materials,

which may be due to the fewer commercially available functional ROMP monomers and limitations of reactivity with some that are available. For example, the carboxylic acid is one of the major moieties utilized in pH-responsive materials. However, the catalysts often used in ROMP are not tolerant of carboxylic acid groups,[26,27] which limits the investigation of pH-responsive carboxylic acid-related materials prepared by ROMP.

In Chapter IV, I presented an easy and efficient method to introduce various functionalities, including carboxylic acids, in films prepared by ROMP. Here, I report a unique approach to prepare pH-responsive, random copolymer films via surface-initiated ROMP and post-polymerization modification, which offers several advantages. First of all, the polymerization method, utilizing SiROMP provides rapid polymerization and great control over film thickness, which allows for the application of pH-responsive films in different levels of thickness. In addition, the unique post-polymerization method introduced in Chapter IV offers great control over copolymer composition, which is favorable for the design of thin films with large pH-responsive changes in properties. Furthermore, the surface-initiated method enables film attachment on surfaces of almost any geometry, which is favorable in biomedical applications and membrane processes.

Experimental Section

Polymerization of NBDAC and Modification to Copolymer Films.

Polymerization of pNBDAC was accomplished in the vapor phase. The ROMP-active substrates removed from the DCM solution of Grubbs 3rd generation catalyst were quickly rinsed with DCM, dried in a stream of nitrogen, and immediately placed into a pre-heated reaction vial

(65 °C) containing NBDAC monomers. The reaction vial is shown in Figure 4.1. NBDAC monomers were then polymerized from the vapor phase to form a smooth thin film. After the surface-initiated polymerization in the vial, the substrates were quickly rinsed with DCM to remove extra monomer on the film surface and then directly exposed to water-ethanol mixtures for 15 min to achieve a partial modification of the film, followed by a second modification with a 50/50 acetone/pH 4 aqueous solution mixture for overnight to obtain the carboxylic acid/ester copolymer film.

Preparation of Buffer Solutions.

pH buffer solutions were prepared according to the procedure in previous literature[12,28] except that NaH_2PO_4 was used instead of KH_2PO_4 and pH 9 buffer solution was prepared by mixing appropriate volumes of 0.1 M Na_2CO_3 with 0.1 M $NaHCO_3$.

Characterization Methods.

Polarization modulation-infrared reflectance-absorption spectroscopy (PM-IRRAS) was performed to estimate the composition of the copolymer films based on the C=O absorbance at different wavenumbers.

The C=O absorbance due to carboxylic acid is at 1732 cm^{-1}, which is not distinguishable comparing to the C=O absorbance due to ester (at 1739 cm^{-1}). Thus, to obtain the copolymer composition, the prepared copolymer films were exposed to a 50/50 acetone/pH 9 buffer solution mixture to convert the carboxylic acid contents to carboxylate. The C=O absorbance due to carboxylate is at 1560 cm^{-1}, which is distinguishable when comparing to the C=O absorbance due to ester (1739 cm^{-1}).

Reference peak ratios were obtained for normalization. Since the infrared intensity of the same number of C=O bonds in different molecular structural environments may vary, the relationship between the areas of C=O absorption bands due to different molecular groups should be obtained to determine the composition. The ratios of the C=O absorption bands before and after the modification were collected for pure ester-modified and carboxylate-modified films as Figure 6.1 shows. The adsorption bands in Figure 6.1 were integrated, and the reference ratios were calculated by Eq.6.1 and Eq. 6.2.

$$r_{ester} = \frac{A_{acyl\ chloride}}{A_{ester}} \tag{6.1}$$

$$r_{carboxylate} = \frac{A_{acyl\ chloride}}{A_{carboxylate}} \tag{6.2}$$

With r_{ester} and $r_{carboxylate}$ calculated, all the areas used in the calculation of copolymer composition can be normalized to the area for the acyl chloride of the original film.

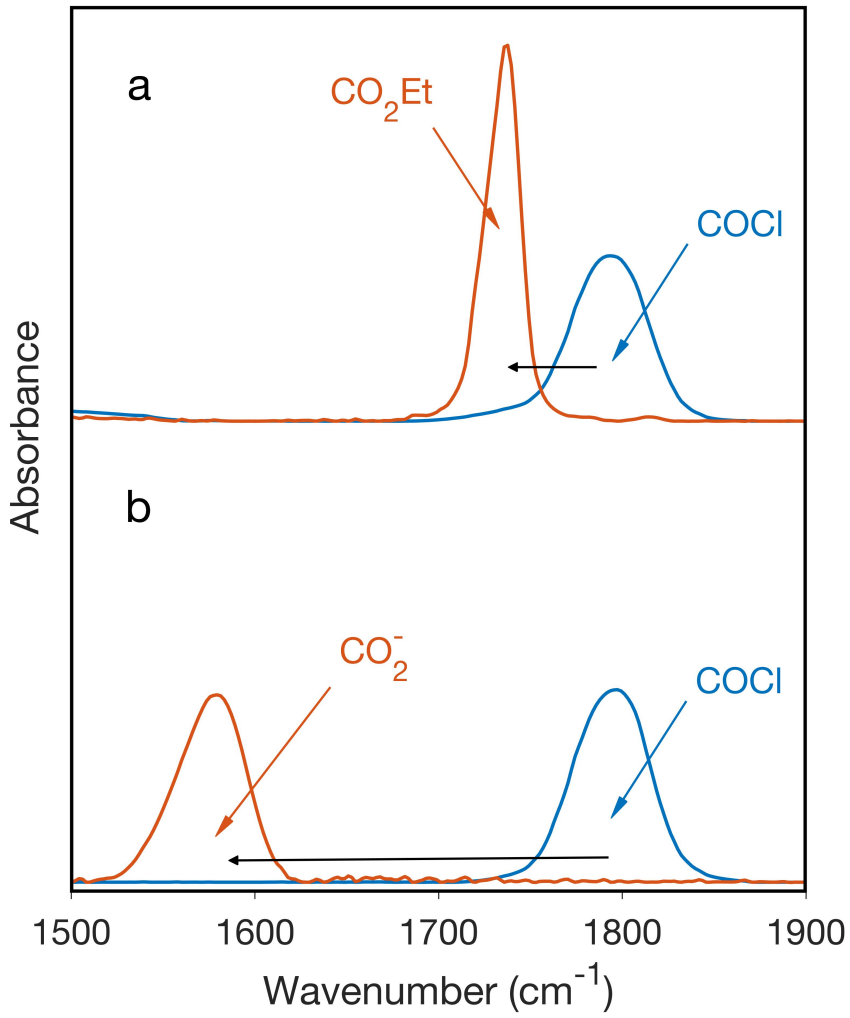

Figure 6.1.(a) IR spectra of the original pNBDAC film (blue; before modification) and a pure ester-modified film (red; after modification) prepared by exposing the pNBDAC film ethanol. (b) IR spectra of the original pNBDAC film (blue; before modification) and the carboxylate-modified film (red; after modification) prepared by exposing the pNBDAC film to water and then pH 9 buffer solution.

IR spectra of the prepared copolymer films after exposed to a 50/50 acetone/pH 9 buffer solution mixture are shown in Figure 6.2. To obtain the ester composition of the film, the peak

areas of the C=O absorbance due to carboxylate and ester were normalized with the C=O absorbance due to the acyl chloride as the reference (see Figure 6.1), and the following equations were used:

$$\text{ester } \% = \frac{A_{co_{ester}} r_{ester}}{A_{co_{ester}} r_{ester} + A_{co\_carboxylate} r_{carboxylate}} \tag{6.3}$$

where $A_{co_{ester}}$ is the area of the ester carbonyl absorption band, and $A_{co\_carboxylate}$ is the area of carboxylate carbonyl absorption band in the spectrum of copolymer. Since all acid chlorides in the film are converted during the reaction, the percentage of carboxylates within the film is simply the difference between the ester % of Eq. 6.3 and 100%.

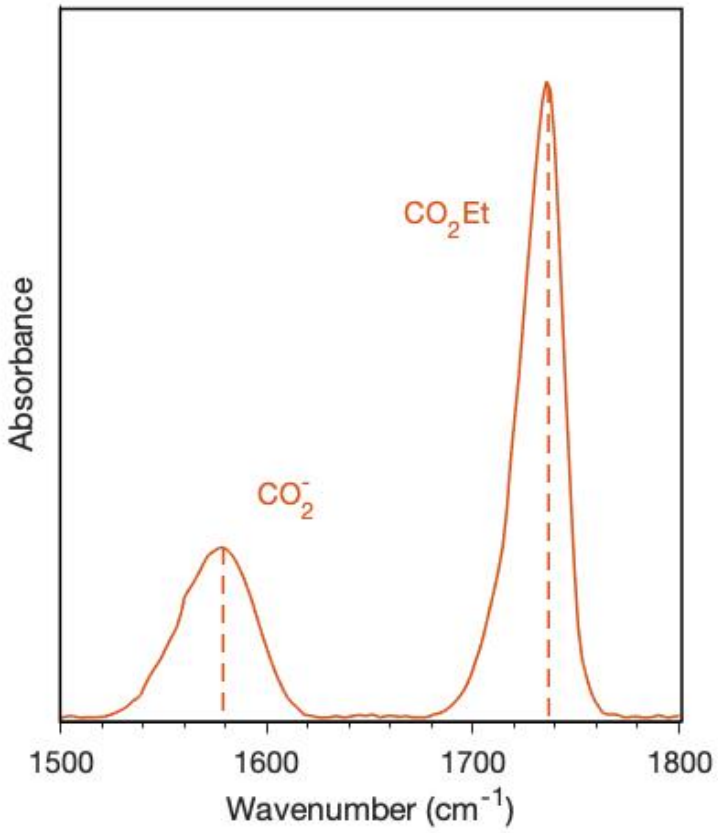

Figure 6.2. The sample spectrum of the ester/carboxylic acid copolymer exposed to pH 9 buffer solution. The areas of the absorption bands were determined, and the composition of the copolymer can be calculated as Eq.6.3.

Results and Discussion

Copolymer Preparation

After the pNBDAC films were prepared via SiROMP, they were immediately exposed to ethanol-water mixtures and characterized after the film modification by PM-IRRAS. Since the absorption band due to C=O stretching in the ester is close to the one due to C=O stretching in the carboxylic acid, the films were exposed to a 50/50 mixture of acetone/pH 9 buffer solution to deprotonate the carboxylic acid groups to carboxylates. Figure 6.3 shows the IR spectrum of the original pNBDAC film and the representative IR spectra of the copolymer films after exposure to pH 4 and pH 9. The spectrum of the pNBDAC film shows absorption bands due to C=O stretching in the acyl chloride (1794 cm^{-1}), the Csp^3-H in-plane bending (1430-1500 cm^{-1}), the Csp^3-H out-of-plane bending (1300-1400 cm^{-1}), and the Csp^2-H out-of-plane bending (900-1100 cm^{-1}). Compared to the spectrum of pNBDAC, the IR spectrum of the film after exposure to the ethanol/water mixture shows a shift of the absorption band due to C=O stretching (1736 cm^{-1}). The broad C=O absorption band at 1736 cm^{-1} results from the overlapping of C=O absorption from the ester (1739 cm^{-1}) and C=O absorption from the carboxylic acid (1732 cm^{-1} or 1710 cm^{-1}). Comparatively, an absorption band due to C=O stretching in the carboxylate (1560 cm^{-1}) appears in the IR spectrum of the copolymer exposed to pH 9, which demonstrates the successful preparation of ester/carboxylic acid copolymer films by modifying pNBDAC films with two different reagents. The ester composition of the copolymer films can be obtained by using Eq.6.3.

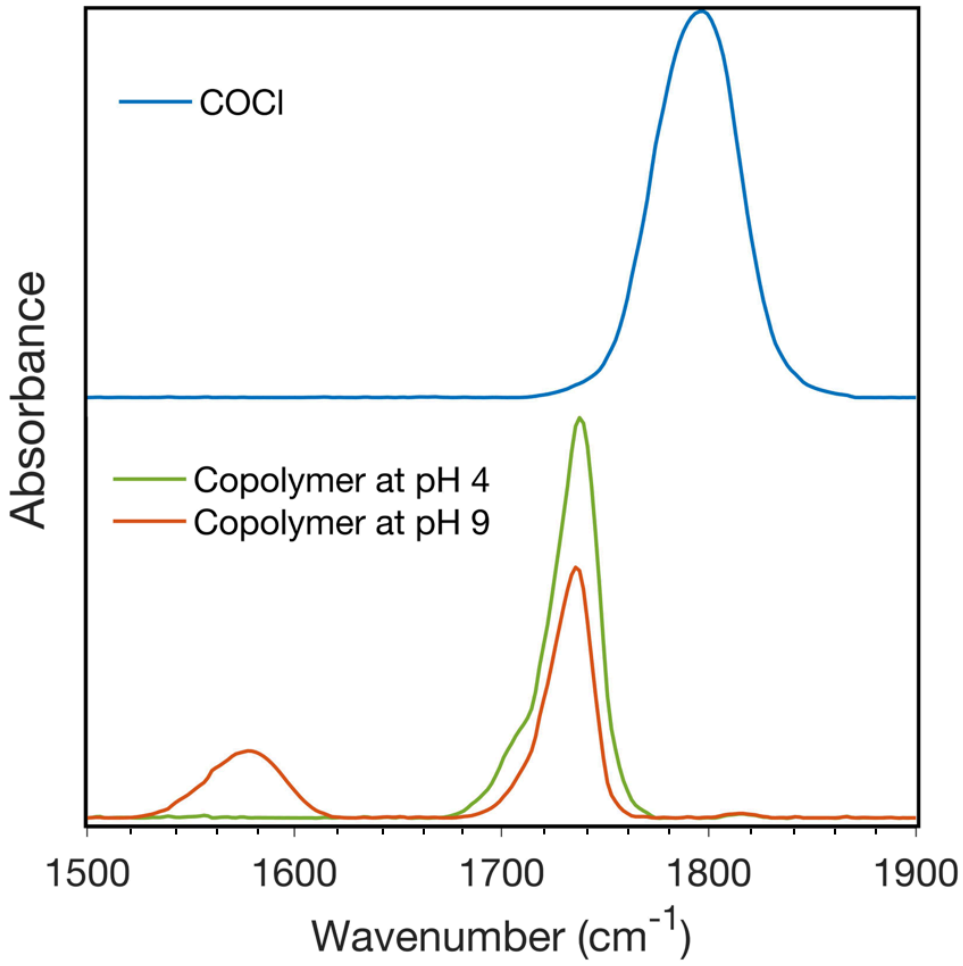

Figure 6.3. IR spectra of the original pNBDAC film and the ester/carboxylic acid copolymer film after exposure to buffer solutions at pH 4 and pH 9.

Investigation of Copolymer Composition

One approach to tailor the film composition is to control the ratio of ethanol to water in the modification step. To determine the feasibility of this method of control, we modified pNBDAC films with ethanol-water mixtures containing various mole fractions of ethanol in the mixture, and we measured the mole fractions of ester groups in the films with PM-IRRAS. The ester mole

percentages in the film are plotted versus the mole fraction of ethanol in the modifying mixtures in Figure 6.4.

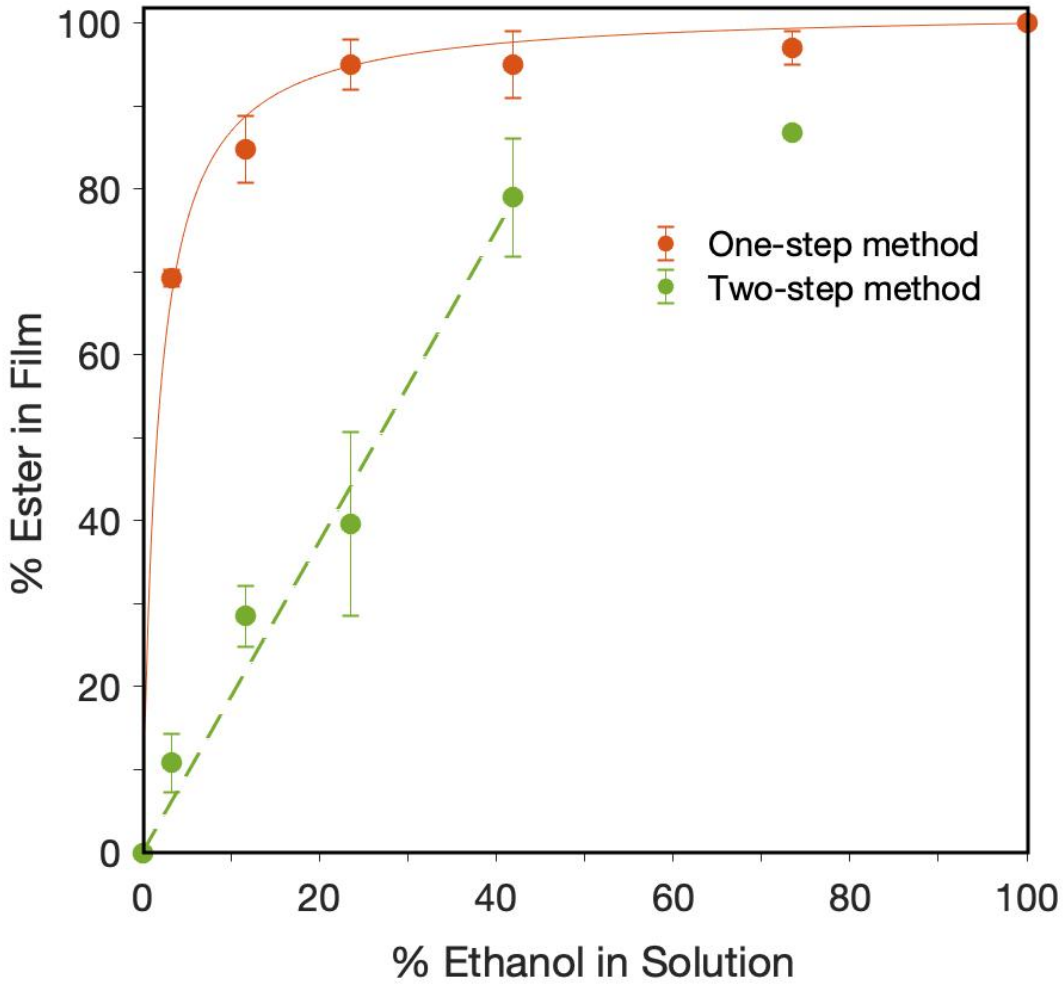

Figure 6.4. Plot of ester molar composition in the resulting film versus the ethanol molar composition in the modifying solution for both one-step and two-step methods. For the two-step method, the x-axis represents the ethanol solution composition in the 15-min first-step exposure. The film was subsequently exposed to an acetone/pH 4 aqueous solution to convert the remaining acyl chlorides to carboxylic acids.

Figure 6.4 shows that even with a percentage as low as 5% of ethanol used in the reagent mixture for modification, we still obtain a high percentage of ester (68 %) in the resulting film, which shows that ethanol dominates the reaction with the pendant acyl chlorides over that of water. To quantify the reactivity difference of ethanol and water with the pNBDAC films, the composition data were fit with a model. The reaction rate of acyl chloride groups with ethanol and water can be written as Eq 6.4 and Eq 6.5.

$$r_E = \frac{dC_{Ester}}{\partial t} = k_E[Ethanol]C_{unreacted} \tag{6.4}$$

$$r_W = \frac{dC_{Acid}}{\partial t} = k_W[Water]C_{unreacted} \tag{6.5}$$

where r_E represents the reaction rate of acyl chloride with ethanol, r_W is the reaction rate with water, k_E and k_W are the corresponding rate constants, $[Ethanol]$ and $[Water]$ are the concentrations of ethanol and water in the mixture. C_{Ester}, C_{Acid}, and $C_{unreacted}$ represent the concentrations of esters, carboxylic acids, and unreacted acyl chlorides in the film. Dividing Eq 6.5 by Eq.6.4 yields

$$\frac{\theta_{Ester}}{\theta_{Acid}} = \frac{r_E}{r_W} = \frac{k_E[Ethanol]}{k_W[Water]} \tag{6.6}$$

where θ_{Ester} is the fraction of esters in the film and θ_{Acid} is the fraction of carboxylic acid groups in the film. Therefore, θ_{Ester} can be expressed as Eq 6.7 and further derived to Eq 6.8 with [Ethanol]/[Water] expressed in terms of an ethanol percentage (E%),

$$\theta_{Ester} = \frac{k_E[Ethanol]}{k_E[Ethanol] + k_W[Water]} \tag{6.7}$$

$$\theta_{Ester} = \frac{\left(\frac{k_E}{k_W}\right)}{\left(\frac{k_E}{k_W}\right) + \frac{1 - E\%}{E\%}} \tag{6.8}$$

By fitting the experimental data with the model, the reaction rate ratio (k_E/k_W) was calculated to be 60 ± 10, quantifying that the reaction of acyl chloride with ethanol is much faster rate than that with water. The much faster reaction rate with ethanol is due to the hydrophobic structure of the polynorbornene-based polymer backbone. The hydrophobic backbone structure results in much lower affinity of water than ethanol within the polymer film, so that the concentration of ethanol within the film is greater than that of water. Therefore, as ethanol dominates the reaction, the curve in Figure 6.4 shows that a small change in ethanol concentration under dilute ethanol conditions can result in a huge difference in the resulting film composition. This sensitivity to ethanol composition shows that we have limited control over film composition if we seek to prepare a copolymer film with a comparatively high percentage of carboxylic acid groups.

I then utilized a two-step modification process to prepare the ester/carboxylic acid copolymer films to obtain a greater control over a broader range of film compositions. Instead of reacting the pNBDAC films in the ethanol-water solution overnight to ensure full completion, we chose to shorten the reaction time to 15 min to achieve a partial modification of the pNBDAC films. In this situation, the percentage of the ester groups in the partially modified films should depend approximately linearly on the concentration of ethanol in the mixture, and thus, we can achieve a greater control over the composition in the films. The partially modified films contained

an intermediate molar percentage of ester groups, a small percentage of carboxylic acids, and the balance of unreacted acyl chloride groups. After the partial modification, the films were exposed to an acetone/pH 4 aqueous solution mixture to convert the remaining acyl chloride groups to carboxylic acids. The resulting films were characterized with IR, and the ester film composition versus ethanol solution composition is also shown in Figure 6.4. The ester composition in the copolymer films is approximately linearly dependent on the concentration of the ethanol in the modifying solution of the first step when the ethanol composition is in the range of 0 – 40% molar. This partial modification method can be used to prepare copolymers with small to large percentages of ester in the final copolymer films with good controllability. These copolymer methods can be extended to prepare other types of copolymer films as long as the functionalities can be achieved via post-polymerization modification of pNBDAC.

pH-Responsive Properties in Ion Transport

The effect of copolymer film composition on the ion transport is shown with impedance spectra in Bode format in Figure 6.5. A pNBDAC film modified with pure ethanol to achieve a homopolymer with ethyl ester side chains exhibits a capacitive spectrum, indicating that the film effectively blocks electrolyte transport. In contrast, a pNBDAC film modified with pure water to achieve a homopolymer with carboxylic acid side chains exhibits a low impedance that is barely higher than a SAM control that is 300x thinner, even at pH 4 at which the carboxylic acids are in the more hydrophobic, protonated form. These results suggest that copolymer films with higher ester mole fractions will exhibit greater barriers to water and ion transport.

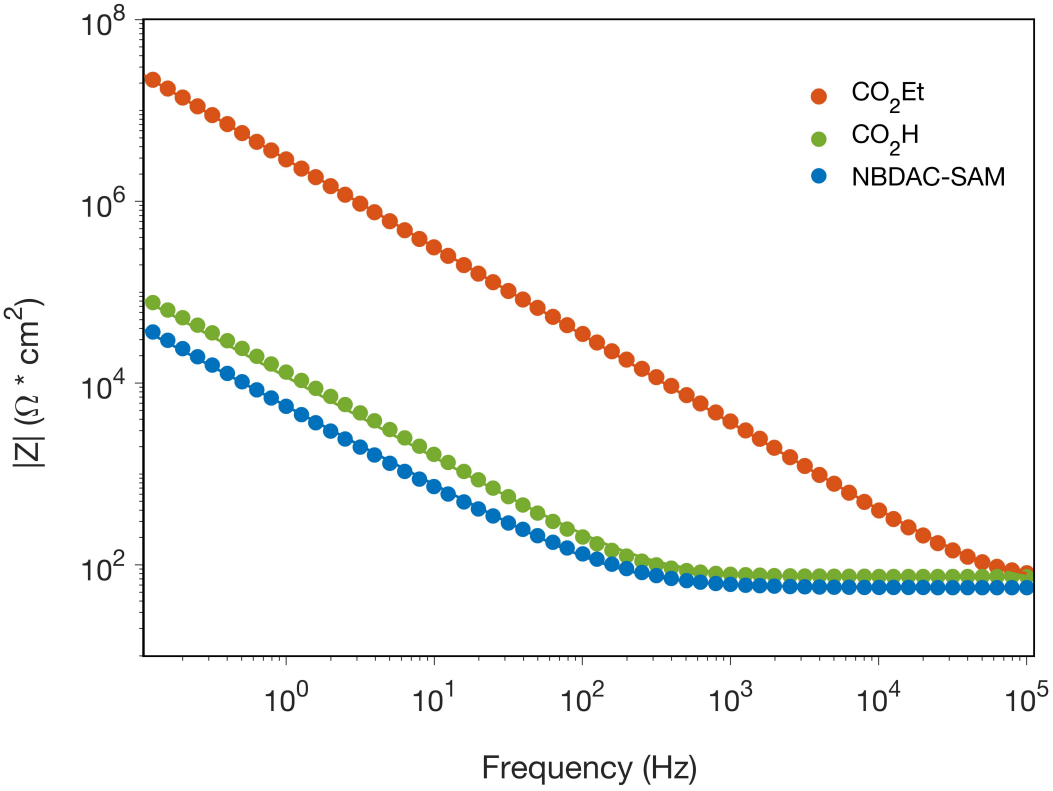

Figure 6.5. EIS spectra of pure ester-modified film, pure carboxylic acid-modified film, and the norbornene-terminated SAM film. The electrolyte consisted of 0.1 M KCl.

The hydrophilicity of these ester/carboxylic acid copolymer films is affected by pH, depending on the degree of deprotonation of the acids. The barrier properties of the films toward ion transport in aqueous solution, therefore, are expected to show a pH-responsive behavior. EIS was used to characterize the effect of pH and film composition on the ion transport properties of the ester/carboxylic acid copolymer films with pH buffer solutions as the electrolytes. EIS measurements for the copolymer films with various compositions were obtained at a wide range of pH from 4 to 11. Figure 6.6 shows Bode magnitude plots of the EIS spectra for films with 25%

and 39% carboxylic acids. The corresponding phase angle plots of the EIS measurements are shown in Appendix B.

For a film with 25% carboxylic acid (Figure 6.6b), the film impedance mildly decreases with pH from 4 to 8 due to the gradual deprotonation of the carboxylic acids to elevate water content within the film and thereby increase film capacitance (reduce capacitive impedance). These effects are also consistent with the decreased slope of the spectrum at pH 8, which indicates the film is acting as a leaky capacitor. As pH is increased from 8 to 9, a dramatic drop of the film impedance is observed, and in fact, the resistance that the film provides against ion transfer decreases from nearly 10^6 at pH 8 to ~10^2 at pH 9. Over this critical range, the concentration of deprotonated carboxylates within the film has reached a threshold where water and ions can now rapidly diffuse throughout the film structure to reach the SAM-coated electrode interface. The EIS spectra from pH 9 to 11 show no film impedance imparted by the copolymer film. Similarly, EIS spectra of the copolymer film with 39% carboxylic acids (Figure 6.6a) also show pH-responsive character, except that the dramatic decrease of the film impedance happens from pH 6 to pH 7 in this case. The increased percentage of carboxylic acid groups provides a more hydrophilic copolymer film that can reach the critical deprotonation threshold at lower pH. Therefore, copolymer composition can be utilized to adjust the critical pH of these pH-responsive copolymer films, where a dramatic decrease of impedance occurs.

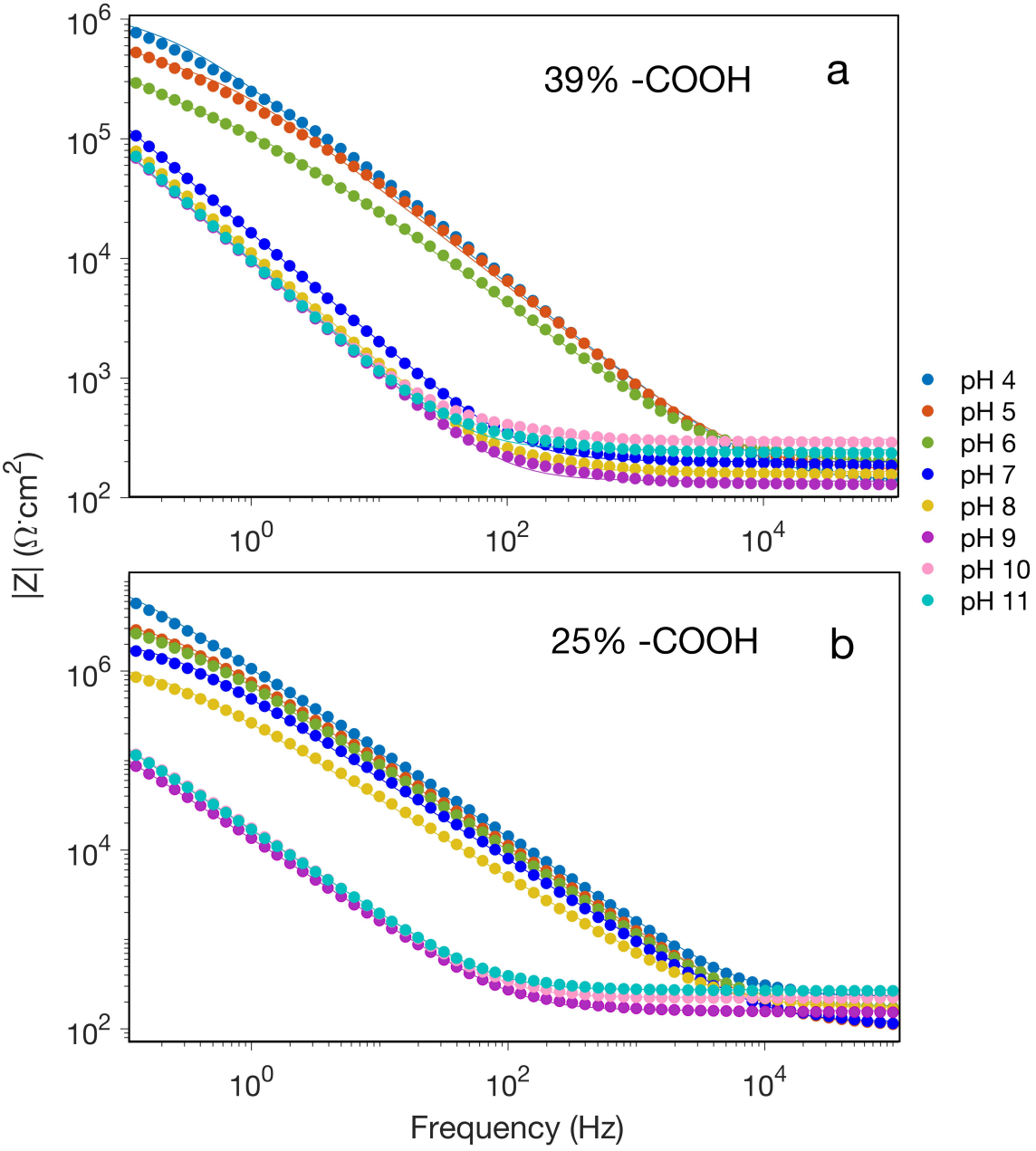

Figure 6.6. pH-dependent EIS spectra of a copolymer film that contains (a) 39% carboxylic acids and (b) 25% carboxylic acids. Solid lines indicate fits of the spectra based on the equivalent circuit model of Figures 3.3 and 3.4.

EIS spectra of ester/acid copolymer films with other compositions (14 % and 49 % -CO_2H) were also collected as Bode plots in Figure 6.7. Different from the copolymer films shown in Figure 6.6, the two films in Figure 6.8 show milder pH-responsive behavior. Considering that the

backbones of these copolymer films are repeating cyclopentyl units, which contribute toward the hydrophobicity of the film, the copolymer film with 14% acid contains a low volume fraction (< 5%) of pH-sensitive -CO_2H groups. Thus, the effect in Figure 6.7b is a slight reduction in capacitive impedance with increasing pH from 4 to 11, with no critical pH observed over this range. This film with low acid content is ideal for applications where a fine tuning of barrier properties with pH is desired. Figure 6.7a shows the opposite case, in which the copolymer film contains a high concentration of carboxylic acid groups so that even at low pH values, the hydrophilicity of the film is already sufficient to swell the film, and as such, ions can transfer directly to the interface with low impedance. This film shows small film resistances at pH 4 and 5 in which the carboxylic acid groups are protonated but no measurable resistances at pH 6 or higher where deprotonation occurs.

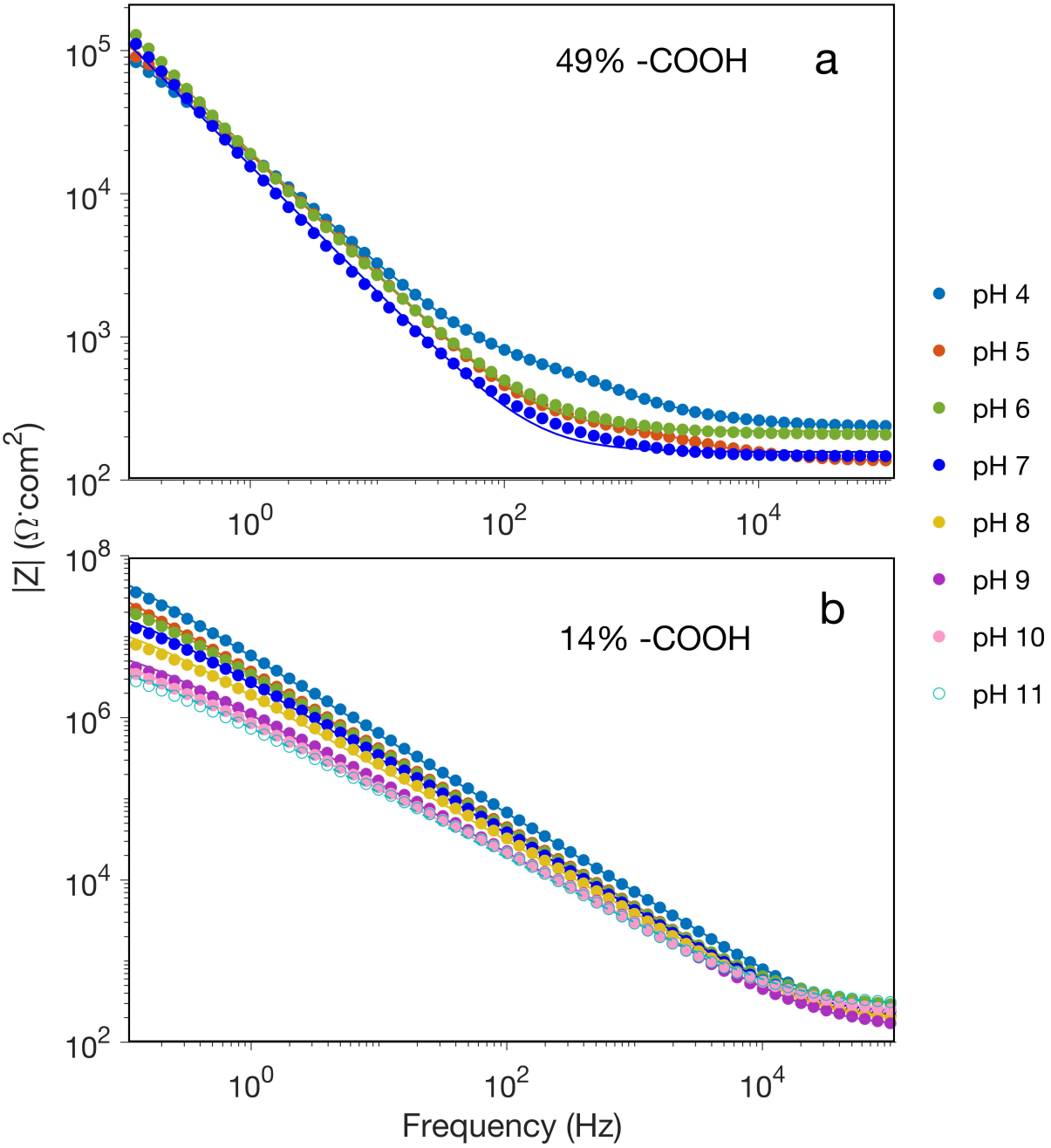

Figure 6.7. pH-dependent EIS spectra of a copolymer film that contains (a) 49% carboxylic acids and (b) 14% carboxylic acids. Dashed lines indicate fits of the spectra based on the equivalent circuit model of Figure 3.3 and 3.4.

The EIS spectra are all fitted with proper equivalent circuits to calculate the film resistances of these copolymer films at each pH. Figure 6.8 shows the calculated polymer film resistances against ion transfer versus pH values. At the same pH, copolymer films with higher carboxylic acid content have lower film resistances, which is consistent with our previous explanation that higher carboxylic acid content reduces the hydrophilicity of the film, resulting in improved interaction of the film with water and lower barrier properties against ion transfer. Also, the critical pH of the pH-responsive barrier properties can be altered via the change of the film composition. Generally, the critical pH for ion transport is reduced by increasing carboxylic acid fraction in the copolymer film. From Figure 6.8, this simple approach of copolymer film preparation where film composition is based on that of a water-ethanol solution, provides a versatile method to design and control the pH-responsive behavior across a wide range of pH values.

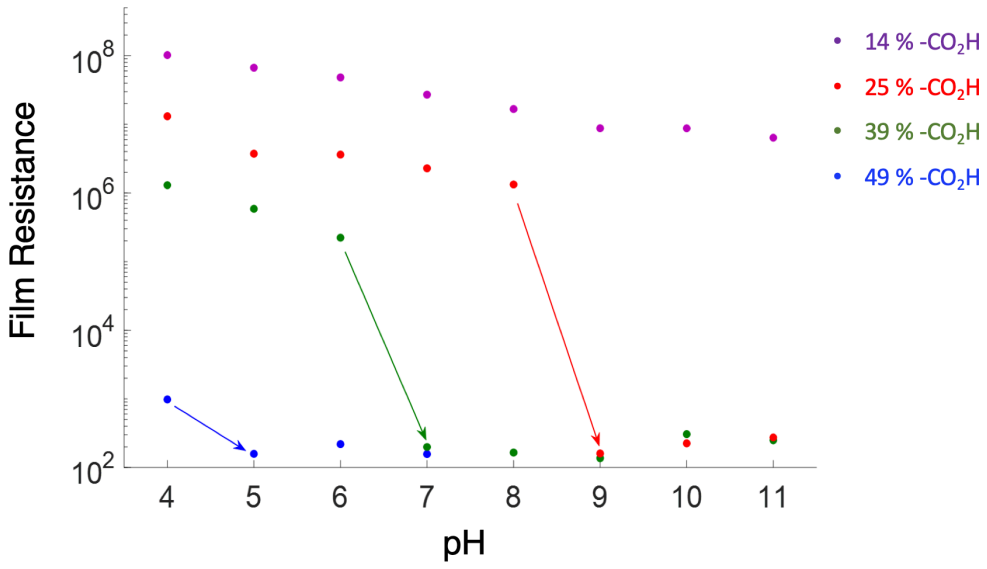

Figure 6.8. Film resistance of copolymer films with different carboxylic acid compositions (mole %) at different pH levels.

Prior research on pH-responsive films by Bai et al.[12] focused on polymethylene-based copolymer films that contained dilute (<5%) molar fractions of carboxylic acids with a small percentage of unreacted ester groups. These films were grown by a surface-catalyzed polymerization specific to gold surfaces in the presence of mixtures of diazomethane and ethyl diazoacetate in ether. The large ~10^4 pH-induced change in film resistance observed here is similar to that reported by Bai et al. The similarity of these dramatic changes is not coincidental as deprotonation of a carboxylic acid to a carboxylate increases the water-octanol partition coefficient of that molecule by a factor of 10^4.[30] Thus, an increase in pH above the critical threshold enhances the interaction of these copolymer groups with water dramatically, on a scale that is comparable to the observed change in film resistance. The advances of the present approach over that of Bai et al. are that the present films are not limited to gold surfaces, film thicknesses can be widely controlled via SiROMP, independent of the final copolymer composition, and copolymer film composition is easily adjusted based on the ethanol-water solution ratio. In addition, the work by Bai et al. did not examine the polymer-water interaction to determine film swelling, as done here (below).

pH-responsive Water Interactions in the Copolymer Film

QCM-D was employed to characterize the interaction of water with the ester/acid copolymer film from pH 11 to 4. QCM-D allows precise measurements of frequency shifts and energy dissipation of a QCM crystal upon loading by a film. Mass loading on the quartz crystal will result in a decrease in the frequency of oscillation, while the change in energy dissipation is directly related to the interaction of the aqueous medium with the polymer film. The frequency and dissipation values for a clean quartz crystal sensor were first collected in a flowing stream of

ultrapure water, and these values for the clean quartz crystal were used as baselines. We then modified the gold part of the crystal sensor to grow an ester/acid copolymer film (34% acid) via SiROMP and subsequent modification as described above.

Figure 6.9 shows the changes in frequency (Δf) and energy dissipation (ΔD) over time for the copolymer-coated crystal as the pH of the buffer solution was incrementally altered from 11 to 4. A large decrease in frequency and a corresponding increase in dissipation occur after the attachment of the copolymer film and exposure to pH 11 buffer. These changes are consistent with the successful addition of a swollen copolymer mass to the quartz crystal. As pH of the aqueous flow is decreased, the frequency increases and dissipation decreases. From pH 11 to 8, the changes in frequency and dissipation are modest, but as pH is further decreased from 8 to 6, more significant jumps in frequency and drops in dissipation are observed, followed again by more gradual changes when pH is reduced to lower values. The Δf as compared to the baseline value correlates with the mass added to the quartz crystal, which has contributions from both film deposition and aqueous solution-film interaction. The stronger the interaction of the film with the aqueous solution, the more "mass" is added to the crystal. Thus, while the copolymer mass is constant with pH, the decrease in Δf (increase in absolute frequency) as pH is reduced represents a weaker interaction of water in the copolymer film. The dramatic decrease in Δf from pH 8 – 6 shows that the film deswells significantly over this range, to dispel the solution as carboxylates are protonated to achieve a more hydrophobic film. Similarly, this evacuation of aqueous solution from the film leads to less energy dissipation during the oscillation, which explains the decreasing trend of dissipation as pH is reduced in Figure 6.9. These results are consistent with the EIS results in Figures 6.6 and 6.8 for a film with similar carboxylic acid content of 39% that show major changes in barrier properties over a similar range of pH.

We fit the results from QCM-D with the Kelvin-Voigt model and obtained the calculated thickness in different pH flows. Figure 6.10 shows that at lower pH, the copolymer film is in a contracted state and the film thickness is less than 100 nm, while at higher pH, the copolymer film is swollen by almost 4x so that the overall thickness significantly increases to more than 200 nm. Figure 6.10 demonstrates the pH-triggered change of film structure and explains the pH-responsive properties of the copolymer film. The major change happens between pH 6 and pH 8 for the copolymer film with 34% carboxylic acid.

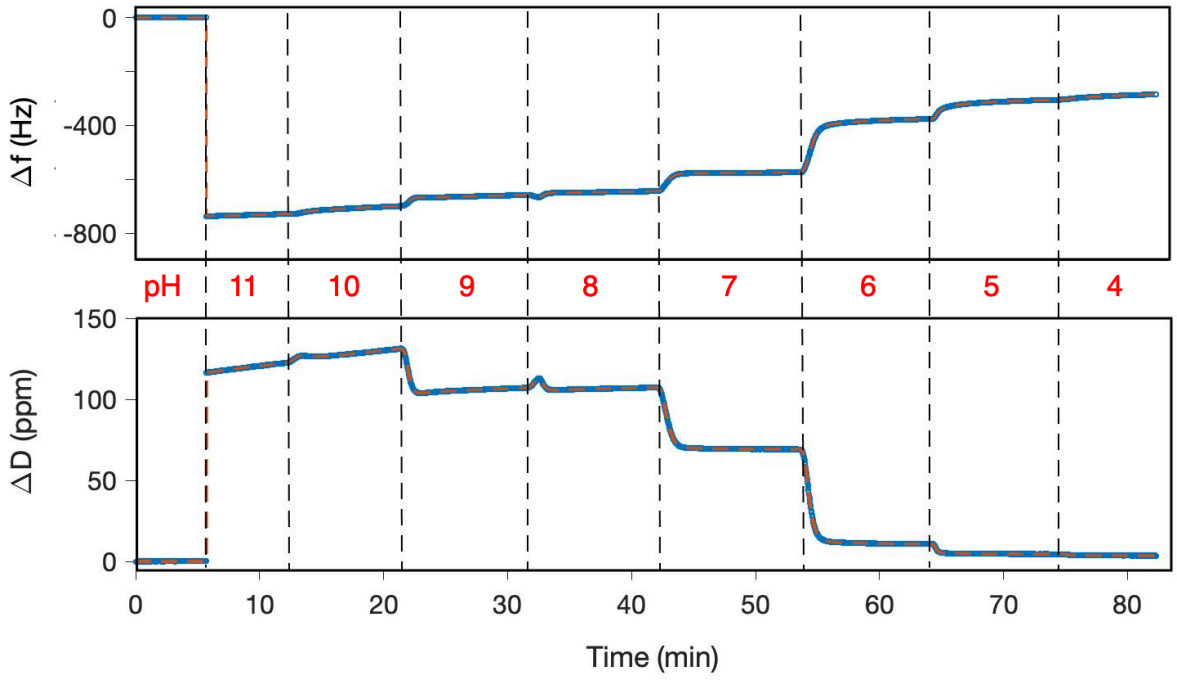

Figure 6.9. QCM-D measurements of a copolymer film with 34% (molar) carboxylic acid groups exposed to flowing buffer solutions in which pH changes gradually from pH 11 to pH 4, as indicated in the intermediate x-axis.

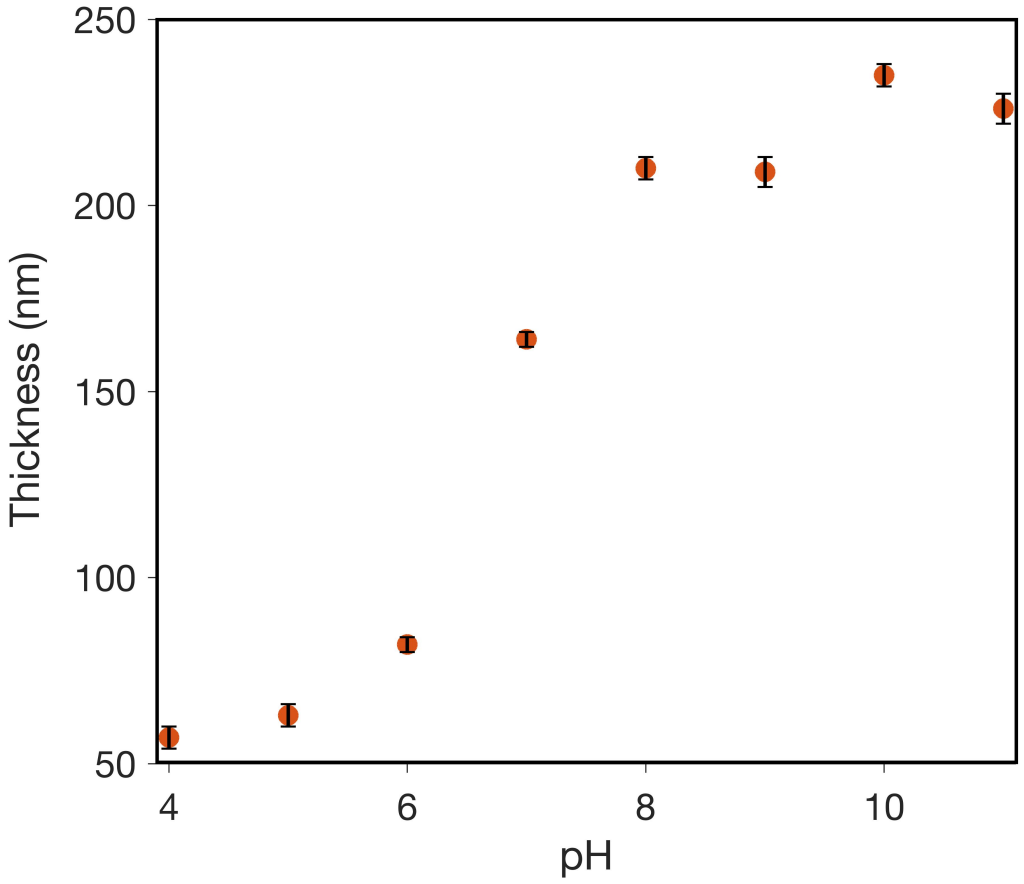

Figure 6.10. pH-dependent thicknesses as measured by QCM-D for copolymer films with 34% (molar) carboxylic acid groups.

The reversibility of the pH-responsive behavior was also investigated with QCM-D. QCM-D measurements of the copolymer films were collected with periodic pH changes between pH 6 and pH 8. Four and half pH change cycles were conducted to examine the reproducibility, and Figure 6.11 shows the changes in frequency (Δf) and energy dissipation (ΔD) along the pH-switching process. The results of Figure 6.11 suggest that the film can be reversibly expanded and contracted over an important range of pH, one unit above and below neutrality. The changes in properties are achieved within 1.5 min, and the corresponding changes in Δf and ΔD in each pH

cycle are almost exactly the same. The film thicknesses in the aqueous flow are also obtained by fitting the experimental data, and the calculated thicknesses at each cycle are shown in Figure 6.12. The changes in the copolymer film structure in the water flow are reversible and highly reproducible, which demonstrates that these ester/carboxylic acid films exhibit a robust and durable pH-responsive performance for applications where film properties are required to be altered reversibly and repeatedly.

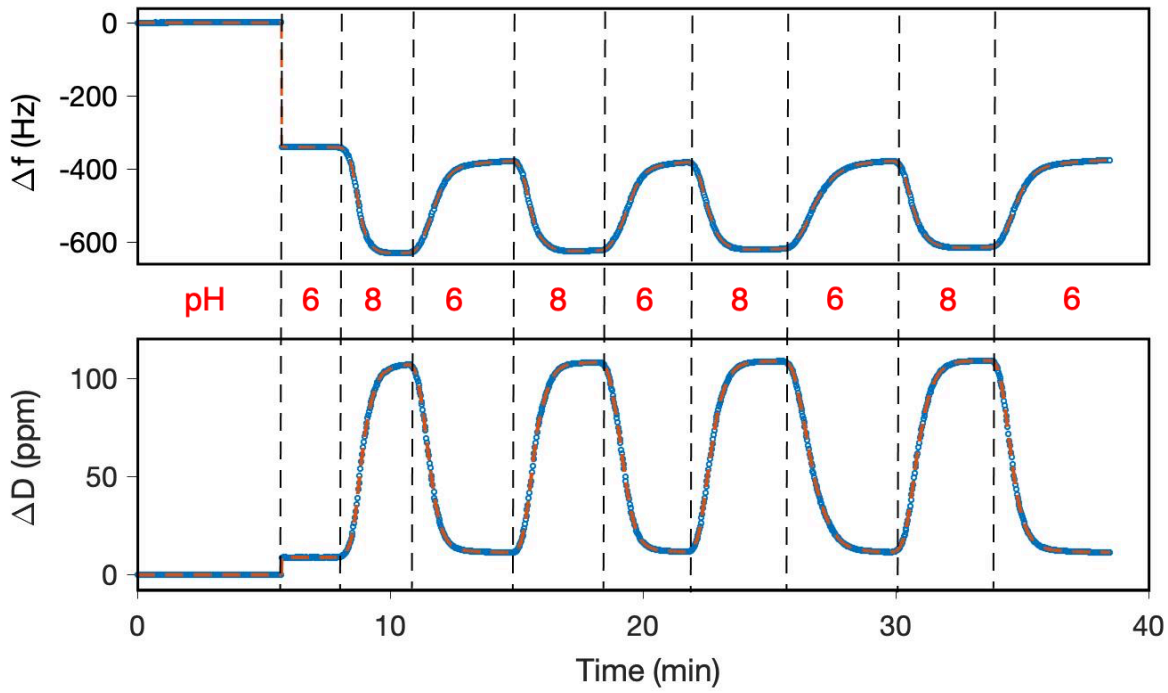

Figure 6.11. QCM-D measurements of a copolymer film with 34% (molar) carboxylic acid groups exposed to flowing buffer solutions in which the pH switches repeatedly between 6 and 8.

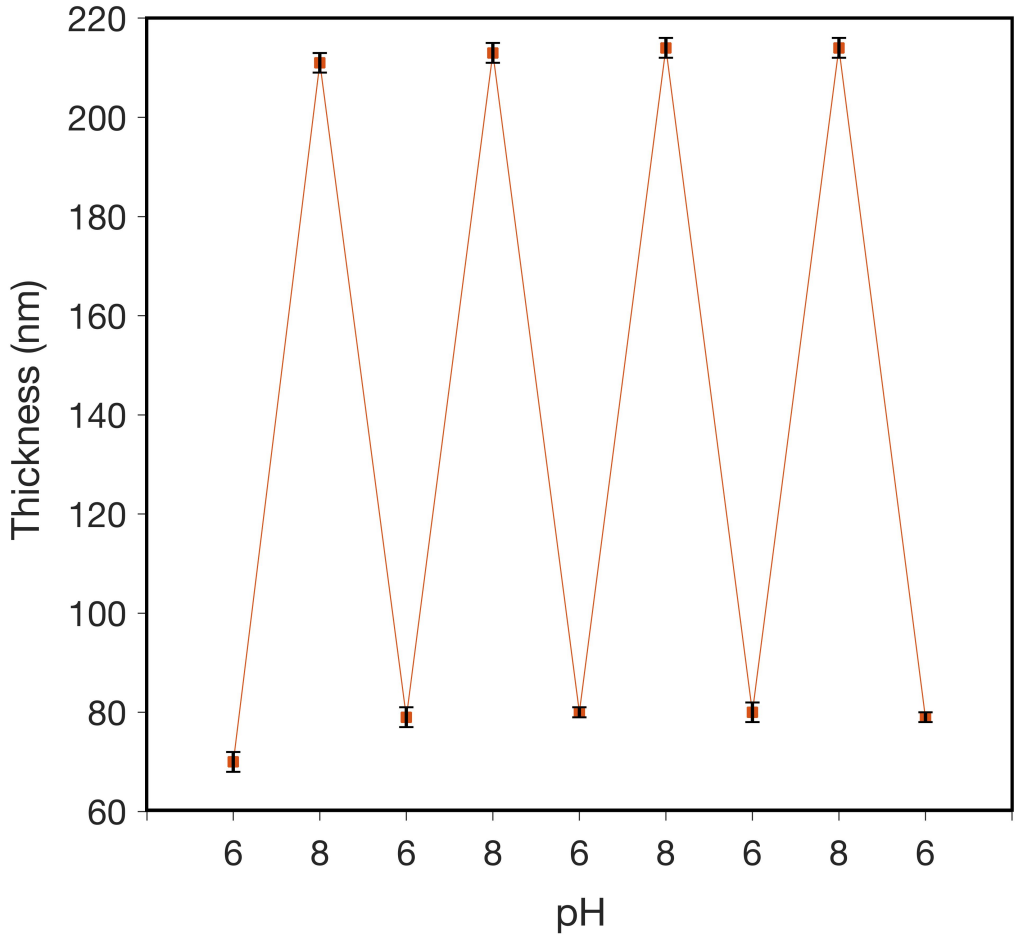

Figure 6.12. Film thickness of a copolymer film with 34% (molar) carboxylic acid groups exposed to flowing buffer solutions in which the pH switches repeatedly between 6 and 8.

Conclusions

The ester/carboxylic acid copolymer films have been successfully prepared by post-polymerization modification of the acyl chlorides of pNBDAC in a mixture of water and ethanol. In the modification process, ethanol has a 60x faster reaction rate than water does. A two-step modification method can be used to tune the copolymer film composition with good control. The copolymer films demonstrate pH-responsive behavior in which the film composition plays an

important role in the pH-induced change of film properties. A dramatic decrease in ionic barrier properties is observed at a critical pH, where most carboxylic acids are deprotonated to carboxylate to enable a contiguous network of aqueous solution through the film. This critical pH of the copolymer is dependent on the film composition. QCM-D measurements were conducted to investigate the interaction of aqueous solution with the film at different pH. At high pH, the existence of the carboxylates in the copolymer films strengthens the interactions of the film with the aqeueous solution and leads to a more swollen film structure. The pH-responsive performance of the copolymer film exhibits high reversibility and reproducibility according to the QCM-D measurements.

References

(1) Chen, J. K.; Chang, C. J. Fabrications and Applications of Stimulus-Responsive Polymer Films and Patterns on Surfaces: A Review. *Materials (Basel)*. **2014**, *7* (2), 805–875.

(2) Chen, Y. C.; Xie, R.; Chu, L. Y. Stimuli-Responsive Gating Membranes Responding to Temperature, PH, Salt Concentration and Anion Species. *J. Memb. Sci.* **2013**, *442*, 206–215.

(3) Tokarev, I.; Minko, S. Stimuli-Responsive Hydrogel Thin Films. *Soft Matter* **2009**, *5* (3), 511–524.

(4) Schmaljohann, D. Thermo- and PH-Responsive Polymers in Drug Delivery. *Adv. Drug Deliv. Rev.* **2006**, *58* (15), 1655–1670.

(5) Chen, J.; Chu, M.; Koulajian, K.; Wu, X. Y.; Giacca, A.; Sun, Y. A Monolithic Polymeric Microdevice for PH-Responsive Drug Delivery. *Biomed. Microdevices* **2009**, *11* (6), 1251–1257.

(6) Luo, T.; Lin, S.; Xie, R.; Ju, X. J.; Liu, Z.; Wang, W.; Mou, C. L.; Zhao, C.; Chen, Q.; Chu, L. Y. PH-Responsive Poly(Ether Sulfone) Composite Membranes Blended with Amphiphilic Polystyrene-Block-Poly(Acrylic Acid) Copolymers. *J. Memb. Sci.* **2014**, *450*, 162–173.

(7) Jin, X.; Hsieh, Y. Lo. PH-Responsive Swelling Behavior of Poly(Vinyl Alcohol)/Poly(Acrylic Acid) Bi-Component Fibrous Hydrogel Membranes. *Polymer (Guildf)*. **2005**, *46* (14), 5149–5160.

(8) Li, J. J.; Zhou, Y. N.; Luo, Z. H. Smart Fiber Membrane for PH-Induced Oil/Water Separation. *ACS Appl. Mater. Interfaces* **2015**, *7* (35), 19643–19650.

(9) Han, Z.; Cheng, C.; Zhang, L.; Luo, C.; Nie, C.; Deng, J.; Xiang, T.; Zhao, C. Toward

Robust PH-Responsive and Anti-Fouling Composite Membranes via One-Pot in-Situ Cross-Linked Copolymerization. *Desalination* **2014**, *349*, 80–93.

(10) Lee, C. H.; Kang, S. K.; Lim, J. A.; Lim, H. S.; Cho, J. H. Electrospun Smart Fabrics That Display PH-Responsive Tunable Wettability. *Soft Matter* **2012**, *8* (40), 10238–10240.

(11) Richter, A.; Paschew, G.; Klatt, S.; Lienig, J.; Arndt, K. F.; Adler, H. J. P. Review on Hydrogel-Based PH Sensors and Microsensors. *Sensors* **2008**, *8* (1), 561–581.

(12) Bai, D.; Habersberger, B.; Jennings, G. K. PH-Responsive Copolymer Films by Surface-Catalyzed Growth. *J. Am. Chem. Soc.* **2005**, *1527*, 16486–16493.

(13) Kocak, G.; Tuncer, C.; Bütün, V. PH-Responsive Polymers. *Polym. Chem.* **2017**, *8* (1), 144–176.

(14) Escalé, P.; Van Camp, W.; Du Prez, F.; Rubatat, L.; Billon, L.; Save, M. Highly Structured PH-Responsive Honeycomb Films by a Combination of a Breath Figure Process and in Situ Thermolysis of a Polystyrene-Block-Poly(Ethoxy Ethyl Acrylate) Precursor. *Polym. Chem.* **2013**, *4* (17), 4710–4717.

(15) Pereira, P. F.; Andrade, C. T. Optimized PH-Responsive Film Based on a Eutectic Mixture-Plasticized Chitosan. *Carbohydr. Polym.* **2017**, *165*, 238–246.

(16) Siepmann, F.; Wahle, C.; Leclercq, B.; Carlin, B.; Siepmann, J. PH-Sensitive Film Coatings: Towards a Better Understanding and Facilitated Optimization. *Eur. J. Pharm. Biopharm.* **2008**, *68* (1), 2–10.

(17) Naficy, S.; Spinks, G. M.; Wallace, G. G. Thin, Tough, PH-Sensitive Hydrogel Films with Rapid Load Recovery. *ACS Appl. Mater. Interfaces* **2014**, *6* (6), 4109–4114.

(18) Lindqvist, J.; Nyström, D.; Östmark, E.; Antoni, P.; Carlmark, A.; Johansson, M.; Hult, A.; Malmström, E. Intelligent Dual-Responsive Cellulose Surfaces via Surface-Initiated

ATRP. *Biomacromolecules* **2008**, *9* (8), 2139–2145.

(19) Sanjuan, S.; Perrin, P.; Pantoustier, N.; Tran, Y. Synthesis and Swelling Behavior of PH-Responsive Polybase Brushes. *Langmuir* **2007**, *23* (10), 5769–5778.

(20) Zhang, Z. B.; Zhu, X. L.; Xu, F. J.; Neoh, K. G.; Kang, E. T. Temperature- and PH-Sensitive Nylon Membranes Prepared via Consecutive Surface-Initiated Atom Transfer Radical Graft Polymerizations. *J. Memb. Sci.* **2009**, *342* (1–2), 300–306.

(21) Yu, H. Y.; Li, W.; Zhou, J.; Gu, J. S.; Huang, L.; Tang, Z. Q.; Wei, X. W. Thermo- and PH-Responsive Polypropylene Microporous Membrane Prepared by the Photoinduced RAFT-Mediated Graft Copolymerization. *J. Memb. Sci.* **2009**, *343* (1–2), 82–89.

(22) Cayre, O. J.; Chagneux, N.; Biggs, S. Stimulus Responsive Core-Shell Nanoparticles: Synthesis and Applications of Polymer Based Aqueous Systems. *Soft Matter* **2011**, *7* (6), 2211–2234.

(23) Faulkner, C. J.; Fischer, R. E.; Jennings, G. K. Surface-Initiated Polymerization of 5-(Perfluoro-n-Alkyl)Norbornenes from Gold Substrates. *Macromolecules* **2010**, *43* (3), 1203–1209.

(24) Njoroge, I.; Kempler, P.; Deng, X.; Arnold, S.; Jennings, G. K. Surface-Initiated Ring-Opening Metathesis Polymerization of Dicyclopentadiene from the Vapor Phase. *Langmuir* **2017**.

(25) Escobar, C. a; Harl, R. R.; Maxwell, K. E.; Mahfuz, N. N.; Rogers, B. R.; Jennings, G. K. Amplification of Surface-Initiated Ring-Opening Metathesis Polymerization of 5-(Perfluoro-n-alkyl)Norbornenes by Macroinitiation. *Langmuir* **2013**, *29*, 12560–12571.

(26) Leitgeb, A.; Wappel, J.; Slugovc, C. The ROMP Toolbox Upgraded. *Polymer (Guildf).* **2010**, *51* (14), 2927–2946.

(27) Bielawski, C. W.; Grubbs, R. H. Living Ring-Opening Metathesis Polymerization. *Prog. Polym. Sci.* **2007**, *32* (1), 1–29.

(28) Bates, R. G.; Bower, V. E. Handbook of Analytical Chemistry; McGraw-Hill: New York, 1963.

(29) Masel, R. I. *Principles of Adsorption and Reaction on Solid Surfaces*; John Wiley & Sons, Inc., 1996.

(30) Schwarzenbach, R. P.; Gschwend, P. M.; Imboden, D. M. *Environmental Organic Chemistry*; John Wiley & Sons, Inc., 2005.

CHAPTER VII

SURFACE-INITIATED POLYMER/IONIC LIQUID GEL FILMS

Introduction

Ionic liquids have gained much attention from the scientific world due to their unique properties such as chemical, thermal, and photocatalytic stability, negligible vapor pressure, non-flammability, relatively high ionic conductivity, and tunability of liquid properties by varying the anion or cation.[1–4] The utilization of ionic liquids in polymer science has also been actively investigated during the past decades. [5–10] The mobility of free ions enhance the electrochemical properties of the polymer and also improve the liquid behavior of the film, which can be applied in applications where phase transition is critical, such as in smart materials.[5–10]

Currently, polymer-IL systems are mainly prepared by two methods.[6–8] One method is the direct in situ polymerization of monomers in the IL environment, and the other is the direct mixing of the pre-synthesized polymer with an IL.[11,12] These two methods have been widely used in polymer-IL gel preparations for many applications such as polymer electrolytes, gas separation membranes, and smart materials; however, both methods have some key limitations. Both direct in situ polymerization in ILs and polymer dissolution in IL require specific IL "design," which limits the choice of polymer and IL to assemble the binary system and contributes toward other issues such as high cost. Also, currently, most preparations are performed in bulk solution, which requires complicated separation processes. In addition, to form a coating, further deposition of the gel onto a surface is required, and the robustness of the attachment to the surface by current deposition techniques is limited. Furthermore, the thinness of the gel film prepared by deposition

techniques is limited to the micrometer scale, as nanoscale films can rarely be achieved. Thus, a new and simpler method that is feasible with multiple ILs and is easily extended to robust surface films would facilitate the further investigation of polymer-IL systems.

In this Chapter I report the preparation of surface-initiated-ion gels containing polydicyclopentadiene (pDCPD) as the matrix polymer, prepared by surface-initiated ring-opening metathesis polymerization (SiROMP) from the vapor phase. Surface-initiated polymerization (SIP), also called the "grafting from" method, which enables the growth of stable polymer films with tunable thicknesses ranging from tens of nanometers up to the micron level.[13,14] Compared to other types of SIP, SiROMP shows more rapid initiation and polymerization due in part to the continuously developed and improved SiROMP catalysts developed by Grubbs and others.[15–19] As such, film thicknesses greater than a few hundred nm can be achieved by SiROMP in under 15 min of polymerization time.[18,20,21] We have recently shown that smooth films of pDCPD with thicknesses of a few hundred nm can be grown by SiROMP upon exposure to the vapor of DCPD for 15 min.[22] Immersion of the pDCPD film into an appropriate solvent containing an IL results in the IL occupying the internal cross-linked structure of the pDCPD. The process enables a precise control over the amount of loaded IL in the pDCPD-IL gel and the thickness of the resulting composite surface film. Here, we investigate the kinetics and mechanism of IL incorporation through this simple immersion method, as well as several crucial properties of the novel pDCPD-IL gel films.

Experimental Section

Preparation of pDCPD-IL Gel Films

The polymerization of pDCPD films from the vapor phase on gold and silicon substrates has been described recently by our group.[22] Figure 7.1 schematically depicts the growth of pDCPD films by SiROMP and the preparation of pDCPD-IL gel films on the gold surface by the simple immersion method. Gold substrates were exposed to 1 mM 4-mercapto-1-butanol solution in ethanol overnight followed by ethanol and water rinses and drying in a stream of nitrogen to develop a hydroxyl-terminated surface. The resulting sample was then soaked in 5 mM NBDAC solution in DCM for at least 30 min followed by rinsing in DCM, ethanol, and water and drying in a stream of nitrogen to yield the acylation product of a surface-tethered norbornenyl group. The sample was subsequently exposed to a 5 mM solution of Grubbs catalyst (2nd generation) in DCM for 12 min and placed into the polymerization reaction vial immediately after a quick DCM rinse. The reaction vial is shown in Figure 7.1. DCPD monomers were then polymerized from the vapor phase to form a smooth thin film. The pDCPD thin films on gold substrates were then immersed into a [bmim][PF_6] solution in DCM for periods of time ranging from 4 to 72 h. The concentration of the IL in DCM was varied between 0.5 mM to 25 mM. By removing the substrate from the [bmim][PF_6] solution, a pDCPD-IL gel film was obtained after the quick evaporation of any remaining DCM into air. Other ILs were investigated, including [bmim][BF_4], [bmim][NTF_2], [bmim][OTf], and [hmim][PF_6], all at 25 mM concentration in the DCM solvent.

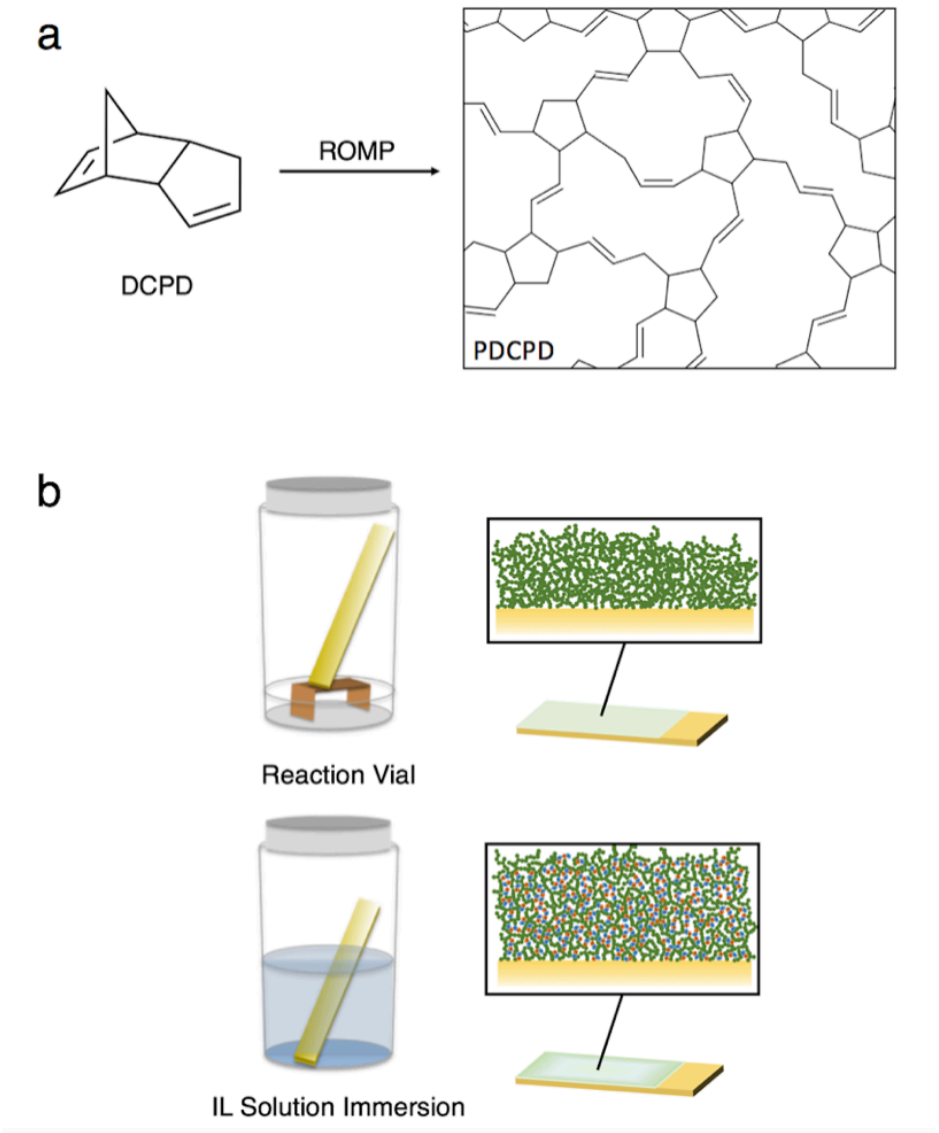

Figure 7.1. (a) Molecular structure of DCPD monomer and schematic of the structure for cross-linked pDCPD. (b) DCPD monomer was placed at the bottom of the vial, with a copper stage used to prevent direct contact between the surface and the liquid monomer. The reaction vial was preheated to 55 °C for 20 min to obtain the equilibrium vapor concentration of monomers in the vial. DCPD monomer was then polymerized from the vapor phase to form a cross-linked surface-initiated polymer film. The pDCPD film was soaked in a solution containing the IL to obtain the pDCPD-IL gel film.

Results and Discussion

Preparation of pDCPD-IL Gel Films on Gold Electrodes

PDCPD films were prepared by SiROMP of DCPD on gold, with monomer in the vapor phase, to achieve film thicknesses of more than 300 nm and roughnesses of less than 20 nm. The pDCPD films were then soaked in a 25 mM [bmim][PF_6] solution in DCM for up to 48 h. Upon removal from the solution, DCM evaporated quickly and the pDCPD-IL gel films on gold surfaces were obtained. To determine whether the IL was successfully incorporated into the polymer films, profilometric thicknesses were measured before and after soaking in the IL solution. Considering that ILs may be deposited as a separate layer atop the film surface, which may affect the film thickness measurements, the profilometry measurements were initially performed with only IL on top of the gold and no thickness was detected, which demonstrates that any IL remaining on the film surface would not affect the profilometric thickness measurements. Figure 7.2 shows a comparison of thickness profiles for the pDCPD film before and after soaking in the IL. The film thickness increases markedly after soaking in the IL, but the roughness of the polymer film does not change with the incorporation of IL. The ratio of increased film thickness over the original pDCPD film thickness was calculated as the IL uptake (U), which is synonymous with the volume expansion of the polymer film due to the presence of the IL, given that the lateral dimensions of the film are many orders of magnitude greater than the thickness. The average IL uptake was calculated for each pDCPD-IL gel film to further investigate the effect of IL loading on film properties.

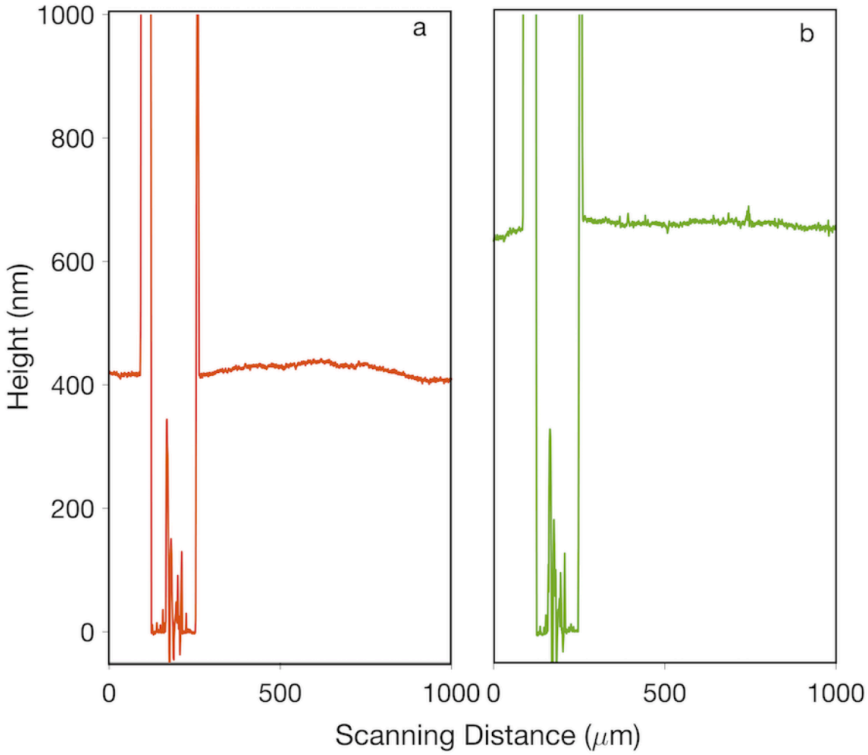

Figure 7.2. (a) Profilometry scan of the original pDCPD film. (b) Profilometry of the film after [bmim][PF_6] incorporation. The valley displays the scratch made down to the gold surface and the two peaks are uplifted polymer that results from scratching. The difference between the valley (gold surface) and the film was calculated as the film thickness. The average thickness and root-mean-square roughness for the pDCPD film shown in (a) are 425 nm and 8 nm. The average thickness and root-mean-square roughness for the pDCPD-IL gel film shown in (b) are 661 nm and 4 nm. Therefore, the incorporated IL results in a 55% thickness increase but minimal change in roughness.

PM-IRRAS was used to verify incorporation of the IL into the pDCPD film. Figure 7.3 shows IR spectra of pure [bmim][PF_6], the original pDCPD film, and the same film after soaking in the IL. The spectrum of [bmim][PF_6] shows absorption bands due to P-F stretching (881 cm^{-1}),

C_{sp3}-H out of plane bending (1100-1200 cm^{-1}), and C=C stretching (1570 cm^{-1}). In the spectrum of pDCPD, the C_{sp2}-H out of plane bending (900-1000 cm^{-1}), the C_{sp3}-H out-of-plane bending (1100-1200 cm-^{1}), and the C=C stretching (1620 cm^{-1}) were observed. The spectrum of the pDCPD film after IL soaking (Figure 7.2(b)) shows all the major peaks for [bmim][PF_6] and pDCPD but with an altered shape of the P-F stretching band, a shift of the P-F stretching band from 867 cm^{-1} to 854 cm^{-1}, and a slight shift of the C_{sp2}-H out of plane bending vibration absorption band from 974 cm^{-1} to 978 cm^{-1}. The changes in the P-F stretching and the C_{sp2}-H out of plane bending absorption bands are attributed to the interaction of incorporated IL molecules with the C=C double bonds in the pDCPD matrix.

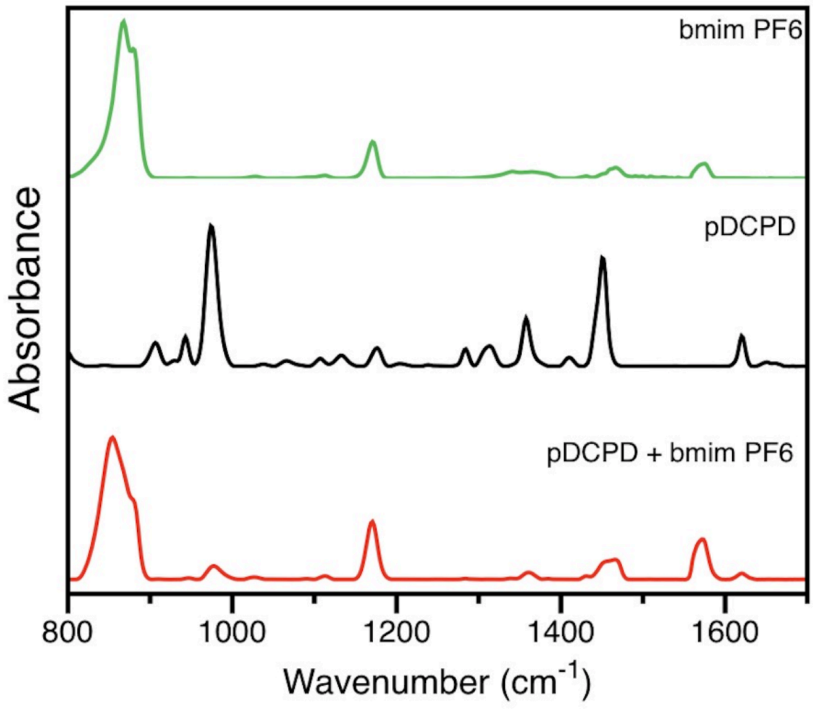

Figure 7.3. FITR spectra of [bmin][PF_6], a pDCPD film, and the pDCPD-IL composite film. Major peaks of pDCPD and [bmin][PF_6] are observed in the spectrum of the composite film after IL immersion

Solvent Effects

The results above suggest a mechanism in which the solvent swells the pDCPD film so that ILs can migrate into the film and achieve stabilizing interactions with the polymer matrix. Therefore, we examined different solvents to assess their effect on the preparation of the polymer-IL gel. Other than DCM with dielectric constant (ε) of 8.93, we examined chloroform ($CHCl_3$) (ε=4.81), ethanol (ε=24.5), dimethylformamide (DMF) (ε=36.7), and water (ε=80.1) as solvents. Bowden et al. have reported that DCM and chloroform swell pDCPD very well while more polar solvents do not.[23] Gold substrates containing pDCPD films were placed into a 25 mM IL solution in different solvents for 48 h. The thicknesses of the films were measured before and after the IL soaking, and the IL uptake for each solvent is listed in Table 7.1. Among the selected solvents, DCM results in the highest IL uptake of 0.49. Significant decreases in IL uptake are observed when the solvent is changed from DCM to the others. Water, ethanol and DMF yield similar IL uptakes, all around 0.13. These polar solvents do not swell pDCPD well, and thus, do not open up the polymer sufficiently to enable high uptake of IL. No uptake is observed for the film exposed to the IL in $CHCl_3$, which swells pDCPD well and was expected to enhance the IL incorporation into pDCPD films. However, [bmim][PF_6] is not soluble in $CHCl_3$, owing to its lower dielectric constant as compared to that for DCM, which reduces effective screening of the electrostatic interactions of the IL. Even though $CHCl_3$ can swell the pDCPD film, the suspended IL aggregates are still too large to penetrate the cross-linked pDCPD films. Also, in the absence of solvent (pure IL), U = 0, revealing that swellability of the polymer film by solvent is a critical component of the mechanism for IL uptake. Hence, of the solvents examined, DCM behaves optimally in the preparation of polymer-IL gels and thus, was used as the solvent for all the experiments described in the remainder of the manuscript.

We also examined different IL species (Table 7.2) to investigate the feasibility of preparing a host of pDCPD-IL gels by this straightforward immersion method. The ILs [bmim][PF_6], [bmim][BF_4], and [hmim][PF_6] were successfully incorporated into the polymer film with IL uptakes ranging from 0.35–0.52. These results indicate that pDCPD is compatible with multiple IL species through this straightforward immersion method. Other ILs, including [bmim][NTF_2] and [bmim][OTf], could not be loaded into pDCPD, which may be due to the mismatch of interactions between the fluorocarbon anions and the hydrocarbon polymer, as fluorocarbons tend to be insoluble in hydrocarbons.[24]

Table 7.1. Uptake of [bmim][PF_6] within the pDCPD-IL gel film prepared with different solvents for the IL.

Solvent	IL uptake
Dichloromethane	0.49 ± 0.04
Chloroform	0
Water	0.14 ± 0.04
Ethanol	0.13 ± 0.05
Dimethylformamide	0.12 ± 0.05

Table 7.2. IL uptake of the pDCPD-IL gel film prepared with different IL species, using dichloromethane as solvent for IL loading.

Ionic Liquid	IL uptake
[bmim][PF_6]	0.49 ± 0.04
[hmim][PF_6]	0.35 ± 0.13

[bmim][BF_4]	0.52 ± 0.08
[bmim][NTF_2]	0
[bmim][OTf]	0

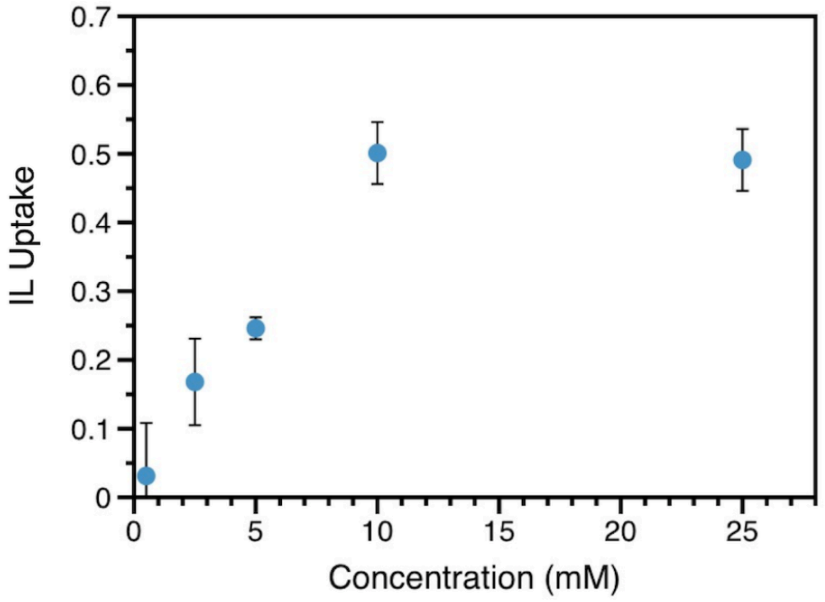

Figure 7.4. The uptake of [bmim][PF_6] within pDCPD-IL gel films immersed in different concentrations of the IL in DCM for 48 h.

IL Concentration Effects and Kinetics.

The IL loading is expected to be controllable by varying the IL solution concentration and the immersion time. Figure 7.4 displays the concentration dependence of IL uptake of the polymer-IL gel films that were soaked in a [bmim][PF_6] solution in DCM for 48 h. A linear dependence of the gel-IL uptake on the IL concentration is obtained at low concentration range (less than 10 mM), suggesting the ability to tune the IL uptake from 0 to 0.5 by varying the IL concentration. The IL

loading cannot be further increased with IL solution concentrations higher than 10 mM. The ceiling of IL uptake is attributed to the limited swelling of pDCPD due to its crosslinked structure.

The IL uptake of the pDCPD-IL films prepared with different IL immersion times in a 25 mM [bmim][PF_6] solution in DCM is displayed in Figure 7.5. The IL incorporation process is relatively slow in the first 4 h and then accelerates from 4 to 36 h, followed by an inhibition as the IL uptake approaches its maximum uptake. This kinetics plot is not consistent with a mechanism based on a diffusion limitation of the IL into the solvent-swollen matrix, followed by entrapment of the IL after removal of the film from the solvent. Diffusion is driven by a concentration gradient, which should result in a faster initial uptake.[25] Similarly, reaction-based kinetic models also predict higher rates at the beginning due to the concentration dependence, and hence, do not fit the experimental data well.[26,27] Instead, the IL incorporation process can be explained as a phase transformation.

The final pDCPD-IL gel is not simply a mixture of IL and polymer matrix but a new phase with special interactions between ions and polymer matrix. The polarizable C=C double bonds that are prevalent within the pDCPD can be induced in the presence of IL to form either electron-deficient or electron-rich π systems, which will then create anion-π or cation-π interactions between the polymer matrix and ions. The existence of the ion-π interactions results in the IR active vibrational frequency shift of the out-of-plane C_{sp2}-H bending absorption band. A blue shift (frequency increase) should be observed if cation-π interactions exist, while a red shift (frequency decrease) should be observed when anion-π interactions exist.[28,29] For our system, a slight shift of the absorption band for C_{sp2}-H out-of-plane bending from 974 cm^{-1} to 978 cm^{-1} is observed after we incorporate IL into the pDCPD film, which suggests that we do have ion-π interactions formed between the ILs and the polymer matrix. The shift is small because both types of ion-π interactions

exist here, which results in both a blue shift and an opposing red shift. The ion-π interactions stabilize ions around the double bonds in pDCPD, and those ions interacting with the polymer matrix can electrostatically attract other ions. More ions aggregate around the polymer matrix, and eventually, a new phase forms. The slow IL incorporation process at the outset may be attributed to the slow formation of the polymer-ion interactions.

The Avrami model, which was developed to describe the time-dependent change of phase in materials, was applied to our results for IL uptake to investigate the mechanism of the IL loading process of pDCPD films.[30–32] In the model, the volume fraction of the transformed phase (Y) as a function of time (t) is given as

$$Y = 1 - e^{-Kt^n} \tag{7.1}$$

where *K* and *n* are two constants in the Avrami model. For IL incorporation, the transformed phase volume can be expressed as the IL uptake while the total available volume for phase change can be expressed as the ceiling IL uptake, limited by the swellability of pDCPD in DCM. Hence, the model equation for our specific case can be written as

$$\frac{U}{U_{max}} = Y = 1 - e^{-Kt^n} \tag{7.2}$$

where U stands for IL uptake and U_{max} is the maximum IL uptake.

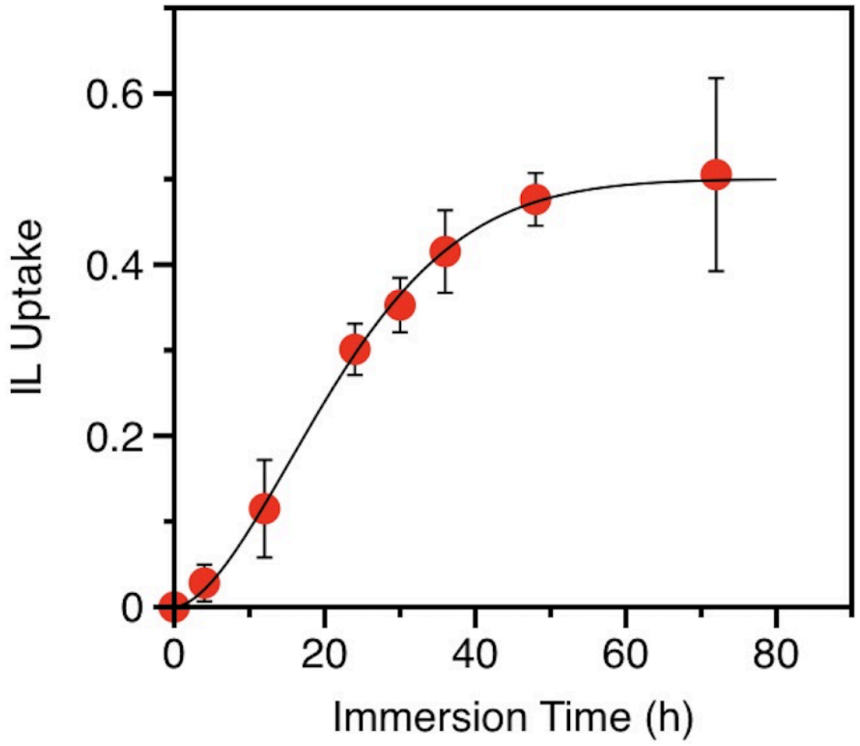

Figure 7.5. The uptake of [bmim][PF_6] in pDCPD-IL gel films immersed in a 25 mM IL solution in DCM for different immersion times. The fitting curve was made based on the calculated K and n value by applying the Avrami model (Eq.7.2). The fitting equation is $U = 0.51(1 - e^{-0.0044t^{1.66}})$

By fitting the experimental data with the Avrami model, the parameter *K* is calculated to be 0.0044 ± 0.0005 min^{-n} and *n* is 1.66 ± 0.3. Generally, the *K* value demonstrates the rate of the phase transformation and is dependent on the IL solution concentration and the type of cation and anion in our case. The parameter *n* generally indicates the dimension of the nucleation and growth of the phase. In our IL incorporation process, the nucleation refers to the process of formation of ion-π interactions while the growth of the phase refers to the ion-attracting and aggregating process. The calculated *n* value is 1.66, suggesting that one dimension growth of the phase

occurred during the IL incorporation process. The phenomenon is attributed to the complexity of the cross-linked structure of the pDCPD matrix. The available space for phase transformation is actually different from site to site. Hence, the nucleation and growth of the new phase also vary due to the special structure of pDCPD films.

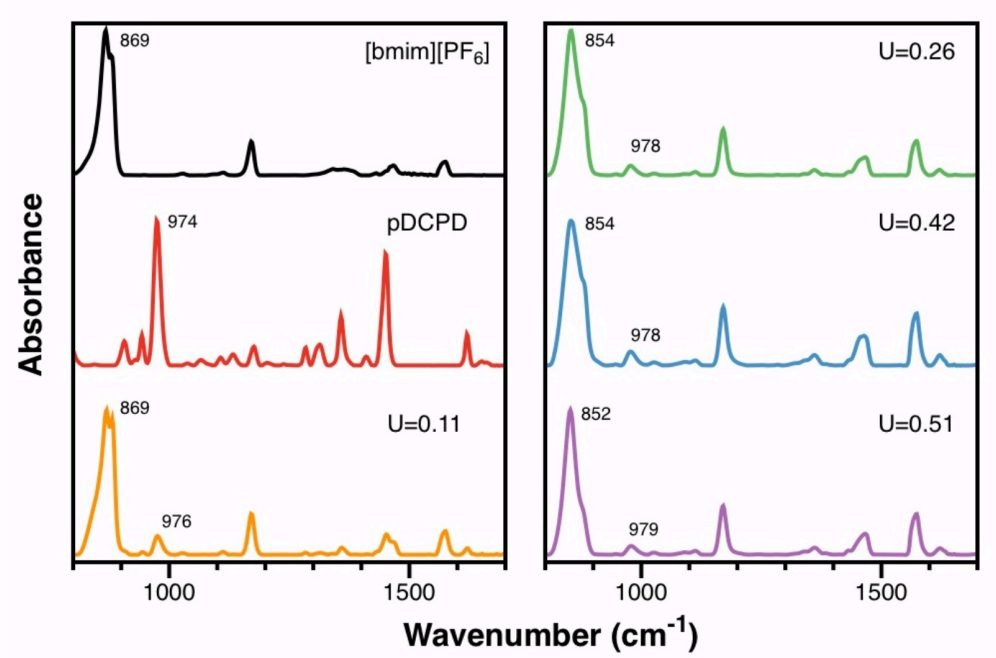

Figure 7.6. PM-IRRAS spectra of [bmim][PF_6] and pDCPD films, as well as a pDCPD-IL gel film with different IL uptakes. Each spectrum is normalized to the maximum peak within this spectral window.

Polarization modulation-infrared reflection-absorption spectra (PM- IRRAS) of [bmim][PF6], the pDCPD film (U = 0), and the pDCPD-IL gel films with different IL uptake (U) are shown in Figure 7.6. From the figure, the gradual shifts of absorption bands due to P-F stretching (from 869 cm^{-1} to 852 cm^{-1}) and out-of-plane C_{SP2}-H bending (from 974 cm^{-1} to 979 cm^{-}

[1]) are observed. The absorption band shifts are labeled in Figure 7.6. These shifts are consistent with the interaction of the ions with the polymer matrix in the pDCPD-IL gel film.

Shear Modulus

The incorporation of IL into the pDCPD matrix is expected to alter the properties of the polymer film. Shear modulus, one of the important mechanical properties for coatings, was investigated by employing the quartz crystal microbalance with dissipation (QCM-D) in an air environment. QCM-D is a technique that allows precise measurements of frequency shifts and energy dissipation factor of a QCM crystal upon loading by a film or coating. The addition of film mass on the quartz crystal will result in a decrease in the frequency of oscillation, while varying viscoelastic properties of the film can be related to the energy dissipation of the coated crystal.[33] We collected the frequency and dissipation values for a clean quartz crystal sensor and used those as the baseline. The changes in frequency (Δf) and energy dissipation (ΔD) as we deposited a self-assembled monolayer (SAM), grew a pDCPD film, and loaded IL to create a pDCPD-IL gel film on the crystal are shown in Figure 7.7. The addition of the SAM on the crystal did not result in a significant decrease in frequency since the mass of the SAM is small and it is robustly coupled to the electrode. In the subsequent steps, both the attachment of the pDCPD film on the crystal and the incorporation of IL into the polymer film result in a dramatic decrease in frequency, which demonstrates that significant masses have been deposited onto the crystal. By applying the Kelvin-Voigt model, a mass ratio of added IL to deposited polymer (0.81) is obtained. The density ratio is 1.34,[34] hence, a volume ratio based on QCM-D data is calculated to be 0.6, which is slightly higher than the IL uptake we measured by the profilometer (0.5). This difference is ostensibly due to the IL deposited on the quartz part of the sensor after IL solution immersion. The change in

dissipation (ΔD) indicates the varying viscoelastic properties of the coated crystal. In the Kelvin-Voigt model, the viscoelastic properties of the film are presented by the complex shear modulus, $G = G' + jG''$, where *j* is the imaginary unit.[35] *G'* is the shear storage modulus, which is a measure of stored energy and describes the elastic behavior of the materials. By fitting our experimental data with the Kelvin-Voigt model, the shear storage modulus *G'* for the pure pDCPD film is 172 MPa, and *G'* for the pDCPD-IL gel film is 204 MPa. This small change in shear storage modulus indicates that the elastic behavior depends more on the structure of the polymer matrix and does not change much with the IL incorporation. *G''* is the shear loss modulus, which is the measure of energy dissipation and describes the viscous behavior of the materials. $G'' = \omega\eta$, where ω is the oscillation frequency and η can be regarded as a coefficient that relates the applied force to the rate of deformation.[35] The pDCPD-IL gel has a 10-time higher η (13.3 mPa·s) than the pure pDCPD film does (1.3 mPa·s). The increased η demonstrates the higher shear loss modulus, which shows that the existence of incorporated IL in the polymer matrix results in a more liquid-like behavior of the material. This result demonstrates the feasibility of the simple immersion method to incorporate IL into polymer matrix and adjust the mechanical properties of polymeric films and coatings.

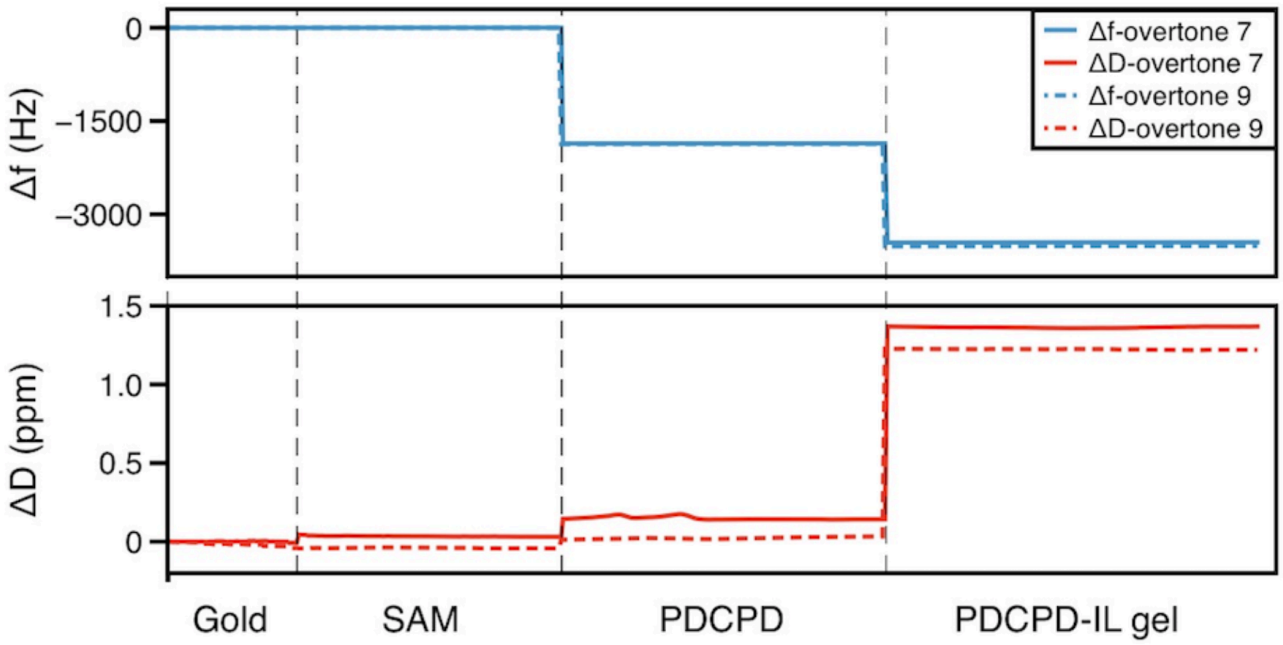

Figure 7.7. QCM-D spectra of the pure quartz crystal, a hydroxyl-terminated SAM, the pDCPD film, and the pDCPD-IL gel film. The experimental data were measured on the fundamental frequency and other odd harmonics. Overtones 7 and 9 were chosen for analysis due to the insufficient energy trapping on low harmonics and interference from anharmonic side bands on high harmonics.[36]

Ion Transport in PDCPD-IL Gel Films

The most widely developed application of polymer-IL composites is as solid-state electrolytes in electrochemical devices. The existence of ions within a polymer matrix or coating generally causes a dramatic enhancement in ion conductance of the materials. Understanding ion transport in these pDCPD-IL gel films is crucial for their potential implementation in electrochemical devices or membranes. Ion transport through pDCPD-IL gel films was investigated with electrochemical impedance spectroscopy (EIS), using an electrochemical cell as

shown in Figure 7.8(a). Two gold substrates were used as the electrodes to sandwich the gel film and pure IL, which served as electrolyte. The pDCPD-IL gel film was prepared on the bottom electrode. A piece of Gamry electrochemical sample mask with a 0.28 cm^2 circular hole was used as the mask to prevent direct contact of the two gold electrodes. A drop of [bmim][PF_6] was then added to fill the unmasked area, followed by placement of the other gold electrode on top and an added clamp that served as stabilization. By applying an AC potential with varying frequencies, the frequency response of the system was recorded and plotted in the format of a Bode magnitude plot. Representative Bode plots of EIS spectra for the NBDAC-terminated SAM without pDCPD, the pDCPD film, and the pDCPD-IL gel film with different levels of IL uptake are shown in Figure 7.8(b).

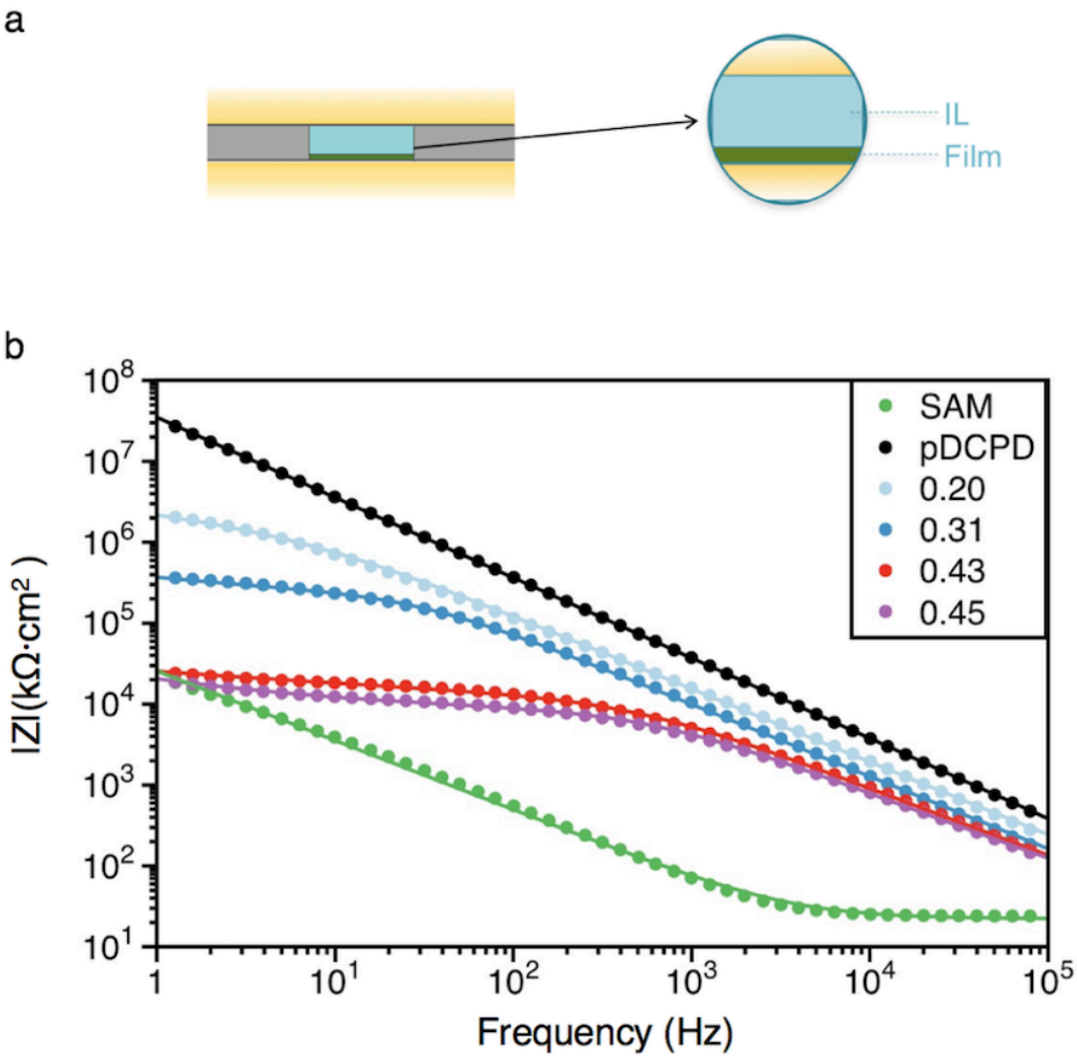

Figure 7.8. (a) Scheme of the electrochemical cell used in the EIS measurements. (b) Bode magnitude plots of EIS spectra using pure IL as the electrolyte for working electrodes containing an NBDAC-modified SAM (control), the pDCPD polymer film, and a pDCPD-IL gel film with different IL uptakes (0.20, 0.31, 0.43, 0.45). The solid curves represent a fit of the data with the equivalent circuit shown in Figure 7.9.

The EIS spectrum of pDCPD exhibits the behavior of a pure capacitor and demonstrates an extremely high film impedance, which is attributed to its low dielectric constant and its cross-

linked structure. The perfect capacitive response indicates that ions of the contacting IL do not penetrate into the pure pDCPD film. These results suggest that the IL, by itself, is incapable of swelling the polymer film. With IL loaded into the polymer matrix, the ion transport ability is significantly changed. In the Bode plots, the magnitudes of the plateaus of the spectra in the low frequency region reflect the resistances of the films against ion migration, which is termed film resistance. A quantitative analysis was done by fitting the obtained EIS spectra with an equivalent circuit model. The equivalent circuit model we used to fit the data for pDCPD-IL gel films is shown in Figure 7.9 Considering the leakage of the capacitors, constant phase elements (CPEs) were used in lieu of capacitors to fit the experimental data. The impedance of the CPE is given by Eq. 7.3,

$$Z_{CPE} = \frac{1}{Y_0(j\omega)^{\alpha}} \tag{7.3}$$

where Y is a constant with units of S□/Ω•cm^2 and □□is a dimensionless constant between 0 and 1. The effective capacitance can be converted from CPE by Eq. 7.4.

$$C = Y_0(\omega_m'')^{\alpha-1} \tag{7.4}$$

where the ω_m'' is the frequency at which the imaginary part of the impedance is a maximum.

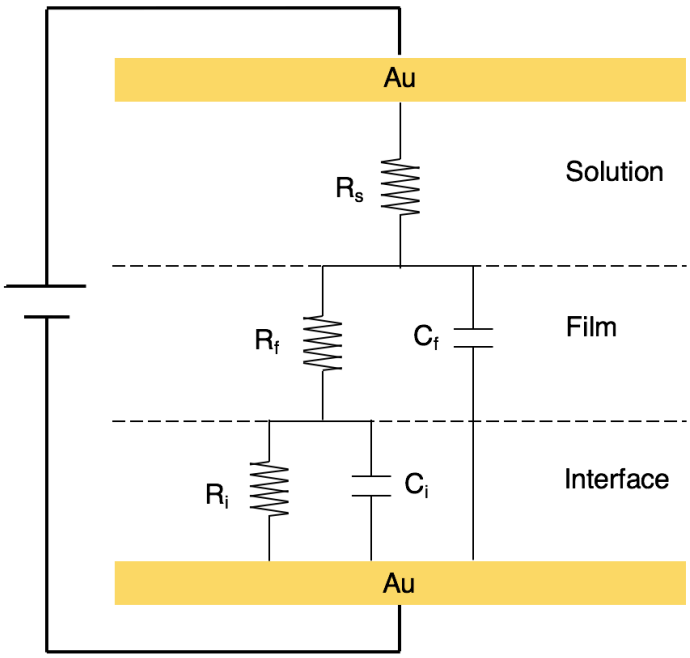

Figure 7.9. The equivalent circuit model used to fit the EIS spectra for pDCPD-IL gel films. The circuit model consists of a solution resistance (R_s), connected in series with a film capacitance (C_f) and a film resistance (R_f), that is in series with an interfacial capacitance (C_i) and an interfacial resistance (R_i). Constant phase elements (CPEs) were used in lieu of capacitors to obtain the best fit of the EIS spectra.

The fitted electrochemical parameters are listed in Table 7.3. The film resistance changes from more than 100 MΩ·cm^2 for pure pDCPD to as low as ~0.01 MΩ·cm^2 as the IL becomes incorporated into the polymer film—a four-order-of-magnitude decrease. The dramatic decrease with IL uptake demonstrates the existence of conducting, IL-filled pathways within the polymer matrix and reflects the potential of polymer-IL gels as solid-state electrolytes. The film capacitance also increases from 4.3 nF to 33 nF as the incorporation of the IL boosts the overall dielectric

constant of the composite film. Considering that the IL is ion-conductive and causes capacitor leakage, the effect of incorporated IL on the overall dielectric constant of the gel film cannot be simply described using a traditional linear model. Also, as we incorporate additional IL into the pDCPD film, the dramatic decrease in film resistance can lead to greater capacitor leakage and a less purely capacitive behavior.

Another control experiment was performed with only the NBDAC-modified SAM on the gold substrate. The difference between the spectra of the polymer-IL gel films and the spectra of the control experiment indicate the effect of the pDCPD-IL gel film. At low frequency, the spectrum of the film with an IL uptake of 0.45 merges with the control spectrum, which demonstrates that at low frequency, the impedance of the pDCPD-IL gel film is negligible, as ions have sufficient time to transport through the film in a similar manner as transferring in bulk IL. In this case, the effect of the pDCPD-IL gel film disappears and the impedance response only depends on the interface.

Table 7.3. Film resistance and film capacitance values of the pDCPD-IL gel obtained from a fit of EIS spectra of Figure 7.8(b) with the equivalent circuit shown in Figure 7.9

IL Uptake (U)	IL Volume Percentage (%)	Film Resistance ($k\Omega \cdot cm^2$)	Film Capacitance (nF/cm^2)

0	0	>30000*	4.3 ± 0.1
0.20	17	>2000*	20.8 ± 0.9
0.31	24	244 ± 19	25.1 ± 1.1
0.43	30	9.4 ± 2.5	29.9 ± 3.6
0.45	31	8.6 ± 0.3	33.3 ± 3.0

* Film resistances of pure pDCPD and the pDCPD-IL gel film with an IL uptake of 0.2 cannot be determined accurately via modeling fitting because no obvious plateaus exist in the frequency range from 1 Hz to 100 kHz.

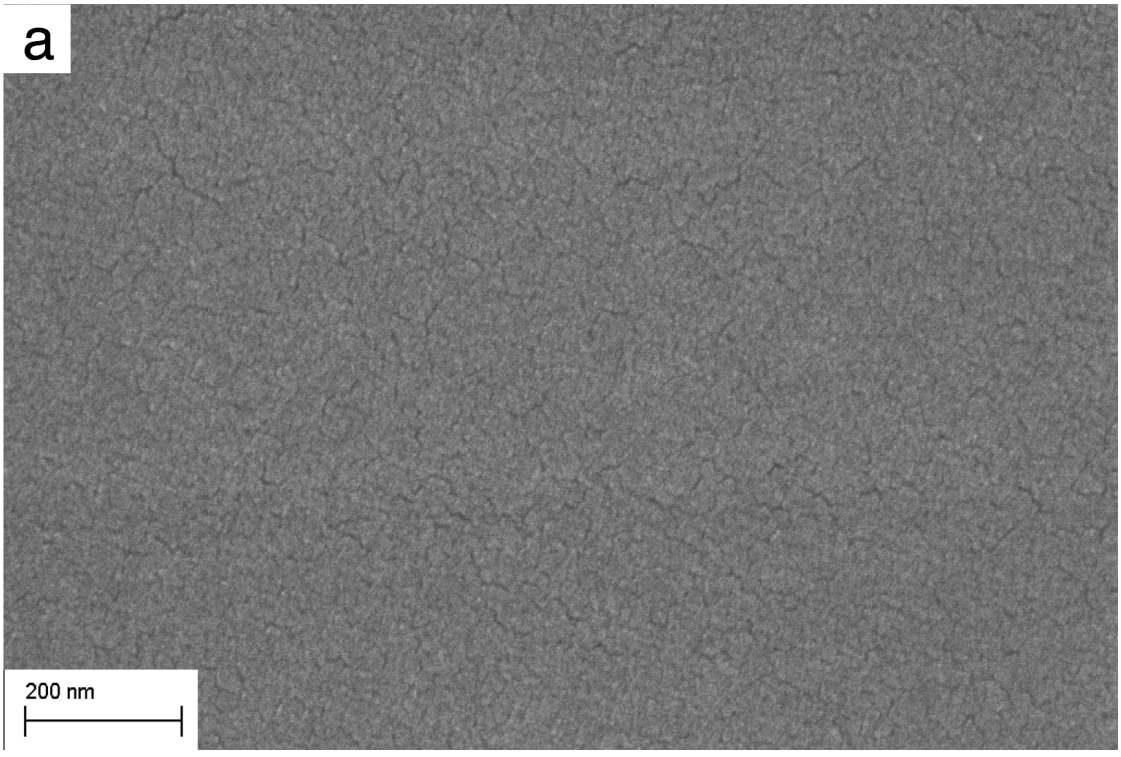

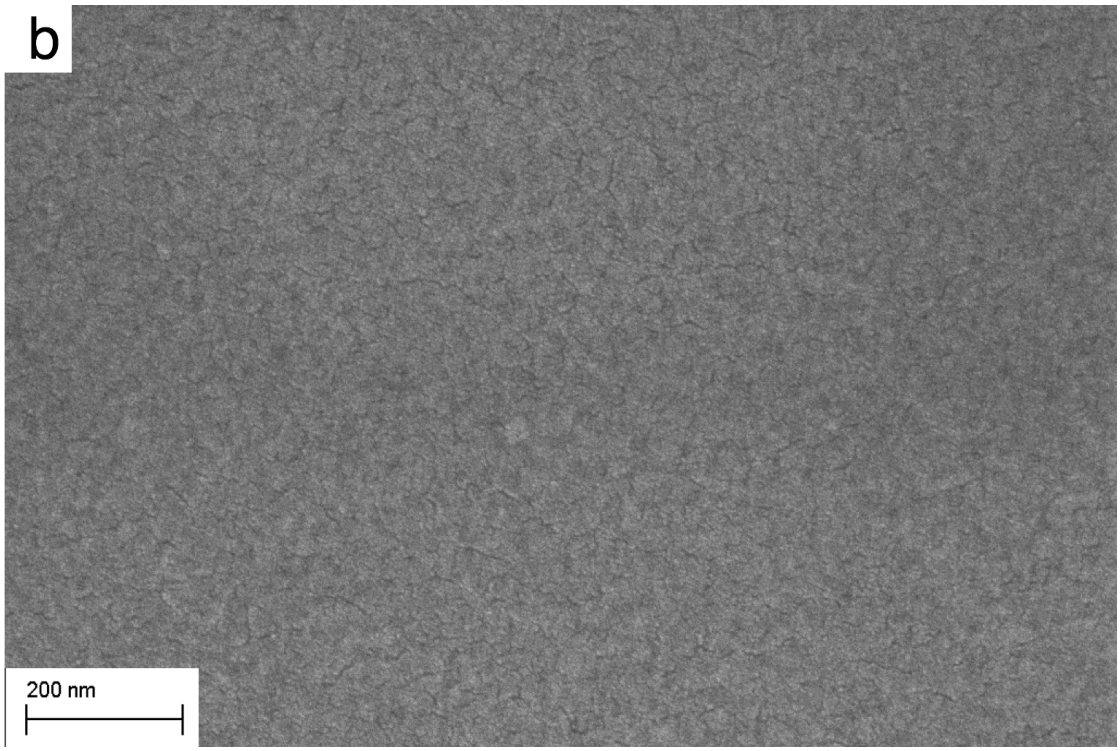

Figure 7.10. (a) The SEM image of pure pDCPD film (b) The SEM image of pDCPD-IL gel film (U = 0.49).

Scanning electron microscopy (SEM) was used to investigate the morphology of the pure pDCPD film and the pDCPD-IL gel film (U = 0.49). Figure 7.10 demonstrates similarity between the grown pDCPD film and the pDCPD-IL gel film after the IL incorporation. The result is consistent with the comparison of roughness shown in Figure 7.2. The IL incorporation does not result in a change in surface morphology. Also, the SEM images show that the films are smooth and uniform, which demonstrates an advantage of surface-initiated polymerization in the preparation of polymer/IL gel films and coatings.

Conclusions

PDCPD-IL gel films were successfully prepared by incorporating ILs into surface-initiated pDCPD films using a simple immersion method. The ILs incorporate into surface-initiated pDCPD and form stabilizing interactions with the C=C double bonds of the polymer as the solvent swells the polymer matrix. The method is proven to be feasible in preparing pDCPD-IL gels with different IL species that are soluble in the IL and within the pDCPD matrix. The successful incorporation of the IL is proven by the increased thickness of the final resulting gel, as well as changes in the IR spectra. The IL uptake of the resulting gel is dependent on the solvent, IL solution concentration, and the sample immersion time. DCM as solvent enables the highest IL uptake due to the high swellability of pDCPD and high solubility of the IL in DCM. The process of the IL incorporation can be regarded as a phase transformation process that can be described by the Avrami model. The film properties of pDCPD were also changed as the IL becomes incorporated into the polymer matrix. QCM-D measurements show that pDCPD-IL gel film has a higher shear loss modulus than that of the pure pDCPD films, and EIS spectra display dramatic decreases in film resistance with the IL loaded into the polymer film. We expect that this process can be extended to other polymer compositions and ILs to generate robustly bound, ion-conductive gel films with controlled thicknesses on a variety of substrates.

References

(1) Marsh, K. N.; Boxall, J. A.; Lichtenthaler, R. Room Temperature Ionic Liquids and Their Mixtures - A Review. *Fluid Phase Equilib.* **2004**, *219* (1), 93–98.

(2) Qian, W.; Texter, J.; Yan, F. Frontiers in Poly(Ionic Liquid)s: Syntheses and Applications. *Chem. Soc. Rev.* **2017**, *46* (4), 1124–1159.

(3) Yuan, J.; Mecerreyes, D.; Antonietti, M. Poly(Ionic Liquid)s: An Update. *Prog. Polym. Sci.* **2013**, *38* (7), 1009–1036.

(4) Mecerreyes, D. Polymeric Ionic Liquids: Broadening the Properties and Applications of Polyelectrolytes. *Prog. Polym. Sci.* **2011**, *36* (12), 1629–1648.

(5) Snedden, P.; Cooper, A. I.; Scott, K.; Winterton, N. Cross-Linked Polymer - Ionic Liquid Composite Materials. *Macromolecules* **2003**, 4549–4556.

(6) Kokorin, A. *Ionic Liquids: Applications and Perspectives*; InTech: Rijeka, 2011.

(7) Lu, J.; Yan, F.; Texter, J. Advanced Applications of Ionic Liquids in Polymer Science. *Prog. Polym. Sci.* **2009**, *34* (5), 431–448.

(8) Ueki, T.; Watanabe, M. Macromolecules in Ionic Liquids: Progress, Challenges, and Opportunities. *Macromolecules* **2008**, *41* (11), 3739–3749.

(9) Xie, Z. L.; Huang, X.; Taubert, A. Dyeionogels: Proton-Responsive Ionogels Based on a Dye-Ionic Liquid Exhibiting Reversible Color Change. *Adv. Funct. Mater.* **2014**, *24* (19), 2837–2843.

(10) Terasawa, N. High-Performance Transparent Actuator Made from Poly(Dimethylsiloxane)/Ionic Liquid Gel. *Sensors Actuators B Chem.* **2018**, *257*, 815–819.

(11) Singh, T.; Trivedi, T. J.; Kumar, A. Dissolution, Regeneration and Ion-Gel Formation of

Agarose in Room-Temperature Ionic Liquids. *Green Chem.* **2010**, *12* (6), 1029.

(12) Vidinha, P.; Lourenço, N. M. T.; Pinheiro, C.; Brás, A. R.; Carvalho, T.; Santos-Silva, T.; Mukhopadhyay, A.; Romão, M. J.; Parola, J.; Dionisio, M.; Cabral, J. M. S.; Afonso, C. a M.; Barreiros, S. Ion Jelly: A Tailor-Made Conducting Material for Smart Electrochemical Devices. *Chem. Commun. (Camb).* **2008**, No. 44, 5842–5844.

(13) Olivier, A.; Meyer, F.; Raquez, J. M.; Damman, P.; Dubois, P. Surface-Initiated Controlled Polymerization as a Convenient Method for Designing Functional Polymer Brushes: From Self-Assembled Monolayers to Patterned Surfaces. *Prog. Polym. Sci.* **2012**, *37* (1), 157–181.

(14) Jennings, G. K.; Brantley, E. L. Physicochemical Properties of Surface-Initiated Polymer Films in the Modification and Processing of Materials. *Adv. Mater.* **2004**, *16* (22), 1983–1994.

(15) Grubbs, R. H. Olefin Metathesis. *Tetrahedron* **2004**, *60* (34), 7117–7140.

(16) Vougioukalakis, G. C.; Grubbs, R. H. Ruthenium-Based Heterocyclic Carbene-Coordinated Olefin Metathesis Catalysts. *Chem. Rev.* **2010**, *110* (3), 1746–1787.

(17) Bielawski, C. W.; Grubbs, R. H. Living Ring-Opening Metathesis Polymerization. *Prog. Polym. Sci.* **2007**, *32* (1), 1–29.

(18) Lerum, M. F. Z.; Chen, W. Surface-Initiated Ring-Opening Metathesis Polymerization in the Vapor Phase: An Efficient Method for Grafting Cyclic Olefins with Low Strain Energies. *Langmuir* **2011**, *27* (9), 5403–5409.

(19) Love, J. A.; Sanford, M. S.; Day, M. W.; Grubbs, R. H. Synthesis, Structure, and Activity of Enhanced Initiators for Olefin Metathesis. *J. Am. Chem. Soc.* **2003**, *125* (33), 10103–10109.

(20) Faulkner, C. J.; Fischer, R. E.; Jennings, G. K. Surface-Initiated Polymerization of 5-(Perfluoro-n-Alkyl)Norbornenes from Gold Substrates. *Macromolecules* **2010**, *43* (3), 1203–1209.

(21) Escobar, C. a; Harl, R. R.; Maxwell, K. E.; Mahfuz, N. N.; Rogers, B. R.; Jennings, G. K. Amplification of Surface-Initiated Ring-Opening Metathesis Polymerization of 5-(Perfluoro-n-alkyl)Norbornenes by Macroinitiation. *Langmuir* **2013**, *29*, 12560–12571.

(22) Njoroge, I.; Kempler, P.; Deng, X.; Arnold, S.; Jennings, G. K. Surface-Initiated Ring-Opening Metathesis Polymerization of Dicyclopentadiene from the Vapor Phase. *Langmuir* **2017**.

(23) Bowden, N. B.; Gupta, A.; Long, T. R. High-Density Polydicyclopentadiene. US 8778186B2, 2014.

(24) Mukerjee, P. Fluorocarbon-Hydrocarbon Interactions in Micelles and Other Lipid Assemblies, at Interfaces, and in Solutions. *Colloids Surfaces A Physicochem. Eng. Asp.* **1994**, *84* (1), 1–10.

(25) Wu, F. C.; Tseng, R. L.; Juang, R. S. Initial Behavior of Intraparticle Diffusion Model Used in the Description of Adsorption Kinetics. *Chem. Eng. J.* **2009**, *153* (1–3), 1–8.

(26) Tseng, R. L.; Wu, F. C.; Juang, R. S. Characteristics and Applications of the Lagergren's First-Order Equation for Adsorption Kinetics. *J. Taiwan Inst. Chem. Eng.* **2010**, *41* (6), 661–669.

(27) Wu, F. C.; Tseng, R. L.; Huang, S. C.; Juang, R. S. Characteristics of Pseudo-Second-Order Kinetic Model for Liquid-Phase Adsorption: A Mini-Review. *Chem. Eng. J.* **2009**, *151* (1–3), 1–9.

(28) Kim, D.; Hu, S.; Tarakeshwar, P.; Kim, K. S.; Lisy, J. M. Cation-π Interactions: A

Theoretical Investigation of the Interaction of Metallic and Organic Cations with Alkenes, Arenes, and Heteroarenes. *J. Phys. Chem. A* **2003**, *107* (8), 1228–1238.

(29) Kim, D.; Tarakeshwar, P.; Kim, K. S. Theoretical Investigations of Anion-π Interactions: The Role of Anions and the Nature of π Systems. *J. Phys. Chem. A* **2004**, *108* (7), 1250–1258.

(30) Avrami, M. Kinetics of Phase Change. I General Theory. *J. Chem. Phys.* **1939**, *7* (12), 1103–1112.

(31) Avrami, M. Kinetics of Phase Change. II Transformation-Time Relations for Random Distribution of Nuclei. *J. Chem. Phys.* **1940**, *8* (2), 212–224.

(32) Avrami, M. Granulation, Phase Change, and Microstructure Kinetics of Phase Change. III. *J. Chem. Phys.* **1941**, *9* (2), 177–184.

(33) Rodahl, M.; Kasemo, B. A Simple Setup to Simultaneously Measure the Resonant Frequency and the Absolute Dissipation Factor of a Quartz Crystal Microbalance. *Rev. Sci. Instrum.* **1996**, *67* (9), 3238–3241.

(34) Wypych, G. *Handbook of Polymers*, 2nd ed.; ChemTec Publishing: Toronto, 2016.

(35) Reviakine, I.; Johannsmann, D.; Richter, R. P. Hearing What You Cannot See and Visualizing What You Hear: Interpreting Quartz Crystal Microbalance Data from Solvated Interfaces. *Anal. Chem.* **2011**, *83* (23), 8838–8848.

(36) Steinem, C.; Andreas, I. *Piezoelectric Sensors*; Springer-Verlag Berlin Heidelberg: New York, 2007.

CHAPTER VIII

CONCLUSIONS AND FUTURE WORK

Conclusions

The results presented in this thesis demonstrate the preparation of compositionally versatile polymer thin films via vapor phase surface-initiated ring-opening metathesis polymerization (SiROMP). This work capitalizes on the advantages and characteristics of surface-initiated polymer thin films and on the compositional versatility of the poly(trans-5-norbornene-2,3-dicarbonyl chloride) (pNBDAC)-based thin films and poly(dicyclopentadiene) (pDCPD)/ionic liquid (IL) composite films to explore their applications in untapped polymer coating systems and more efficient polymer coating processes.

Results in Chapter IV demonstrate the application of poly(acyl chloride)s in polymer modification and functional polymer preparation. The successful preparation of pNBDAC via vapor phase SiROMP provides an efficient method to achieve various functionalities in polymer films. Vapor phase SiROMP enables us to obtain pNBDAC films as thick as 400 nm with good controllability, while the easy reaction of acyl chlorides with water, alcohols and amines provide high-yield routes to introduce an unlimited range of chemical functionalities. The introduction of aromatic rings, pH-responsive tertiary amines, large molecules like fluorescein, and long hydrocarbon chains to the polymer film has been examined. The modification of pNBDAC is an easy and rapid process, while steric hindrances may result in incomplete conversions when modifying the acyl chloride groups with large molecules like fluorescein or 1-hexadecanol. The post-polymerization modification of pNBDAC provides the platform to design the properties of the film. Polymer films modified with a series of n-alcohols with different hydrocarbon chain length (n) were investigated. The surface wettability of the films can be adjusted from 40° to 117° as n increases from 0 to 8. Further increases from n = 8 to n = 16 result in a more dense array of oriented methyl groups on the surface, as evidenced by increases of hexadecane contact angles. The film impedance against

ion transport changes dramatically when the carboxylic acid/carboxylate groups in the films are replaced with hydrocarbon-capped esters. The increase in carbon chain length results in an increase in the ionic barrier, which is due to the increase in film thickness to accommodate these longer side chains and the associated increase in methylene crystallinity.

Chapter V introduces an application of the pNBDAC modification method for functional polymer film preparation described in Chapter IV. The acyl chloride groups in pNBDAC were reacted with hydroxylamine to form hydroxamic acid groups, which are able to chelate various transition metal ions to form stable complexes. Our hydroxamic acid-modified films show a high degree of chelation (~ 70%) at solution concentrations as low as 30 μM with most divalent metal ions Fe^{2+}, Cu^{2+}, Ni^{2+}, Co^{2+}, Zn^{2+}, while multivalent ions like Fe^{3+} and Zr^{4+} are not chelated to high loadings within the film. The low chelation of our polymer films with multivalent ions may be due to the special structure of the polymer repeat unit, where the two hydroxamic acid groups located adjacently are oriented away from each other in a trans conformation. Chelation with metal ions requires hydroxamic acid groups placed almost center symmetric, which would require contributions from hydroxamic acids on other repeat units or chains. Because of the special structure repeat unit, the chelation of divalent metal ions by hydroxamic acids occurs between different units or different chains, which creates ion-mediated cross-links to enhance the thermal and pH stabilities, mechanical properties, and ionic barrier properties of the polymer films. We show that these polymer films can chelate metal ions originating from corrosion, which demonstrates the application of metal corrosion detection when interfaced with an appropriate detection strategy.

Chapter VI reports an ester/carboxylic acid random copolymer film prepared by modification of pNBDAC with solutions containing different ratios of water to ethanol. Due to the much higher reactivity of ethanol than water within the film, the composition of the copolymer films is best controlled to complete modification of the pendant acyl chlorides by exposure to an ethanol-water solution for a short time (15 min) followed by exposure to pure water for longer times. This two-step modification method provides an almost linear control of the film composition with solution composition, which is favorable in tuning the pH-responsive properties of the films. The copolymer films with molar carboxylic acid compositions

between 25 and 39% show huge (up to 10^4 times) pH-responsive switches in ionic barrier properties. At the critical pH for property change, a sufficient fraction of carboxylic acids are deprotonated to carboxylates to surpass a threshold in the hydrophilicity of the film and thereby cause a dramatic drop in the barrier properties against ion transfer. The critical pH of the pH-responsive films is elevated for films with lower carboxylic acid fractions, demonstrating a dependence on film hydrophobicity. QCM-D measurements of the ester/carboxylic acid films also show the pH-responsive behavior and provide key complementary information on film-water interactions. According to QCM-D measurements, copolymer films with 34% carboxylic acid exhibit a 3x greater thickness in high pH solution than in low pH solution due to the absorption of water and ions into the film upon deprotonation/ionization of the carboxylic acid groups. The QCM-D measurements also demonstrate high reversibility and reproducibility of the pH-responsive performance of these copolymer films.

Chapter VII introduces another compositionally versatile system with a different base polymer film: pDCPD/IL composite thin films. In this work, I introduce a new strategy to prepare ionogel thin films by a combination of SiROMP to prepare the pDCPD base film, followed by a simple immersion in a solvent that contains the IL to be incorporated to create the gel. The ILs form stabilizing interactions with C=C double bonds of the polymer as solvent swells the polymer matrix. The IL uptake of the composite can be altered by varying solvent, the IL solution concentration, and the film immersion time. The incorporation process of the IL into the polymer matrix is explained as a phase transformation process described by Avrami model. The presence of the ILs changes both mechanical properties and ion transfer properties based on the results from QCM-D and EIS, respectively. The pDCPD matrix can accommodate various ionic liquids depending on the anion species, and we expect the method can be extended to many other polymer films, which enables the design of many unique polymer/IL binary systems.

Future Work

The results in this thesis present a unified theme to demonstrate functional (co)polymer thin films and composites by exploiting simple reactions and processes from base films prepared by vapor-phase

SiROMP. To aid in the utility and understanding of these compositionally versatile films, I suggest the following topics of research that could be addressed in the near term.

A new route to metal-chelating hydroxamic acid-modified films is presented in this thesis. Results in Chapter V show that the chelation of the polymer films with metal ions can be achieved at low centration and with a comparatively fast kinetics according to QCM-D measurements. However, a more detailed analysis of the kinetics of the chelation process at different concentrations is worthy of more exploration. Also, as related to the kinetics, the chelation stabilities of different transition metal ions are not clarified in this thesis.[1] Therefore, a thorough kinetics study with the investigation of chelation stabilities of different metal ions at low, intermediate, and high loadings should provide greater fundamental understanding of the chelation process in these thin films. Chapter V also demonstrates the feasibility of the hydroxamic acid-modified films to chelate metal ions that originate from corrosion and therefore, its potential utilization in the detection of corrosion. However, Chapter V presents only a brief demonstration of metal chelation when the film is extremely close to the surface. Experiments like growing polymer films directly on the metal surface and then detecting the metal ion capture at the early stage of corrosion are necessary to further investigation this application. In addition, analytical methods to detect the metal loading of the film through the walls of a metal pipe will enable this metal-sensitive film to be incorporated as part of a robust sensing system for the non-destructive structural health monitoring of piping networks.

Chapter VI demonstrates the successful preparation of ester/carboxylic acid copolymer films with pH-responsive barrier and structural properties. The copolymer film shows low ion transfer resistance and highly swollen structure when exposed to high pH solutions, and the pH-responsive behavior can be utilized in many applications such as sensors, separation membranes, or biomedical studies. In many of these applications, the opposite pH-responsive performance is required, where films should swell and have elevated water interaction at low pH. Tertiary amine groups can be introduced into the polymer films to achieve the pH-responsive behavior at low pH. The protonation of the tertiary amine groups in acidic environments can provide ionic moieties in the polymer and increase the overall hydrophilicity to further change the film properties, such as structural properties and barrier properties.[2,3] A further investigation of

pH-responsive films made of tertiary amine/ester/carboxylic acids may be worthy of exploration. Theoretically, tertiary amines are comparatively hydrophobic at high pH while carboxylic acids deprotonate to become hydrophilic at high pH. The polymer film containing small percentages of both tertiary amines and carboxylic acids is expected to switch to more hydrophilic status at either low pH or high pH, with hydrophobic status observed only in the middle range of pH where both amines and acids are not sufficiently ionized. Such pH-responsive performance that introduces a third "state" of the film can be utilized in sensors where deviation from a middle range pH is required.

Chapter IV demonstrates the compositional versatility of the pNBDAC film as a platform for the introduction of functionality. In Chapter IV, I show that the modification of pNBDAC films with large molecules is not perfectly complete, which can be attributed to steric hindrance. Inspired by the phenomenon, a novel method to prepare double-layer polymer films with different functionalities via two-step SiROMP may become feasible. To obtain the double-layer system, high molecular weight polymers with abundant hydroxyl groups such as PVA, PHEMA, cellulose, or agarose may be used. If such polymers are used in pNBDAC modification for a short time, the polymers are too large to penetrate into the polymer film and would likely modify only the surface region of the pNBDAC films, which results in a film structure where the surface is covered by a hydroxyl-abundant polymer layer while the interior of the film remains as unreacted acyl chlorides. Then, the film can be modified with other reagents to functionalize the inner film and the hydroxyl groups on the surface can be initiated to grow another layer of pNBDAC film that can be modified differently from the inner layer. The double-layer preparation method can be utilized in polymer coating preparations when multiple functionalities are required. For instance, the bottom layer could be hydrophobic to provide protective performance, with the top layer showing "smart" stimulus-responsive surface behavior. An interesting example would be a film that offers both corrosion protection and metal-chelating capabilities for inhibition and detection of corrosion.

References

(1) Martell, A. E. CHELATION: STABILITY AND SELECTIVITY. *Ann. N. Y. Acad. Sci.* **1960**, *88* (2), 284–292.

(2) Amalvy, J. I.; Wanless, E. J.; Li, Y.; Michailidou, V.; Armes, S. P.; Duccini, Y. Synthesis and Characterization of Novel PH-Responsive Microgels Based on Tertiary Amine Methacrylates. *Langmuir* **2004**, *20* (21), 8992–8999.

(3) Zhu, L.; Powell, S.; Boyes, S. G. Synthesis of Tertiary Amine-Based PH-Responsive Polymers by RAFT Polymerization. *J. Polym. Sci. Part A Polym. Chem.* **2015**, *53* (8), 1010–1022.

APPENDIX A

THE KINETICS OF THE ANION EXCHANGE PROCESS FOR PIL THIN FILMS PREPARED BY SIROMP

Introduction

Poly(ionic liquid)s (pIL) are a special class of polyelectrolyte produced from the polymerization of monomers containing IL constituents. Compared to other polymers, especially other polyelectrolytes, pILs carry IL species in each of the repeating units, which is expected to induce higher ion mobility within the polymer, simpler property modifications by ion exchange, and broader ranges in glass transition temperature (T_g).[1–3] Compared to ILs, pILs are solid in most cases and exhibit much improved mechanical properties, enhanced processability, improved durability, and spatial controllability.[1–3] PILs have been researched for years and have successfully been prepared through multiple polymerization techniques such as free radical polymerization,[4,5] atom transfer radical polymerization (ATRP),[6,7] and ring-opening metathesis polymerization (ROMP).[8–10] This research, for the first time, investigates the kinetics of anion exchange in thin pIL thin films. The study of the kinetics will help better understand the characteristics of pIL films and determine the effects of anion content on film properties that are necessary to utilize pILs in applications.

Ionic Liquid Monomer Synthesis.

The syntheses of norbornene-tethered IL monomers norbornenyl propylene dimethyl imidazolium hexafluorophosphate ($[N_3 - dIm][PF_6]$) (N represents the norbornene group, where the subscript 1 in N_1 is the carbon number between the norbornene group and imidazolium group) and norbornenyl methylene dimethyl imidazolium hexafluorophosphate ($[N_1 - dIm][PF_6]$) have been achieved via the Diels-Alder reaction of dicyclopentadiene with 5-bromo-1-pentene or 3-bromo-1-propene followed by the addition of the 1,2-dimethylimidazole across the C–Br bond to form the dimethylimidazolium terminus. Anion exchange of Br^- with PF_6^- produced the final monomer. The IL monomers were polymerized directly from the surface via SiROMP to obtain PIL films in which the film thickness is tunable by varying the monomer concentration.

PIL Film Smoothing.

The growth of current pIL films shows that the roughness of the polymer film is very high with respect to film thickness. The roughness is more than 150 nm for a 300-nm thick pIL film (Figure A.1). The significant roughness is contributed to inevitable chain transfer during the polymerization process. As chain polymerization proceeds, polymer chains containing an active metal alkylidene species on its terminus can react with nearby olefin functional groups on the same chain to release a cyclic species into the solution.[11] The activated metal alkylidene may then initiate polymerization in the monomer-rich solution and the polymer chains formed in solution may be bound to the grown polymer films in a physical way during the polymerization process. The attachment of those chains that formed in solution to the pIL film is assumed to be weaker than surface-initiated chains, and we hypothesize that those chains will be removed with external force such as sonication. Hence, sonication was attempted to smooth the film, and after some

experimentation, a smoothing process was successfully achieved by sonicating the obtained polymer films in dichloroethane (DCE). The roughness of the polymer film is nearly unchanged after 5 min and then decreases dramatically as sonication proceeds for 1 h (Figure A.1). The roughness and roughness/thickness ratio over various sonication times have been plotted to quantify the effectiveness of the smoothing process.

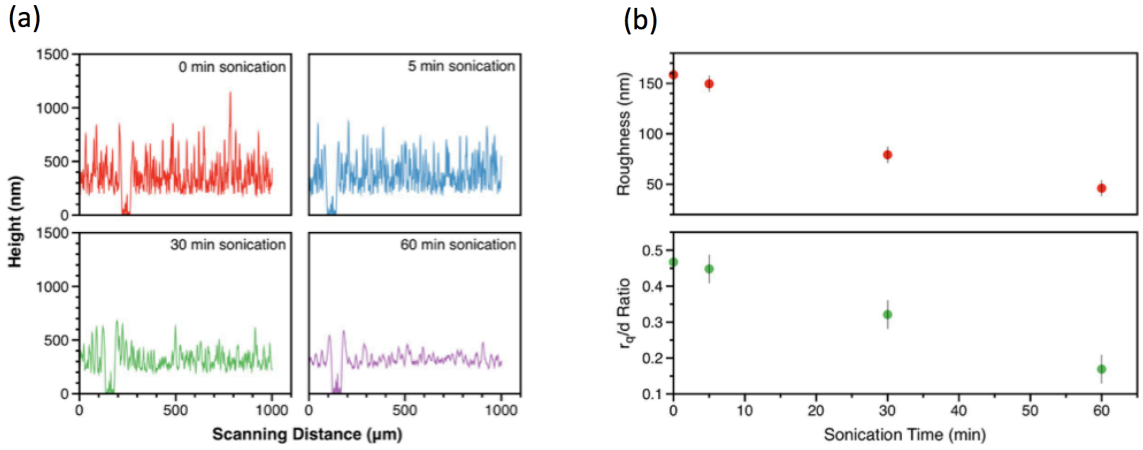

Figure A.1. (a) Profile of pIL films sonicated for 0 min, 5 min, 30 min and 180 min. (b) Roughness (nm) and roughness/thickness ratio of pIL films sonicated for various times.

According to our proposed mechanism, significant roughness is caused by the physical attachment of polymer chains in the bulk solution, which is expected to be almost independent to the film thickness. Films with different thicknesses were prepared and no obvious increase in roughness was observed for a much thicker film. After performing the sonication process for over 90 min, smoother thin PIL films with roughness < 30 nm were obtained for further investigation.

Anion Exchange of PIL Films

One of the unique characteristics of PILs is that their properties may be altered via an anion exchange process. Many researchers have investigated the anion exchange of PILs in bulk solution, which is a slow process and requires a difficult separation process.[12–16] Also, even though anion exchange has been applied to alter polymer properties or during copolymer synthesis, the kinetics of their ion exchange process was not well resolved due to the complexity of the experimental process. As SIP has begun to be applied for the growth of pIL thin films, the ion exchange process can be achieved much more easily from these films without any additional separation processes beyond simple rinsing, as compared to that for bulk polymers. The kinetics of the ion exchange process for pIL thin films will be studied here to provide fundamental insight as to the ion exchange rates for pIL thin films.

We have investigated the kinetics of anion exchange for our more hydrophobic PF_6-laden PIL films with the hydrophilic ion ClO_4^- to investigate effects of anion hydrophobicity, temperature, and thickness on the rate of exchange. The smoothed poly($[N_3 - dIm][PF_6]$) film (300 nm thick) was exposed to a 0.2 M $LiClO_4$ solution for 2 h. FTIR spectra were taken for both the original pIL (PF_6^- film) and the film after anion exchange (Figure A.2a). The strong P-F stretching absorption band at 865 cm^{-1} completely disappears after ion exchange, and a new peak appears at 1118 cm^{-1}, due to the Cl-O absorption band. A complete anion exchange is achieved based on the FTIR spectra. Also, C-H absorption bands are almost unchanged, which suggests that the structure of the polymer backbone remains the same after the anion exchange process. A series of tests with different ion exchange times (0, 1, 3, 10, 30, 90, 180 min) at constant salt concentration (5 mM) has been performed, and the FTIR spectra are shown in Figure A.2b. The

obvious diminution of the PF_6^- peak and increase of the ClO_4^- peak shows that the anion exchange process occurs gradually over 180 min. The kinetics of anion exchange is important to know for further applications such as property tuning and copolymer film synthesis.

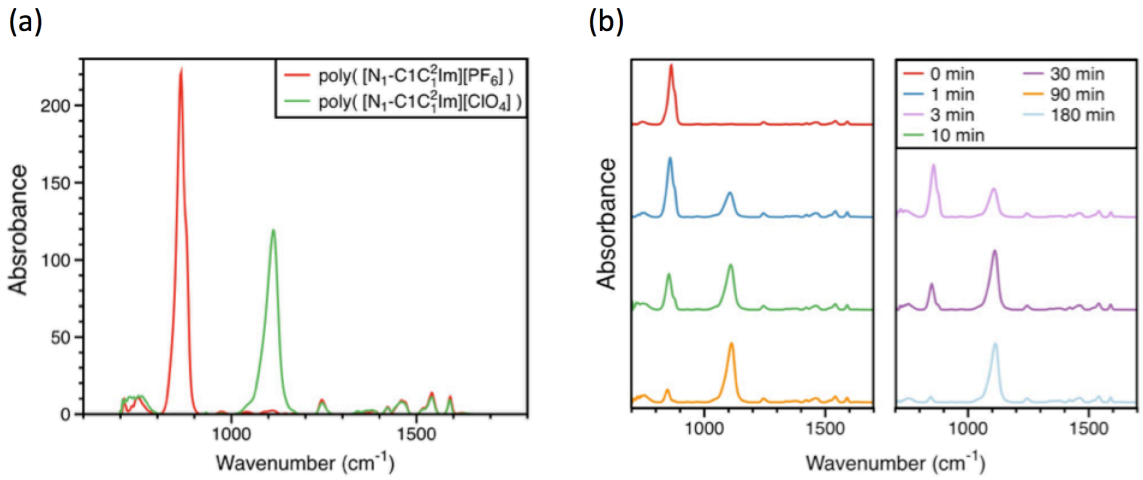

Figure A.2. (a) FTIR spectra of complete anion exchange from PF_6^- to ClO_4^- with a 0.2 M $LiClO_4$(aq) for 2 h (b) FTIR spectra of anion exchange processes from PF_6^- to ClO_4^- with 5 mM $LiClO_4$(aq) for various times.

Kinetics Plots

Utilizing the obtained IR spectra in Figure A.2b, the composition of PF_6^- and ClO_4^- in the ion-exchanged film was estimated, and the conversion of PF_6^- to ClO_4^- conversion was determined. The conversion is plotted versus anion exchange time at different salt concentrations in Figure A.3. The anion exchange reaction proceeded much faster than that expected based on previous results for exchange in bulk solution. For example, 48 h were required for Elabd's group to completely convert poly(1-[(2-methacryl- oyloxy)ethyl]-3-butylimidazolium bromide)

(poly(MEBIm-Br) to poly(1-[(2-methacryl- oyloxy)ethyl]-3-butylimidazolium hydroxide) (poly (MEBIm-OH) by anion exchange.[15] For our PIL thin film anion exchange, the complete conversion of PF_6^- to ClO_4^- can be accomplished after only 30 min with a solution concentration of only 50 mM in $LiClO_4$. The basic trend is consistent with those of other reaction or adsorption processes that proceed rapidly at the beginning due to the abundance of sites, then slow down as sites dwindle until the equilibrium is reached. By lowering the salt solution concentration to 5 mM and 1 mM, slower exchange processes are observed. (Figure A.3a)

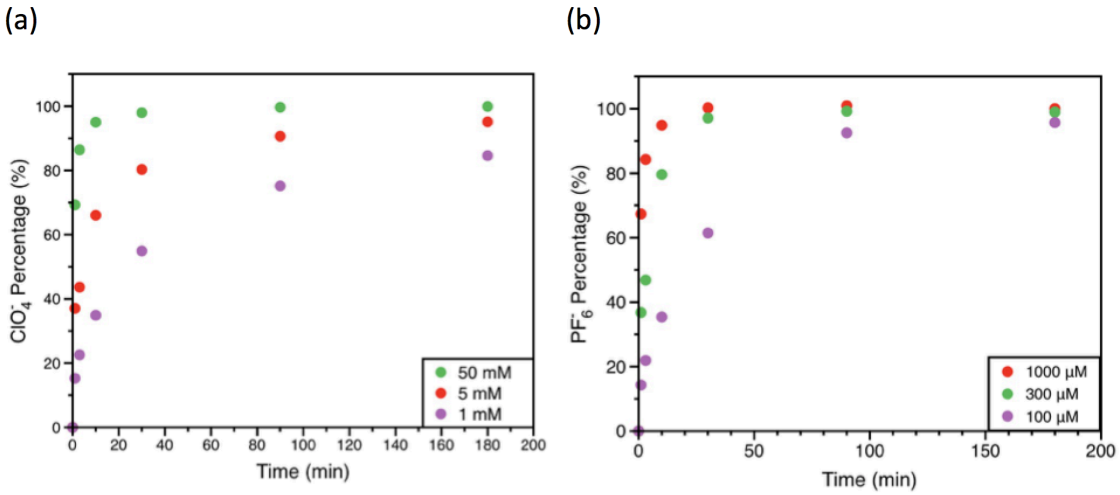

Figure A.3. (a) Conversion plot at various times for anion exchange from PF_6^- to ClO_4^- with a $LiClO_4$ aqueous solution. (b) Conversion plot at various times for anion exchange from ClO_4^- to PF_6^- using a KPF_6 aqueous solution.

Since PF_6^- and ClO_4^- have different water affinities, the ion exchange behavior in the aqueous solution should be different. Hence, after anion-exchanging the original pIL (PF_6^-) film to (ClO_4^-) film, the reverse anion exchange from (ClO_4^-) back to (PF_6^-) was also performed (Figure A.3b). The reverse anion exchange exhibits dramatically faster rates, and the complete conversion

can be achieved within 30 min with a salt solution concentration as low as 1 mM. As such, we investigated lower concentrations for the reverse anion exchange. The phenomenon can be explained by the different hydrophilicity of PF_6^- and ClO_4^- ions. As a more hydrophilic ion, the ClO_4^- that originally occupied the polymer film should have a greater tendency to escape toward the aqueous solution. Likewise, PF_6^- ions are more driven to transport into the hydrophobic polymer film to escape the aqueous phase.

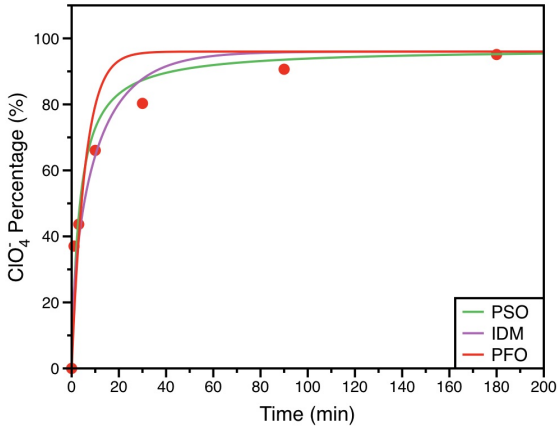

Figure A.4. PFO (RMSE = 11.84), PSO (RMSE = 6.79) and IDM (RMSE = 6.27) model fitting for anion exchange from PF_6^- to ClO_4^- with a 5mM salt solution

Kinetics Model

Different kinetics models were employed to fit the experimental data to determine rate constants. Due to the similarity of the ion exchange process and solid-liquid phase adsorption processes, three commonly employed kinetics models for adsorption: pseudo-first-order model (PFO),[17] pseudo-second-order model (PSO)[18], and intraparticle diffusion model (IDM)[19], have been applied to fit the experimental results for the ion exchange process from PF_6^- to ClO_4^- with a 5 mM $LiClO_4$ salt solution (Figure A.4). Root mean squared errors (RMSE) were calculated for

each model. We found that the pseudo-first-order (PFO) exhibits the poorest fitting (RMSE=11.84), while the PSO (RMSE=6.79) and IMD (RMSE=6.27) fittings are similarly, yet mildly accurate for these data. Additional model fittings were done with all the forward and reverse ion exchange runs. The fitting results are shown in (Figure A.5 a-d). Based on the results, PSO gives improved fitting for anion exchange at high salt concentration while IMD has better predictions for the process at low salt concentration. Due to the lack of error bars on the experimental data at this stage, it is not wise to make a conclusion as to which model best describes the anion exchange process. More experimental data are required for both forward and reverse experiments and more model-fittings should be investigated.

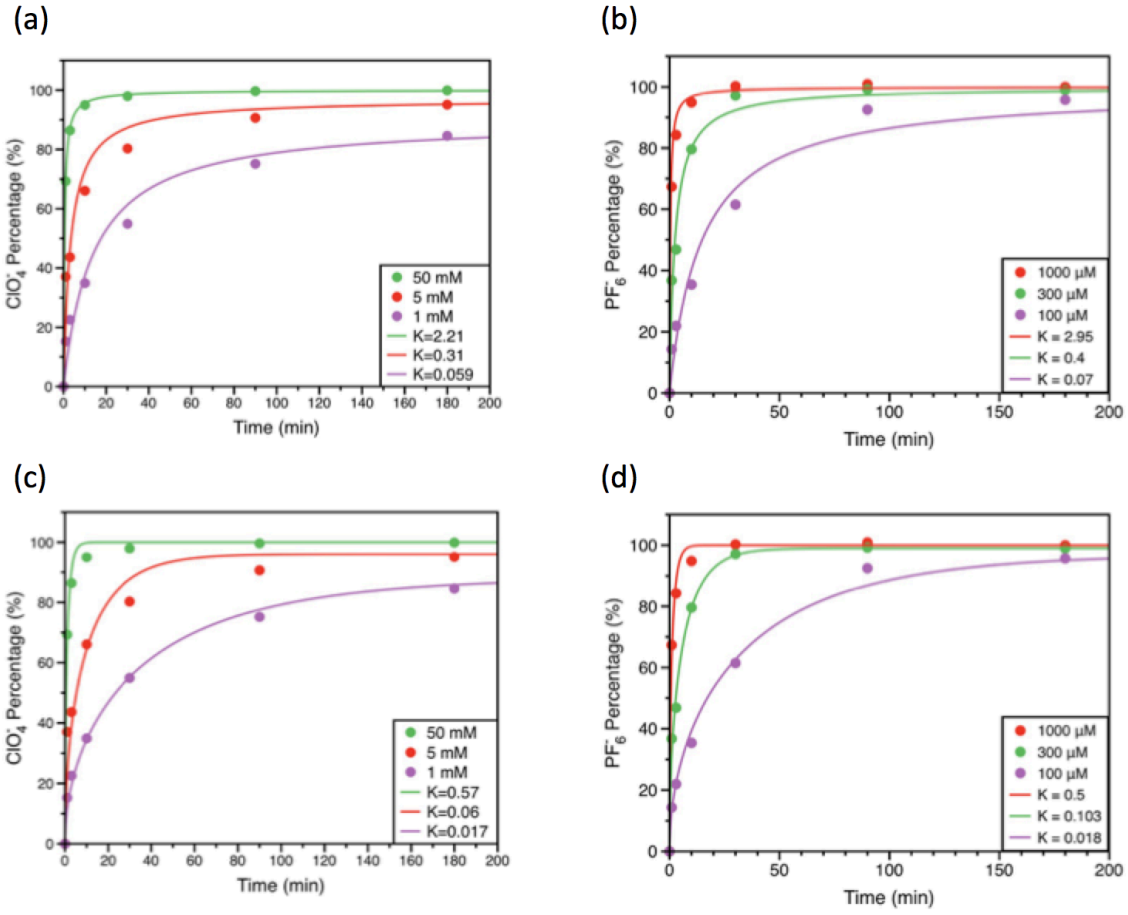

Figure A.5. (a) PSO model-fitting for the anion exchange process from PF_6^- to ClO_4^-. (b) PSO model-fitting for the anion exchange process from PF_6^- to ClO_4^-. (c) IDM model-fitting for the anion exchange process from ClO_4^- to PF_6^-. (d) IDM model-fitting for the anion exchange process from ClO_4^- to PF_6^-.

Temperature Effects

A study on the effect of temperature was performed for the anion exchange process. Increasing temperature is expected to affect both the rate of anion exchange in the film and the equilibrium composition. A set of anion exchange experiments was performed at 60 °C with a 5 mM $LiClO_4$ aqueous solution, and the time-dependent conversion was compared to that at room temperature (Figure A.6). A significantly faster rate is observed for anion exchange at 60 °C, which is consistent with our prediction. More sets of anion exchange at lower temperatures are required for a full study on temperature effects.

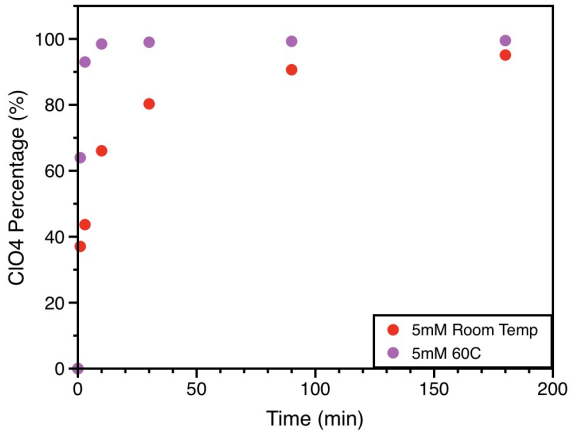

Figure A.6. The anion exchange kinetics plot for a $[N_3 - dIm][PF_6]$ film exposed to 5 mM $LiClO_4$ aqueous solution at room temperature and at 60 °C.

References

(1) Yuan, J.; Antonietti, M. Poly(Ionic Liquid)s: Polymers Expanding Classical Property Profiles. *Polymer (Guildf)*. **2011**, *52* (7), 1469–1482.

(2) Yuan, J.; Mecerreyes, D.; Antonietti, M. Poly(Ionic Liquid)s: An Update. *Prog. Polym. Sci.* **2013**, *38* (7), 1009–1036.

(3) Mecerreyes, D. Polymeric Ionic Liquids: Broadening the Properties and Applications of Polyelectrolytes. *Prog. Polym. Sci.* **2011**, *36* (12), 1629–1648.

(4) Grubjesic, S.; Seifert, S.; Firestone, M. A. Cytoskeleton Mimetic Reinforcement of a Self-Assembled N.N' -Dialkylimidazolium Ionic Liquid Monomer by Copolymerization. *Macromolecules* **2009**, *42* (15), 5461–5470.

(5) Huang, J.; Tao, C.-A.; An, Q.; Zhang, W.; Wu, Y.; Li, X.; Shen, D.; Li, G. 3D-Ordered Macroporous Poly(Ionic Liquid) Films as Multifunctional Materials. *Chem. Commun. (Camb)*. **2010**, *46* (6), 967–969.

(6) He, X.; Yang, W.; Pei, X. Preparation , Characterization , and Tunable Wettability of Poly (Ionic Liquid) Brushes via Surface-Initiated Atom Transfer Radical Polymerization. *Society* **2008**, 4615–4621.

(7) Ding, S.; Tang, H.; Radosz, M.; Shen, Y. Atom Transfer Radical Polymerization of Ionic Liquid 2-(1-Butylimidazolium-3-Yl)Ethyl Methacrylate Tetrafluoroborate. *J. Polym. Sci. Part A Polym. Chem.* **2004**, *42* (Copyright (C) 2014 American Chemical Society (ACS). All Rights Reserved.), 5794–5801.

(8) Vygodskii, Y. S.; Shaplov, A. S.; Lozinskaya, E. I.; Filippov, O. A.; Shubina, E. S.;

Bandari, R.; Buchmeiser, M. R. Ring-Opening Metathesis Polymerization (ROMP) in Ionic Liquids: Scope and Limitations. *Macromolecules* **2006**, *39* (23), 7821–7830.

(9) Wang, J.; He, X.; Zhu, H.; Chen, D. RSC Advances Preparation of a ROMP-Type Imidazolium- Functionalized Norbornene Ionic Liquid Block Copolymer and the Electrochemical Property For. *RSC Adv.* **2015**, *5*, 43581–43588.

(10) Ye, Q.; Gao, T.; Wan, F.; Yu, B.; Pei, X.; Zhou, F.; Xue, Q. Grafting Poly(Ionic Liquid) Brushes for Anti-Bacterial and Anti-Biofouling Applications. *J. Mater. Chem.* **2012**, *22* (26), 13123.

(11) Bielawski, C. W.; Grubbs, R. H. Living Ring-Opening Metathesis Polymerization. *Prog. Polym. Sci.* **2007**, *32* (1), 1–29.

(12) Marcilla, R.; Blazquez, J. A.; Rodriguez, J.; Pomposo, J. A.; Mecerreyes, D. Tuning the Solubility of Polymerized Ionic Liquids by Simple Anion-Exchange Reactions. *J. Polym. Sci. Part A Polym. Chem.* **2004**, *42* (1), 208–212.

(13) Carrasco, P. M.; Ruiz De Luzuriaga, A.; Constantinou, M.; Georgopanos, P.; Rangou, S.; Avgeropoulos, A.; Zafeiropoulos, N. E.; Grande, H. J.; Cabañero, G.; Mecerreyes, D.; Garcia, I. Influence of Anion Exchange in Self-Assembling of Polymeric Ionic Liquid Block Copolymers. *Macromolecules* **2011**, *44* (12), 4936–4941.

(14) Vijayakrishna, K.; Mecerreyes, D.; Gnanou, Y.; Taton, D. Polymeric Vesicles and Micelles Obtained by Self-Assembly of Ionic Liquid-Based Block Copolymers Triggered by Anion or Solvent Exchange. *Macromolecules* **2009**, *42* (14), 5167–5174.

(15) Ye, Y.; Elabd, Y. A. Relative Chemical Stability of Imidazolium-Based Alkaline Anion Exchange Polymerized Ionic Liquids. *Macromolecules* **2011**, *44* (21), 8494–8503.

(16) Isik, M.; Fernandes, A. M.; Vijayakrishna, K.; Paulis, M.; Mecerreyes, D. Preparation of

Poly(Ionic Liquid) Nanoparticles and Their Novel Application as Flocculants for Water Purification. *Polym. Chem.* **2016**, *7* (8), 1668–1674.

(17) Tseng, R. L.; Wu, F. C.; Juang, R. S. Characteristics and Applications of the Lagergren's First-Order Equation for Adsorption Kinetics. *J. Taiwan Inst. Chem. Eng.* **2010**, *41* (6), 661–669.

(18) Wu, F. C.; Tseng, R. L.; Huang, S. C.; Juang, R. S. Characteristics of Pseudo-Second-Order Kinetic Model for Liquid-Phase Adsorption: A Mini-Review. *Chem. Eng. J.* **2009**, *151* (1–3), 1–9.

(19) Wu, F. C.; Tseng, R. L.; Juang, R. S. Initial Behavior of Intraparticle Diffusion Model Used in the Description of Adsorption Kinetics. *Chem. Eng. J.* **2009**, *153* (1–3), 1–8.

APPENDIX B

SUPPLEMENTARY INFORMATION FOR CHAPTER VI

Phase Angle Plots

Figure B.1 shows the phase angle plots for ester/carboxylic acid copolymers with 25 % and 39 % carboxylic acids. In Figure B.1a, as the frequency change from high to low, the phase angles start to decrease almost immediately at 100 kHz, which demonstrate the capacitor behavior of the film at these pH levels. A dramatic change in the phase angle spectra shows from pH 6 to 7. When pH is 7 or higher, the phase angle spectra keep near 0 (resistant behavior from solution) and start to decrease at frequency 100 – 300 Hz, which comes from the capacitor behavior of the SAM interface). The phase angle spectra shows that the copolymer has high film resistance at low pH and almost no film resistance effect at high pH. Figure B.1b shows similar trend, but the property switch happens at pH 9.

Figure B.2 shows the phase angle plots for ester/carboxylic acid copolymers with 14 % and 49 % carboxylic acids. In Figure B.2, phase angles spectra show not much change over different pH values, which is consistent with the conclusion in the Chapter VI that if copolymer films contain too many carboxylic acids (Figure B.2a), the film will be hydrophilic enough even at high pH. In contrast, if copolymer films contain too less carboxylic acids, the overall film will still show relatively high hydrophobicity even with deprotonated carboxylates.

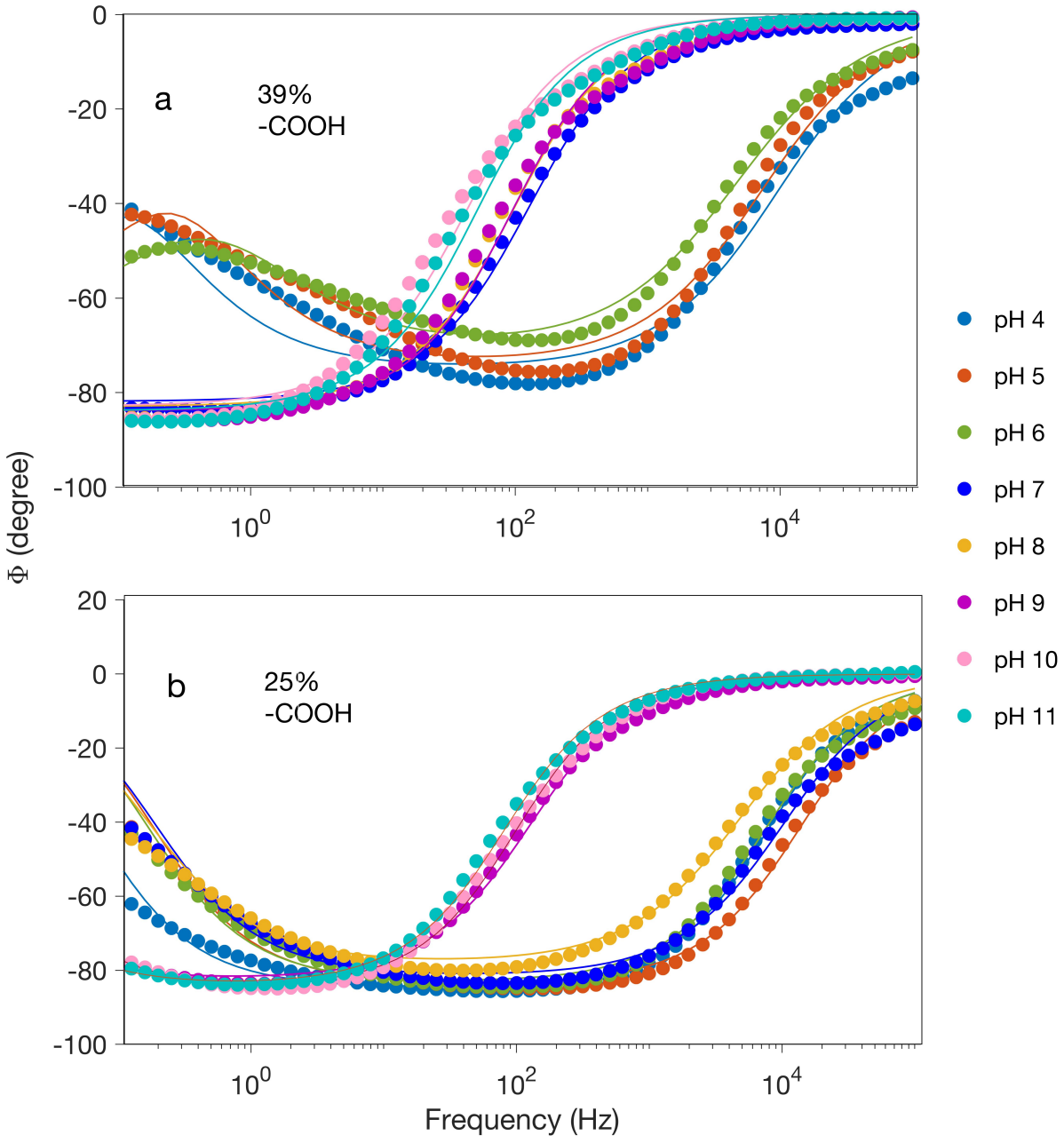

Figure B.1. pH-dependent EIS phase angle measurements of a copolymer film that contains (a) 39% carboxylic acids and (b) 25% carboxylic acids. Solid lines indicate fits of the spectra based on the equivalent circuit model of Figures 3.3 and 3.4.

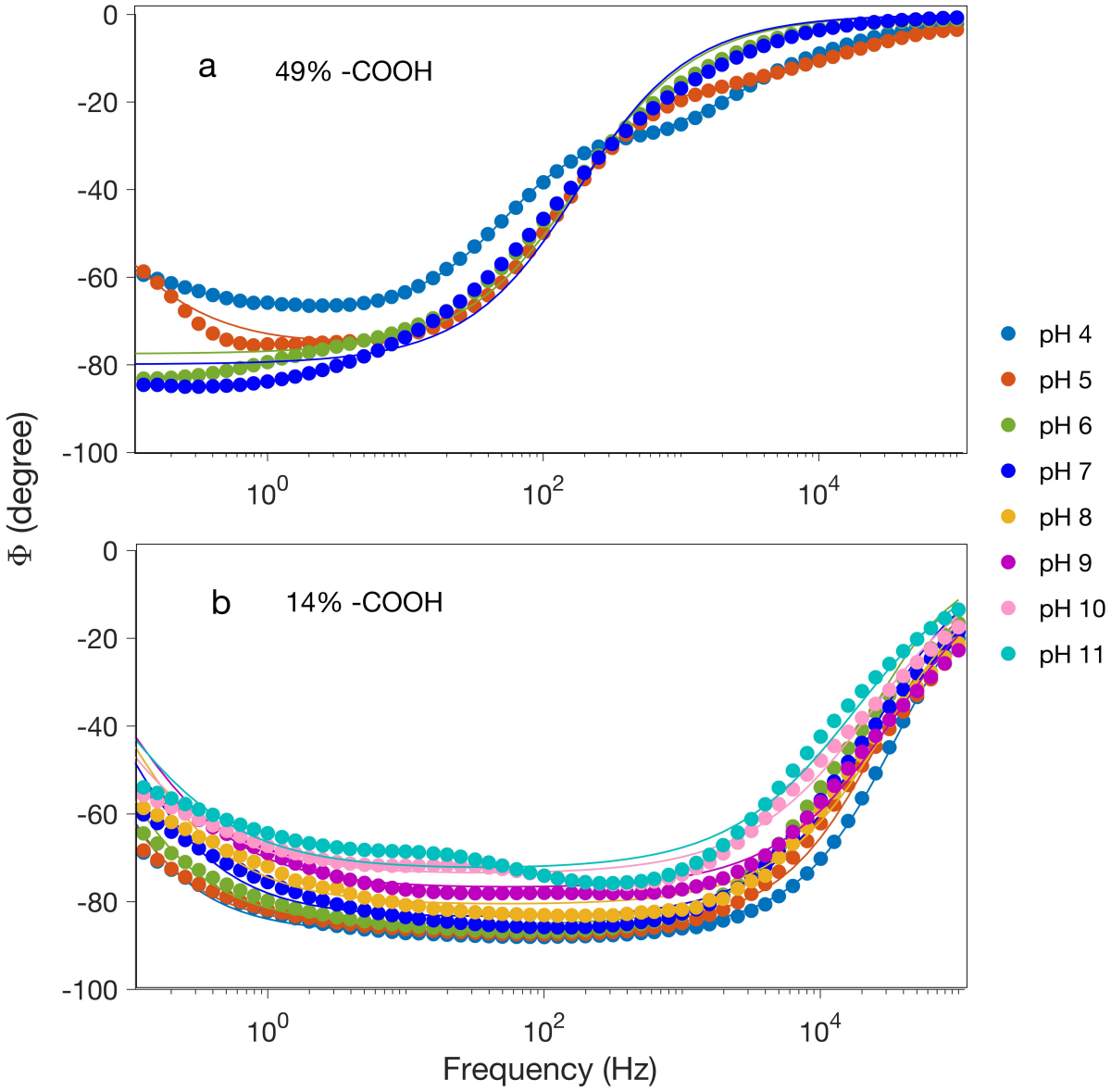

Figure B.2. pH-dependent EIS phase angle measurements of a copolymer film that contains (a) 49% carboxylic acids and (b) 14% carboxylic acids. Solid lines indicate fits of the spectra based on the equivalent circuit model of Figures 3.3 and 3.4.